Causal Feature Selection via Orthogonal Search

Anonymous authors
Paper under double-blind review

Abstract

The problem of inferring the direct causal parents of a response variable among a large set of explanatory variables is of high practical importance in many disciplines. However, established approaches often scale at least exponentially with the number of explanatory variables, are difficult to extend to nonlinear relationships and are difficult to extend to cyclic data. Inspired by *Debiased* machine learning methods, we study a one-vs.-the-rest feature selection approach to discover the direct causal parent of the response. We propose an algorithm that works for purely observational data while also offering theoretical guarantees, including the case of partially nonlinear relationships possibly under the presence of cycles. As it requires only one estimation for each variable, our approach is applicable even to large graphs. We demonstrate significant improvements compared to established approaches.

1 Introduction

Identifying causal relationships is a profound and hard problem pervading experimental sciences such as biology (Sachs et al., 2005), medicine (Castro et al., 2020), earth system sciences (Runge et al., 2019), or robotics (Ahmed et al., 2020). While randomized controlled interventional studies are considered the gold standard, they are in many cases ruled out by financial or ethical concerns (Pearl, 2009; Spirtes et al., 2000). In order to improve the understanding of a system and help design relevant interventions, the subset of causes that have a direct effect (*direct causes*/*direct causal parents*) often needs to be identified based on observations only. Let us consider the setup exemplified in Figure 1, corresponding to a linear structural equation (SEM) for the response Y,

$$Y = \langle \theta, X \rangle + U. \tag{1}$$

where U is an independent exogenous variable with zero mean, $\theta, X \in \mathbb{R}^d$, $Y \in \mathbb{R}$ and $\langle \cdot, \cdot \rangle$ denotes the inner product. We investigate how to find the direct causes of Y among a high-dimensional vector of covariates X, where the covariates have arbitrary non-linear, possibly cyclic relationships among them. In other words, the causal structure of covariates (X) is an arbitrary member of uniquely solvable structural causal models (Simple SCMs), possibly with hidden confounders (As long as there is no hidden confounder for the response variable). Uniquely solvability of SCMs amounts to not having self-cycles in the causal structure, but any other arbitrary non-linear cyclic structure is allowed (Bongers et al., 2021). Practically speaking, almost all causal discovery applications lie under the umbrella of simple SCMs (Bollen, 1989; Sanchez-Romero et al., 2019). Besides, the assumption of not having self-cycles is usually assumed not-limiting in the literature (Lacerda et al., 2012; Rothenhäusler et al., 2015; Bongers et al., 2016). From our formulation, a given entry of θ should be non-zero if and only if the variable corresponding to that particular coefficient is a direct causal parent (Peters et al., 2017), e.g., X_1 and X_2 in Figure 1. We restrict ourselves to the setting of *linear direct causal effects* of Y (LDC, as specified in Equation 1) and *no feature descending from* Y (NFD). LDC is justified as an approximation when the effects of each causal feature are weak such that the possibly non-linear effects can be linearized; NFD is justified in some applications where we can exclude any influence of Y on a covariate. This is, for example, the case when X are genetic factors, and Y is a particular trait/phenotype. Our method, in particular, comes handy in this case due to the relatively complex non-linear cyclic structure of these genetic factors in high-dimensional regimes (Yao et al., 2015; Meinshausen et al., 2016; Warrell & Gerstein, 2020).

While applicable to full graph discovery rather than the simplified problem of finding causal parents, state-of-the-art methods for causal discovery often rely on strong assumptions or the availability of interventional data or have prohibitive computational costs explained in section 1.1 in more detail. In addition to and despite their strong assumptions, causal discovery methods may perform worse than simple regression baselines (Heinze-Deml et al., 2018; Janzing, 2019; Zheng et al., 2018).

While plain regression techniques have appealing computational costs, they come without guarantees. When using unregularized least-square regression to estimate θ, there can be infinitely many possible choices for θ recovered with equivalent prediction accuracy for regressing Y, especially in the case of over-parametrized models. However, none of these choices provide any information about the features which, when intervened upon, directly cause the output variable Y. On the other hand, when using a regularized method such as Lasso, a critical issue is the bias induced by regularization (Javanmard & Montanari, 2018).

When knowing the distinction between covariates and direct causes, Double ML approaches (Chernozhukov et al., 2018a) have shown promising bias compensation results in the context of high dimensional observed confounding of a single variable. In the present paper, we generalize them to the problem of finding direct causes. Our key contributions are:

- We show that under the assumption that no feature of X is a child of Y, the Double ML (Chernozhukov et al., 2018) principle can be applied in an iterative and parallel way to find the subset of direct causes with observational data.
- Our approach has a computational complexity requirement polynomial (fast) time in dimension d.
- Our method provides asymptotic guarantees that the set can be recovered from observational data. Importantly, this result neither requires linear interactions among the covariates, faithfulness, nor acyclic structure.
- Extensive experimental results demonstrate the state-of-the-art performance of our method. Our approach significantly outperforms all other methods (even though underlying data generation conditions favor them), especially in the case of non-linear interactions between covariates, despite relying only on linear projection.

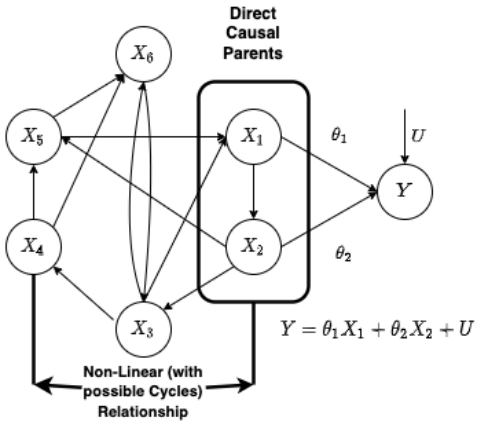

Figure 1: Graphical representation of Causal Feature Selection in our setting, for the case of two direct causal parents of Y, X_1 and X_2, out of variables $\{X_1, \cdots, X_{11}\}$, such that $Y = \theta_1 X_1 + \theta_2 X_2 + U$, U being an independent zero-mean noise. We propose an approach to find X_1 and X_2 under assumptions discussed in the text. An example of this setup in the real-world is finding genes which directly cause a phenotype.

1.1 Related work

The question of finding direct causal parents is also addressed in the literature as mediation analysis (Baron & Kenny, 1986; Hayes, 2017; Shrout & Bolger, 2002). Several principled approaches have been proposed (relying, for instance, on Instrumental Variables (IVs)) (Angrist & Imbens, 1995; Angrist et al., 1996; Bowden & Turkington, 1990) to test for a single direct effect in the context of specific causal graphs. Extensions of the IV-based approach to generalized IVs-based approaches (Brito & Pearl, 2012; Van der Zander & Liskiewicz, 2016) are the closest known result to discovering direct causal parents. However, no algorithm is provided in Brito & Pearl (2012) to identify the instrumental set. Subsequently, an algorithm is provided in Van der Zander & Liskiewicz (2016) for discovering the instrumental set in the simple setting where all the interactions are linear and the graph is acyclic. In contrast, our method allows non-linear cyclic interaction amongst the variables.

Several other works have also tried to address the problem of discovering causal features. The authors review work on causal feature selection in Guyon & Aliferis (2007). More recent papers on causal feature selection have appeared since (Cawley, 2008; Paul, 2017; Yu et al., 2018), but none of those claims to recover all the

direct causal parents asymptotically or non-asymptotically as we do in our case. There has been another line of works on inferring causal relationships from observational data, most of which require strong assumptions, such as faithfulness (Mastakouri et al., 2019; Pearl, 2009; Spirtes et al., 2000). Classical approaches along these lines include the PC-algorithm (Spirtes et al., 2000), which can only reconstruct the network up to a Markov equivalence class. Another approach is to restrict the class of interactions among the covariates and the functional form of the signal-noise mixing (typically considered additive) or the distribution (e.g., non-Gaussianity) to achieve identifiability (see (Hoyer et al., 2009; Peters et al., 2014)); this includes linear approaches like LiNGAM (Shimizu et al., 2006) and nonlinear generalizations with additive noise (Peters et al., 2011). For a recent review of the empirical performance of structure learning algorithms and a detailed description of causal discovery methods, we refer to (Heinze-Deml et al., 2018). Recently, there have been several attempts at solving the problem of causal inference by exploiting the invariance of a prediction under a causal model given different experimental settings (Ghassami et al., 2017; Peters et al., 2016). The computational cost to run both algorithms is exponential in the number of variables when aiming to discover the full causal graph.

Our method mainly takes inspiration from Debiased/Double ML method (Chernozhukov et al., 2018a) which utilizes the concept of orthogonalization to overcome the bias introduced due to regularization. We will discuss this in detail in the next section. Considering a specific example, the Lasso suffers from the fact that the estimated coefficients are shrunk towards zero, which is undesirable (Tibshirani & Wasserman, 2017). To overcome this limitation, a debiasing approach was proposed for the Lasso in several papers (Javanmard & Montanari, 2014; 2018; Zhang & Zhang, 2014). However, unlike our approach, Debiased Lasso methods do not recover all the non-zero coefficients of the parameter vector θ under the generic assumptions of the present work.

2 Methodology

Before describing the proposed method, we quickly discuss Double ML and Neyman orthogonality in the next section, which will be helpful in building the theoretical framework for our method.

2.1 Double Machine Learning (Double ML)

Given a fixed set of policy variables D and control variables X acting as common causes of D and Y, we consider the partial regression model of Equation (2),

$$\begin{aligned} Y &= D\theta_0 + g_0(X) + U, \quad \mathbb{E}\left[U|X, D\right] = 0 \\ D &= m_0(X) + V, \quad \mathbb{E}\left[V|X\right] = 0, \end{aligned} \tag{2}$$

where Y is the outcome variable, U, V are disturbances and $g_0, m_0 : \mathbb{R}^d \to \mathbb{R}$ are (possibly non-linear) measurable functions. An unbiased estimator of the causal effect parameter θ_0 can be obtained via the orthogonalization approach as in Chernozhukov et al. (2018a), which is obtained via the use of the "Neyman Orthogonality Condition" described below.

Neyman Orthogonality Condition: The traditional estimator of θ_0 in Equation (2) can be simply obtained by finding the zero of the empirical average of a score function ϕ such that $\phi(W; \theta, g) = D^\top(Y - D\theta - g(X))$. However, the estimation of θ_0 is sensitive to the bias in the estimation of the function g. Neyman (Neyman, 1979) proposed an orthogonalization approach to get an estimate for θ_0 that is more robust to the bias in the estimation of nuisance parameter (m_0, g_0). Assume for a moment that the true nuisance parameter is η_0 (which represents m_0 and g_0 in Equation (2)) then the orthogonalized "score" function ψ should satisfy the property that the Gateaux derivative operator with respect to η vanishes when evaluated at the true parameter values:

$$\partial_\eta \mathbb{E}\psi(W; \theta_0, \eta_0)[\eta - \eta_0] = 0\,. \tag{3}$$

The corresponding Orthogonalized or Double/Debiased ML estimator $\check{\theta}_0$ solves

$$\frac{1}{n}\sum_{i=1}^{n}\psi(W;\check{\theta}_0,\hat{\eta}_0)=0,$$

where $\hat{\eta}_0$ is the estimator of η_0 and ψ satisfies condition in Equation (3). For the partially linear model discussed in Equation (2), the orthogonalized score function ψ is,

$$\psi(W;\theta,\eta)=(Y-D\theta-g(X))(D-m(X)) \tag{4}$$

with $\eta=(m,g)$.

From Double ML to Causal Discovery: The distinction between policy variables and confounding variables is not always known in advance, which motivates us to consider the more general setting of causal discovery. To this end, we consider a set of variables $X=\{X_1,X_2,\cdots X_d\}$ which includes direct causal parents of the outcome variable Y as well as other variables. We also reiterate our assumption that the relationship between the outcome variable and direct causal parents of the outcome variable is linear. The relationship among other variables can be cyclic and nonlinear. We now provide a general approach to scanning putative direct causes scaling "polynomially" in their number (see *Computational Complexity* paragraph in next section), based on the application of a statistical test and Double ML estimators. We describe first the algorithm and then provide theoretical support for its performance.

2.2 Informal Search Algorithm Description

We provide pseudo-code for our proposed method (CORTH Features) in Algorithm 1. Intuitively, the idea is to do a one-vs-rest split for each variable in turn and try to estimate the link between that particular variable and the outcome variable using Double ML. To do so, we decompose Equation (1) to single out a variable $D=X_k$ as policy variable and take the remaining variables $Z=X_{-k}=X\backslash X_k$ as multidimensional control variables, and run Double ML estimation assuming the partial regression model presented in Section 2.1, which now takes the form

$$\begin{aligned}&Y=D\theta_k+g_k(Z)+U,\quad \mathbb{E}\left[U|Z,D\right]=0\\&D=m_k(Z)+V,\quad \mathbb{E}\left[V|Z\right]=0.\end{aligned} \tag{5}$$

The step-wise description of our estimation algorithm goes as follows:

(a) Select one of the variables X_i to estimate its (hypothetical) linear causal effect θ on Y.
(b) Set all of the other variables X_{-i} as the set of possible confounders.
(c) Use the Double ML approach to estimate the parameter θ i.e. the causal effect of X_i on Y.
(d) If the variable X_i is not a causal parent, the distribution of the conditional covariance χ_i (Proposition 3) is a Gaussian centered around zero. We use a simple normality test for χ_i to select or discard X_i as one of the direct causal parents of Y.

We iteratively repeat the procedure on each of the variables until completion. Pseudo-code for the entire procedure is given below in Algorithm 1.

Note that Equation (5) is not necessarily a correct structural equation model to describe the true underlying causal structure. In general, for instance, when D actually causes Z, it is non-trivial to show that the Double ML estimation of parameter θ_k will be unbiased (see Section 2.3).

Remarks on Algorithm 1: $X_i^{[k]}$ is a vector which corresponds to the samples chosen in the k^{th} subsampling procedure, $X_{\backslash i}^{[k]}=(X_1^{[k]},\ldots,X_{i-1}^{[k]},X_{i+1}^{[k]},\ldots,X_d^{[k]})$ for any $i\in[d]$. In general the subscript i represents the estimation for the i^{th} variable and super-script k represents the k^{th} subsampling procedure. K represents the set obtained after sample splitting. $m_i^{[\backslash k]}$ are (possibly nonlinear) parametric functions fitted using $(1^{st},\ldots,k-1^{th},k+1^{th},\ldots,K^{th})$ subsamples.

Algorithm 1 Efficient Causal Orthogonal Structure Search (CORTH Features)

Input: response $Y \in \mathbb{R}^N$, covariates $\mathbb{X} \in \mathbb{R}^{N \times d}$, significance level α, number of partitions K.
Split N observations into K-fold random partitions, I_k for $k = 1, 2 \ldots, K$, each having $n = N/K$ observations.
for $i = 1, \ldots, d$ **do**
  for Subsample $k \in [K]$ **do**
    $D_k \leftarrow X_i^{[k]}$ and $Z_k \leftarrow X_{\setminus i}^{[k]}$
    Fit $m_i^{[\setminus k]}(Z_{\setminus k})$ to $D_{\setminus k}$ and fit $g_i^{[\setminus k]}(Z_{\setminus k})$ to $Y^{[\setminus k]}$
    $\hat{V}_i^{[k]} \leftarrow D_k - m_i^{[\setminus k]}(Z_k)$
    $\check{\theta}_i^{[k]} \leftarrow \big(\frac{1}{n}\sum_{j \in I_k} \hat{V}_{ij}^{[k]} D_{kj}\big)^{-1} \frac{1}{n} \sum_{j \in I_k} \hat{V}_{ij}^{[k]} (Y_{ij}^{[k]} - g_{ij}^{[\setminus k]}(Z_{kj}))$
    $\hat{\chi}_i^{[k]} \leftarrow \frac{1}{n}\sum_{j \in I_k} \big(- Y_j^{[k]} m_{ij}^{[\setminus k]}(Z_{kj}) - D_{kj} g_{ij}^{[\setminus k]}(Z_{kj}) + m_{ij}^{[\setminus k]}(Z_{kj}) g_{ij}^{[\setminus k]}(Z_{kj}) + \hat{V}_{ij}^{[k]} D_{kj}\big)$
    $(\hat{\sigma}_i^{[k]})^2 \leftarrow \frac{1}{n}\sum_{j \in I_k} \big(- Y_j^{[k]} m_{ij}^{[\setminus k]}(Z_{kj}) - D_{kj} g_{ij}^{[\setminus k]}(Z_{kj}) + m_{ij}^{[\setminus k]}(Z_{kj}) g_{ij}^{[\setminus k]}(Z_{kj}) + \hat{V}_{ij}^{[k]} D_{kj} - \hat{\chi}_i^{[k]}\big)^2$
  end for
  $\hat{\theta}_i \leftarrow \frac{1}{K}\sum_{k \in K} \check{\theta}_i^{[k]}$, $\hat{\chi}_i \leftarrow \frac{1}{K}\sum_{k \in K} \hat{\chi}_i^{[k]}$ and $\hat{\sigma}_i^2 \leftarrow \frac{1}{K}\sum_{k \in K} (\hat{\sigma}_i^{[k]})^2$
end for
for $i \in [d]$ **do**
  Gaussian normality test for $\hat{\chi}_i \approx N\Big(0, \frac{\hat{\sigma}_i^2}{N}\Big)$ with α significance level and select i^{th} feature if null-hypothese is rejected.
end for
Return Decision Vector

Computational Complexity: For each subset randomly selected from the data, we fit two lasso estimators. Accelerated coordinate descent (Nesterov, 2012) can be applied to optimize the lasso objective. To achieve ε error, $\mathcal{O}\left(d\sqrt{\kappa_{\max}} \log \frac{1}{\varepsilon}\right)$ number of iterations are required where $\kappa_{\max}$ is the maximum of the two condition number for both the problems and each iteration requires $\mathcal{O}(nd)$ computation. Hence, the computational complexity of running our approach is only polynomial in d.

2.3 Orthogonal Scores

Now we describe the execution of our algorithm for a simple graph with 3 nodes. Let us consider the following linear structural equation model as an example of our general formulation:

$$Y := \theta_1 X_1 + \theta_2 X_2 + \varepsilon_3, \; X_2 := a_{12} X_1 + \varepsilon_2, \text{ and } X_1 := \varepsilon_1. \tag{6}$$

Example 1. *Let us consider the system whose structural equation model is given in Equation* (5)*. If ε_1, ε_2 and ε_3 are independent uncorrelated noise terms with zero mean, then Algorithm 1 will recover the coefficients θ_1 and θ_2.*

A detailed proof is given in Appendix A.1. While the estimation of the parameter θ_1 is in line with the assumed partial regression model of Equation (6), the estimation of θ_2 does not follow the same. However, it can be seen from the proof that θ_2 can also be estimated from the orthogonal score in Equation (4).

We now show that this result holds for a more general graph structure given in Figure 2, allowing for non-linear cyclic interactions among features.

Proposition 2. *Assume the partially linear Gaussian model of Figure 2, denote $X_{-k} = [Z_1^\top, Z_2^\top]^\top$ the control variables, $\boldsymbol{\gamma} = (\boldsymbol{\gamma}_1, \boldsymbol{\gamma}_2, \boldsymbol{\gamma}_{12})$ the parameter vector of the (possibly non-linear) assignments between putative parents of Y, and $\boldsymbol{\beta} = (\boldsymbol{\beta}_1, \boldsymbol{\beta}_2)$, the vector of causal coefficients for encoding linear effects of X_{-k} on outcome Y. Then, independently of the $\boldsymbol{\gamma}$ parameters and of the functional form of the associated assignments between parents of Y, the score*

$$\psi(W; \theta, \boldsymbol{\beta}) = (Y - X_k\theta - X_{-k}^\top \boldsymbol{\beta})(X_k - r_{XX_{-k}} X_{-k}), \tag{7}$$

with $r_{XX_{-k}} = \mathbb{E}[X_k {X_{-k}}^\top]\mathbb{E}[X_{-k}{X_{-k}}^\top]^{-1}$*, follows the Neyman orthogonality condition for the estimation of* θ *with nuisance parameters* $\boldsymbol{\eta} = (\beta, \boldsymbol{\gamma})$ *which reads*

$$\mathbb{E}\left[(Y - X_k\theta - {X_{-k}}^\top\boldsymbol{\beta})(X_k - r_{XX_{-k}}X_{-k})\right] = 0\,.$$

Please refer to Appendix A.2 for the proof. Comparing the score in Equation (7) with the score in Equation (4), there are two takeaways from Proposition 2: (i) the orthogonality condition remains invariant irrespective of the causal direction between X_k and Z, and (ii) the second term in Proposition 2 replaces function m by the (unbiased) linear regression estimator for modelling all the relations; given that the relation between Z and Y is linear, even if relationships between Z and X_k are non-linear (See Appendix B for concrete examples). Combining with the Double ML theoretical results (Chernozhukov et al., 2018a), this suggests that regularized predictors based on Lasso or ridge regression are tools of choice for fitting functions (m, g).

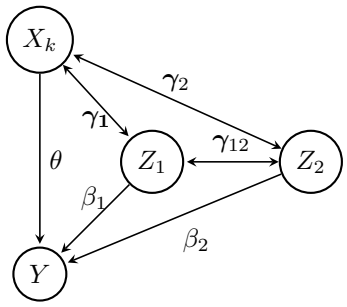

Figure 2: A generic example of identification of a causal effect θ in the presence of causal and anti-causal interactions between the causal predictor and other putative parents, and possibly arbitrary cyclic and nonlinear assignments for all nodes except Y (see Proposition 2). We have $X_{-k} = Z_1 \cup Z_2$.

2.4 Statistical Test

Now that we have illustrated and justified the fitting procedure of our algorithm, we provide a theoretically grounded statistical decision criterion for the direct causes after the model has been fitted. Consider (Y, X), $Y \in \mathbb{R}$, $X \in \mathbb{R}^d$, satisfying

$$Y = \langle \theta, X \rangle + U, \tag{8}$$

$$E(Y^2) < \infty,\ E(U^2) < \infty,\ E(U) = 0, E(U \mid X_j) = 0, \quad \forall j,\ \text{and } E(\|X\|_2^2) < \infty, \tag{9}$$

$$E\left[(X_j - E(X_j \mid X_{-j}))^2\right] \neq 0, \quad \text{for all } j \in \{1, \ldots, p\}. \tag{10}$$

where U is an exogenous variable and X_{-j} represents all the variables except X_j. The assumptions made with the above formulation are standard in the orthogonal machine learning literature (Rotnitzky et al., 2019; Smucler et al., 2019; Chernozhukov et al., 2018). Let us define the quantity $\chi_j = E\left[(Y - E(Y \mid X_{-j}))\,(X_j - E(X_j \mid X_{-j}))\right]$ for $j \in \{1, \cdots, d\}$, which is the expected conditional covariance of X_j given X_{-j}.

Proposition 3. *Let* $PA_Y = \{j \in \{1, \ldots, p\} : \theta_j \neq 0\}$*. For each* $j \in \{1, \ldots, p\}$ *let* X_{-j} *be the vector equals to* X *but excluding coordinate* j *and define* θ_{-j} *similarly. Define for* $j \in \{1, \ldots, p\}$

$$\chi_j = \mathbb{E}\left[(Y - \mathbb{E}(Y \mid X_{-j}))\,(X_j - \mathbb{E}(X_j \mid X_{-j}))\right],$$

which also has the double robustness property (Chernozhukov et al., 2018; Rotnitzky et al., 2019) then under the conditions given in Equations (8) *to* (10)*,*

a) If $j \in PA_Y$ *then* $\chi_j = \theta_j \mathbb{E}\left[(X_j - \mathbb{E}(X_j \mid X_{-j}))^2\right]$.

b) If $j \notin PA_Y$ *then* $\chi_j = 0$.

c) We also have (with notations of Prop. 2) $\chi_j = \mathbb{E}\left[(Y - \mathbb{E}(Y \mid X_{-j}))\left(X_j - r_{XX_{-k}}X_{-j}\right)\right]$.

Proof. Take $j \in PA_Y$. Then, from Equation (8)

$$\begin{aligned}
\mathbb{E}(Y \mid X_{-j}) &= \mathbb{E}(\langle \theta, X \rangle \mid X_{-j}) + \mathbb{E}(U \mid X_{-j}) = \mathbb{E}(\langle \theta_{-j}, X_{-j} \rangle \mid X_{-j}) + \theta_j \mathbb{E}(X_j \mid X_{-j}) \\
&= \langle \theta_{-j}, X_{-j} \rangle + \theta_j \mathbb{E}(X_j \mid X_{-j}) = \langle \theta, X \rangle - \theta_j X_j + \theta_j \mathbb{E}(X_j \mid X_{-j}) \\
&= Y - U - \theta_j (X_j - \mathbb{E}(X_j \mid X_{-j})).
\end{aligned}$$

Thus

$$\begin{aligned}\chi_j &= \mathbb{E}\left[(U + \theta_j(X_j - \mathbb{E}(X_j \mid X_{-j})))\,(X_j - \mathbb{E}(X_j \mid X_{-j})\right] \\ &= \mathbb{E}\left[U(X_j - \mathbb{E}(X_j \mid X_{-j})\right] + \theta_j \mathbb{E}\left[(X_j - \mathbb{E}(X_j \mid X_{-j})^2\right] \\ &= \theta_j \mathbb{E}\left[(X_j - \mathbb{E}(X_j \mid X_{-j})^2\right].\end{aligned}$$

Now take $j \notin PA_Y$. Then

$$\mathbb{E}(Y \mid X_{-j}) = \mathbb{E}(\langle \theta, X\rangle \mid X_{-j}) + \mathbb{E}(U \mid X_{-j}) = \langle \theta, X\rangle.$$

Thus, $\chi_j = \mathbb{E}\left[U(X_j - \mathbb{E}(X_j \mid X_{-j}))\right] = 0$.
For c), we rewrite

$$\begin{aligned}\chi_j &= \mathbb{E}\left[(Y - \mathbb{E}(Y \mid X_{-j}))\left(X_j - r_{XX_{-k}}X_{-j}\right)\right] \\ &+ \mathbb{E}\left[(Y - \mathbb{E}(Y \mid X_{-j}))\left(r_{XX_{-k}}X_{-j} - \mathbb{E}(X_j \mid X_{-j})\right)\right].\end{aligned}$$

Let $\mathcal{G}$ the sub-sigma algebra generated by X_{-j}, under our assumptions, $\mathbb{E}(Y|X_{-j})$ is the orthogonal projection of Y on the subspace of $\mathcal{G}$-measurable square integrable RV's $L^2(\Omega, \mathcal{G})$, so $Y - \mathbb{E}(Y|X_{-j})$ is orthogonal to any elements of $L^2(\Omega, \mathcal{G})$. Noticing that $\left(r_{XX_{-k}}X_{-j} - \mathbb{E}(X_j \mid X_{-j})\right)$ is an element of $L^2(\Omega, \mathcal{G})$, the second right-hand side term of the above equation vanishes and we get the result. □

There are two main implications of the results provided in Proposition 3. (i) χ_j is non-zero only for direct causal parents of the outcome variable, and χ_j has double robustness property as shown in (Rotnitzky et al., 2019; Smucler et al., 2019; Chernozhukov et al., 2018). Having double robustness property means that while computing the empirical version of the χ_j which we denote as $\hat{\chi}_j$, one can use regularized methods like ridge regression or Lasso to estimate the conditional expectation (function m). Afterward, one can perform statistical tests on top of it to decide between zero or non-zero tests. (ii) In line with the above orthogonal score results, we see that this quantity can be estimated using linear (unbiased) regression to fit the function m, although interactions between features may be non-linear.

Next, we discuss the variance of our estimator so that later a statistical test can be used to differentiate between zero and non-zero test. For the sake of convenience, the case of 2 partitions ($K = 2$)[1] is explained here.

Variance of Empirical Estimates of χ_j: Suppose we have n i.i.d. observations indicated by $\mathcal{D}_n = \{(X_i, Y_i), i = 1 \ldots, n\}$. Randomly split the data in two halves, say $\mathcal{D}_{n1}$ and $\mathcal{D}_{n2}$. Take $j \in \{1, \ldots, p\}$. For $k = 1$ let $\overline{k} = 2$, for $k = 2$ let $\overline{k} = 1$. For $k = 1, 2$, compute estimates of $\widehat{\mathbb{E}}^{\overline{k}}(Y \mid X_{-j})$ and $\widehat{\mathbb{E}}^{\overline{k}}(X_j \mid X_{-j})$ using the data in sample $\overline{k}$. Computing $\widehat{\mathbb{E}}^{\overline{k}}(Y \mid X_{-j})$ and $\widehat{\mathbb{E}}^{\overline{k}}(X_j \mid X_{-j})$ can be considered as regularized regression problems. We use Lasso as the estimator for conditional expectation (Equation (12)) in the experiments. Now, we compute the empirical estimates of χ_j. Let,

$$\begin{aligned}\widehat{\chi}_j^k = \mathbb{P}_{nk}\Big[&-Y\widehat{\mathbb{E}}^{\overline{k}}(X_j \mid X_{-j}) - X_j\widehat{\mathbb{E}}^{\overline{k}}(Y \mid X_{-j}) \\ &+\widehat{\mathbb{E}}^{\overline{k}}(Y \mid X_{-j})\,\widehat{\mathbb{E}}^{\overline{k}}(X_j \mid X_{-j}) + YX_j\Big].\end{aligned}$$

and

$$\begin{aligned}\left(\widehat{\sigma}_j^k\right)^2 = \mathbb{P}_{nk}\Big[\Big(&-Y\widehat{\mathbb{E}}^{\overline{k}}(X_j \mid X_{-j}) - X_j\widehat{\mathbb{E}}^{\overline{k}}(Y \mid X_{-j}) \\ &+\widehat{\mathbb{E}}^{\overline{k}}(Y \mid X_{-j})\,\widehat{\mathbb{E}}^{\overline{k}}(X_j \mid X_{-j}) + YX_j - \widehat{\chi}_j^k\Big)^2\Big].\end{aligned} \tag{11}$$

$\mathbb{P}_{nk}$ here denotes the empirical average and $\widehat{\sigma}_j^k$ denotes the empirical variance of χ_j. Finally, let

$$\widehat{\chi}_j = \frac{\widehat{\chi}_1 + \widehat{\chi}_2}{2}, \quad \widehat{\sigma}_j^2 = \frac{\left(\widehat{\sigma}_j^1\right)^2 + \left(\widehat{\sigma}_j^2\right)^2}{2}.$$

[1]Extension to arbitrary number of data partitions ($K \geq 2$) is straightforward. Check Algorithm 1.

Theorem 1 of (Smucler et al., 2019) provides conditions under which (see also (Chernozhukov et al., 2018)), when the estimators

$$\widehat{\mathbb{E}}^{\overline{k}}\left(Y \mid X_{-j}\right) \quad \text{and} \quad \widehat{\mathbb{E}}^{\overline{k}}\left(X_j \mid X_{-j}\right) \tag{12}$$

are Lasso-type regularized linear regressions, it holds that asymptotically $\widehat{\chi}_j \approx N\left(\chi_j, \frac{\widehat{\sigma}_j^2}{n}\right)$.

In this case, the test that rejects $\chi_j = 0$ when $|\widehat{\chi}_j| \geq 1.96\frac{\widehat{\sigma}_j}{\sqrt{n}}$ will have approximately 95% confidence level. The probability of rejecting the null when it is false is

$$P\left(|\widehat{\chi}_j| \geq 1.96\frac{\widehat{\sigma}_j}{\sqrt{n}}\right) \geq P\left(|\widehat{\chi}_j - \chi_j| \leq |\chi_j| - 1.96\frac{\widehat{\sigma}_j}{\sqrt{n}}\right) \to 1.$$

In order to account for multiple testing, we use Bonferroni correction.

Comments about Estimator: In this paper, we use Lasso for the nuisance parameter estimation as the variance of the conditional covariance is known (Smucler et al., 2019). One can also use other estimators instead, assuming one obtains a reasonable enough estimate of the nuisance parameter (up to $N^{-1/4}$-neighbourhood (Chernozhukov et al., 2018a)) with the correct variance term, which is beyond the scope of this paper.

Conditional Independence Tests: Asymptotically, the conditional independence testing between Y and X_j given X_{-j} is also a possible solution for our proposed approach. Indeed, d-separation rules imply that true causes are conditionally dependent according to this test, while non-causes are conditionally independent (because X_{-j} is not a collider under our NFD assumption). However, conditional independence testing is challenging in high-dimensional/non-linear settings. Kernel-based conditional independence testing is computationally expensive (Zhang et al., 2012). We used χ_j in the paper because it was already known from previous works (Smucler et al., 2019; Chernozhukov et al., 2018b) that it has double robustness property, which means one can use regularized methods like Lasso to estimate empirical conditional expectation from a finite number of samples and the empirical estimator is still unbiased with controlled variance. Our work is related to the recent work of (Shah & Peters, 2020), which proposes a conditional independence test whose proofs rely heavily on (Chernozhukov et al., 2018a). In this paper, we use for the first time such double ML-based tests for the search problem.

3 Experiments

In this section, we perform extensive empirical evaluation for our method.

3.1 Experimental Setup

For every combination of number of nodes (#nodes), connectivity (p_s), noise level (σ^2), number of observations (z), and non-linear probability (p_n) (see Table C.1), 100 examples (DAGs) are generated and stored as csv files (altogether 72.000 DAGs are simulated, comprising a dataset of overall >10GB). For each DAG, z samples are generated. We provide more details about the parameters (#nodes, p_s, p_n and z) and data generation process in Appendix C.1. For future benchmarking, the generated files with the code will be made available later.

The baselines we compare our method against are: LiNGAM (Shimizu et al., 2006), order - independent PC (Colombo & Maathuis, 2014), rankPC, MMHC (Tsamardinos et al., 2006), GES (Chickering, 2003), rankGES, ARGES (adaptively restricted GES (Nandy et al., 2016)), rankARGES, FCI+ (Claassen et al., 2013), PCI (Shah & Peters, 2020), and Lasso (Tibshirani, 1996), which are suitable for observational data. The CompareCausalNetworks R Package[2] is used to run most of the baselines methods. We use 10-fold cross-validation to choose the parameters of all approaches. Recall, Fall-out, Critical Success Index, Accuracy, F1

[2] `https://cran.r-project.org/web/packages/CompareCausalNetworks/index.html`

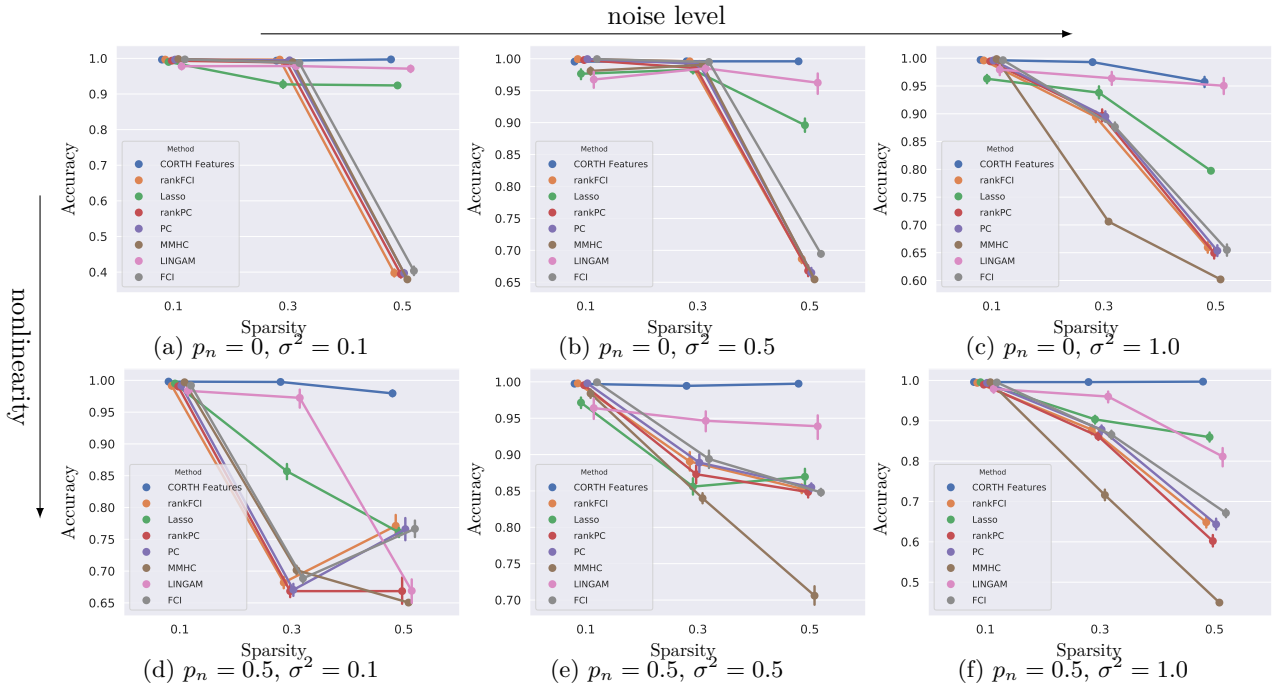

(a) $p_n = 0$, $\sigma^2 = 0.1$ (b) $p_n = 0$, $\sigma^2 = 0.5$ (c) $p_n = 0$, $\sigma^2 = 1.0$

(d) $p_n = 0.5$, $\sigma^2 = 0.1$ (e) $p_n = 0.5$, $\sigma^2 = 0.5$ (f) $p_n = 0.5$, $\sigma^2 = 1.0$

Figure 3: Overall performance for a single random DAG with 100 simulations for each setting, having 20 nodes and 500 observations.

Score, and Matthews correlation coefficient (Matthews, 1975) are considered as metrics for the evaluation. These metrics are described in Appendix C.2. As direction of the possible causes in the defined setting is determined, the non-directional edges inferred by some baselines, e.g., PC are evaluated as direct causes of the target variable.

Regression Technique and Hyperparameters: We use Lasso as the estimator of conditional expectation for our method because the variance bound for χ_j with Lasso type estimator of conditional expectation (Equation equation 12) is provided in Equation equation 11. Further, using more splits than 2 splits in the experiment relatively increases the performance of parameter estimation. Plots for parameter estimation are provided in Appendix E.

Method	Number of Nodes					
	10		20		50	
	ACC	F1	ACC	F1	ACC	F1
GES	0.85	0.78	0.74	0.53	0.70	0.32
rankGES	0.85	0.75	0.74	0.51	0.70	0.32
ARGES	0.80	0.58	0.75	0.52	0.71	0.22
rankARGES	0.79	0.57	0.75	0.51	0.71	0.22
FCI+	0.87	0.81	0.83	0.70	0.77	0.49
LINGAM	**0.95**	0.89	0.89	0.78	0.75	0.39
PC	0.86	0.79	0.82	0.66	0.76	0.46
rankPC	0.85	0.77	0.81	0.64	0.75	0.43
MMHC	0.84	0.74	0.77	0.51	0.73	0.28
PCI	0.92	0.87	0.88	0.78	0.77	0.49
Lasso	0.91	0.90	0.90	0.87	0.77	0.63
`CORTH Features`	**0.95**	**0.93**	**0.95**	**0.91**	**0.80**	**0.66**

Table 1: Performance across all the settings for different number of nodes (10,20 and 50). Each entry in the table is averaged over 18000 simulations.

3.2 Results

Results aggregated by the number of nodes (corresponding to 18000 simulations per entry in the table), connectivity level (corresponding to 24000 simulations per entry in the table), the number of observations over all simulations (corresponding to 24000 simulations per entry in the table) are illustrated in Tables 1 to 3 respectively[3]. Our method performs better than the competing baselines in terms of accuracy and F1 score, especially for more connected structures, despite data being generated according to DAG causal structures, which, dissimilar to our method, is an essen-

[3]Please refer to Appendix C.3 for thorough tables for all parameters.

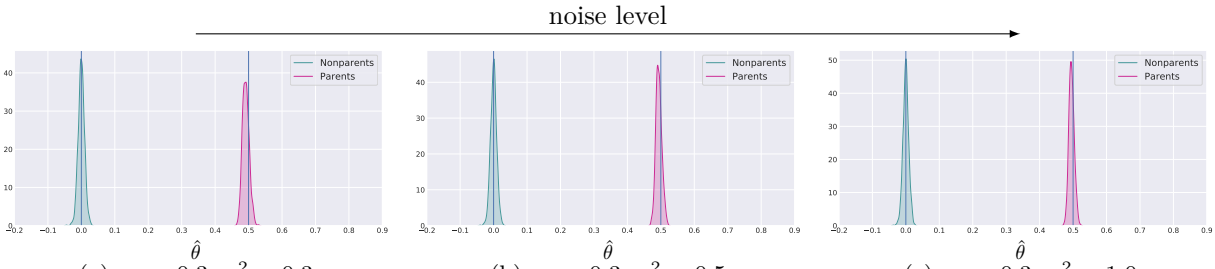

(a) $p_n = 0.3$, $\sigma^2 = 0.3$ (b) $p_n = 0.3$, $\sigma^2 = 0.5$ (c) $p_n = 0.3$, $\sigma^2 = 1.0$

Figure 4: Distribution of the estimated θ values for the true and false causal parents in 100 simulations of the graph with 20 nodes, 20000 observations and 0.3 as connectivity. The vertical lines indicate the ground truth values for the linear coefficients corresponding to causal parents.

tial condition for them. To provide a visual comparison, we plot the accuracy of all the methods w.r.t. the connectivity parameter (p_s) in Figure 3 for different values of p_n and σ^2 on 1800 samples.

It can be observed that the accuracies of the competing baselines significantly drop with increasing noise level and nonlinearity, while our method is more robust to them. More plots are given in Appendix F and Appendix G for several other combinations of varying parameters in the simulation. We also extensively compare all the metrics (Recall, Fall-out, Critical Success Index, Accuracy, F1 Score, and Matthews correlation coefficient) for all the methods in Appendix C.3. According to these metrics, our approach performs better than baselines in most cases regardless of the set of parameters used for generating data. Our method shows in particular stability in performance w.r.t. the number of nodes (Table C.3), partially non-linear relationships (Table C.4), connectivity (table C.2), number of observations (table C.6), and noise level (table C.5). We also show the plot of parameter estimation for direct causal parents vs. non-causal parents in Figure 4. In the plots and tables, we denote our approach as `CORTH Features`.

Method	Connectivity					
	0.1		0.3		0.5	
	ACC	F1	ACC	F1	ACC	F1
GES	0.961	0.825	0.815	0.598	0.646	0.482
rankGES	0.954	0.790	0.809	0.584	0.642	0.475
ARGES	0.965	0.828	0.805	0.501	0.612	0.330
rankARGES	0.959	0.801	0.802	0.494	0.611	0.328
FCI+	0.974	0.853	0.866	0.714	0.734	0.629
LINGAM	0.966	0.796	0.896	0.753	0.827	0.727
PC	0.975	0.849	0.861	0.689	0.718	0.588
rankPC	0.971	0.831	0.852	0.670	0.701	0.560
MMHC	0.978	0.867	0.830	0.561	0.639	0.397
PCI	0.986	0.920	0.906	0.759	0.783	0.661
Lasso	0.976	0.925	0.876	0.811	0.800	0.778
`CORTH Features`	**0.988**	**0.934**	**0.926**	**0.858**	**0.847**	**0.814**

Table 2: Performance across all the settings for different sparsities. Each single entry in the table is averaged over 24000 simulations. Our method is almost state of the art in every case.

3.3 Scaling Causal Inference to Large Graphs

Figure 5 shows the runtime of the method in seconds as a function of the graph's size. Notice that the runtime of our algorithm in the log-log plot is roughly linear, supporting our above statement about the computational time being polynomial in d. Since we used 5000 observations, any additional overhead is coming from cross-validation.

Method	Number of Observations					
	100		500		1000	
	ACC	F1	ACC	F1	ACC	F1
GES	0.797	0.588	0.811	0.650	0.815	0.666
rankGES	0.788	0.561	0.806	0.636	0.810	0.652
ARGES	0.780	0.489	0.799	0.576	0.803	0.595
rankARGES	0.776	0.473	0.795	0.566	0.800	0.584
FCI+	0.837	0.671	0.865	0.755	0.871	0.771
LINGAM	0.840	0.650	0.908	0.743	0.941	0.883
PC	0.830	0.642	0.858	0.732	0.866	0.752
rankPC	0.821	0.617	0.849	0.711	0.855	0.733
MMHC	0.800	0.557	0.820	0.625	0.826	0.642
PCI	0.829	0.594	0.914	0.853	0.931	0.893
Lasso	0.870	**0.812**	0.889	0.848	0.893	0.854
`CORTH Features`	**0.883**	0.78	**0.935**	**0.906**	**0.942**	**0.920**

Table 3: Performance across all the settings for different number of observations. Each single entry in the table is averaged over 24000 simulations. Our method is almost state of the art in every case.

3.4 Real-World Data

We also apply our algorithm to a recent COVID-19 Dataset (Einstein, 2020) where the task is to predict COVID-19 cases (confirmed using RT-PCR) amongst suspected ones. For an existing and exten-

sive analysis of the dataset with predictive methods, we refer to Schwab et al. (2020). We apply our algorithm to discover the features which directly cause the diagnosed infection. We found that the following were the most common causes across different runs of our approach: Patient age quantile, Arterial Lactic Acid, Promyelocytes, and Base excess venous blood gas analysis. Lacking medical ground truth, we report these not as corroboration of our approach but rather as a potential contribution to causal discovery in this challenging problem. It is encouraging that some of these variables are consistent with other studies Schwab et al. (2020). Details on data preprocessing and more results are available in Appendix D.

4 Discussion

A recent empirical evaluation of different causal discovery methods highlighted the desirability of more efficient search algorithms (Heinze-Deml et al., 2018). In the present work, we provide identifiability results for the set of direct causal parents, including the case of partially nonlinear cyclic models, as well as a highly efficient algorithm that scales well w.r.t. the number of variables and exhibits state-of-the-art performance across extensive experiments. Our approach builds on the Double ML method for the partial regression setting of Chernozhukov et al. (2018a); however, we show it can be applied to different underlying causal structures, which is the key for the purpose of search, as this structure is not always known in advance. Whilst not amounting to full causal graph discovery, identification of causal parents is of major interest in real-world applications, e.g., when assaying the causal influence of genes on the phenotype. A natural direction worth exploring is to extend this approach for discovering direct causal parents in the case when nonlinear relationships exist between the output variable and its direct causal parents.

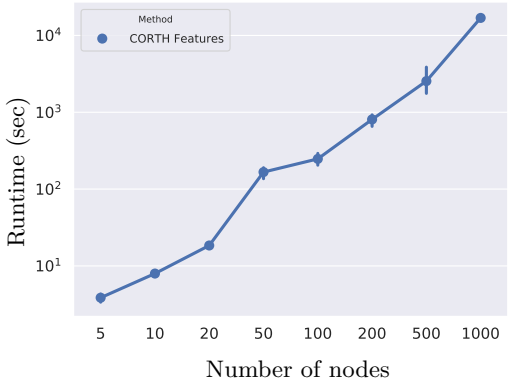

Figure 5: Runtime as a function of the number of variables for 10 simulations per number of nodes. In these simulations connectivity, number of observations, nonlinaer prob., and noise level are set to 0.3, 5000, 0, and 1 respectively.

References

Ossama Ahmed, Frederik Träuble, Anirudh Goyal, Alexander Neitz, Yoshua Bengio, Bernhard Schölkopf, Manuel Wüthrich, and Stefan Bauer. Causalworld: A robotic manipulation benchmark for causal structure and transfer learning. *arXiv preprint arXiv:2010.04296*, 2020.

Joshua D Angrist and Guido W Imbens. Identification and estimation of local average treatment effects. Technical report, National Bureau of Economic Research, 1995.

Joshua D Angrist, Guido W Imbens, and Donald B Rubin. Identification of causal effects using instrumental variables. *Journal of the American statistical Association*, 91(434):444–455, 1996.

Reuben M Baron and David A Kenny. The moderator–mediator variable distinction in social psychological research: Conceptual, strategic, and statistical considerations. *Journal of personality and social psychology*, 51(6), 1986.

Kenneth A Bollen. *Structural equations with latent variables*, volume 210. John Wiley & Sons, 1989.

Stephan Bongers, Jonas Peters, Bernhard Schölkopf, and Joris M Mooij. Theoretical aspects of cyclic structural causal models. *arXiv preprint arXiv:1611.06221*, 2016.

Stephan Bongers, Patrick Forré, Jonas Peters, and Joris M Mooij. Foundations of structural causal models with cycles and latent variables. *The Annals of Statistics*, 49(5):2885–2915, 2021.

Roger J Bowden and Darrell A Turkington. *Instrumental variables*, volume 8. Cambridge university press, 1990.

Carlos Brito and Judea Pearl. Generalized instrumental variables. *arXiv preprint arXiv:1301.0560*, 2012.

Daniel C Castro, Ian Walker, and Ben Glocker. Causality matters in medical imaging. *Nature Communications*, 11(1):1–10, 2020.

Gavin C Cawley. Causal & non-causal feature selection for ridge regression. In *Causation and Prediction Challenge*, 2008.

Victor Chernozhukov, Denis Chetverikov, Mert Demirer, Esther Duflo, Christian Hansen, Whitney Newey, and James Robins. Double/debiased machine learning for treatment and structural parameters, 2018a.

Victor Chernozhukov, Whitney Newey, and James Robins. Double/de-biased machine learning using regularized riesz representers. *arXiv preprint arXiv:1802.08667*, 2018b.

Victor Chernozhukov, Whitney K. Newey, and Rahul Singh. Learning L2 Continuous Regression Functionals via Regularized Riesz Representers. *arXiv preprint arXiv:1809.05224*, Sep 2018.

David Maxwell Chickering. Optimal structure identification with greedy search. *J. Mach. Learn. Res.*, 3 (null):507–554, March 2003. ISSN 1532-4435. doi: 10.1162/153244303321897717. URL `https://doi.org/10.1162/153244303321897717`.

Tom Claassen, Joris M. Mooij, and Tom Heskes. Learning sparse causal models is not np-hard. In *Proceedings of the Twenty-Ninth Conference on Uncertainty in Artificial Intelligence*, UAI'13, pp. 172–181, Arlington, Virginia, USA, 2013. AUAI Press.

Diego Colombo and Marloes H. Maathuis. Order-independent constraint-based causal structure learning. *Journal of Machine Learning Research*, 15(116):3921–3962, 2014. URL `http://jmlr.org/papers/v15/colombo14a.html`.

Hospital Israelita Albert Einstein. Diagnosis of COVID-19 and its clinical spectrum, 2020. https://www.kaggle.com/einsteindata4u/covid19.

Patrick Forré and Joris M Mooij. Markov properties for graphical models with cycles and latent variables. *arXiv preprint arXiv:1710.08775*, 2017.

AmirEmad Ghassami, Saber Salehkaleybar, Negar Kiyavash, and Kun Zhang. Learning causal structures using regression invariance. In *Advances in Neural Information Processing Systems*, pp. 3011–3021, 2017.

Isabelle Guyon and Constantin Aliferis. Causal feature selection. In *Computational methods of feature selection*. Chapman and Hall/CRC, 2007.

Andrew F Hayes. *Introduction to mediation, moderation, and conditional process analysis: A regression-based approach*. Guilford publications, 2017.

Christina Heinze-Deml, Marloes H Maathuis, and Nicolai Meinshausen. Causal structure learning. *Annual Review of Statistics and Its Application*, 5:371–391, 2018.

Patrik O Hoyer, Dominik Janzing, Joris M Mooij, Jonas Peters, and Bernhard Schölkopf. Nonlinear causal discovery with additive noise models. In *Advances in neural information processing systems*, pp. 689–696, 2009.

Dominik Janzing. Causal regularization. In *Advances in Neural Information Processing Systems*, 2019.

Adel Javanmard and Andrea Montanari. Confidence intervals and hypothesis testing for high-dimensional regression. *The Journal of Machine Learning Research*, 15(1), 2014.

Adel Javanmard and Andreas Montanari. Debiasing the lasso: Optimal sample size for gaussian designs. *The Annals of Statistics*, 46(6A), 2018.

Gustavo Lacerda, Peter L Spirtes, Joseph Ramsey, and Patrik O Hoyer. Discovering cyclic causal models by independent components analysis. *arXiv preprint arXiv:1206.3273*, 2012.

Atalanti Mastakouri, Bernhard Schölkopf, and Dominik Janzing. Selecting causal brain features with a single conditional independence test per feature. In *Advances in Neural Information Processing Systems 32*, pp. 12532–12543, 2019.

Brian W Matthews. Comparison of the predicted and observed secondary structure of t4 phage lysozyme. *Biochimica et Biophysica Acta (BBA)-Protein Structure*, 405(2):442–451, 1975.

Nicolai Meinshausen, Alain Hauser, Joris M Mooij, Jonas Peters, Philip Versteeg, and Peter Bühlmann. Methods for causal inference from gene perturbation experiments and validation. *Proceedings of the National Academy of Sciences*, 113(27):7361–7368, 2016.

Preetam Nandy, Alain Hauser, and Marloes Maathuis. High-dimensional consistency in score-based and hybrid structure learning. *Annals of Statistics*, 46, 03 2016. doi: 10.1214/17-AOS1654.

Yu Nesterov. Efficiency of coordinate descent methods on huge-scale optimization problems. *SIAM Journal on Optimization*, 22(2):341–362, 2012.

Jerzy Neyman. C (α) tests and their use. *Sankhyā: The Indian Journal of Statistics, Series A*, 1979.

Michael Paul. Feature selection as causal inference: Experiments with text classification. In *Proceedings of the 21st Conference on Computational Natural Language Learning (CoNLL 2017)*, pp. 163–172, 2017.

Judea Pearl. *Causality*. Cambridge university press, 2009.

Jonas Peters, Joris Mooij, Dominik Janzing, and Bernhard Schölkopf. Identifiability of causal graphs using functional models. In *Proceedings of the 27th Annual Conference on Uncertainty in Artificial Intelligence (UAI)*, pp. 589–598, 2011.

Jonas Peters, Joris M Mooij, Dominik Janzing, and Bernhard Schölkopf. Causal discovery with continuous additive noise models. *The Journal of Machine Learning Research*, 15(1):2009–2053, 2014.

Jonas Peters, Peter Bühlmann, and Nicolai Meinshausen. Causal inference by using invariant prediction: identification and confidence intervals. *Journal of the Royal Statistical Society: Series B (Statistical Methodology)*, 78(5):947–1012, 2016.

Jonas Peters, Dominik Janzing, and Bernhard Schölkopf. *Elements of causal inference: foundations and learning algorithms*. MIT press, 2017.

Dominik Rothenhäusler, Christina Heinze, Jonas Peters, and Nicolai Meinshausen. Backshift: Learning causal cyclic graphs from unknown shift interventions. *Advances in Neural Information Processing Systems*, 28, 2015.

Andrea Rotnitzky et al. Characterization of parameters with a mixed bias property. *arXiv preprint arXiv:1904.03725*, 2019.

Jakob Runge, Sebastian Bathiany, Erik Bollt, Gustau Camps-Valls, Dim Coumou, Ethan Deyle, Clark Glymour, Marlene Kretschmer, Miguel D Mahecha, Jordi Muñoz-Marí, et al. Inferring causation from time series in earth system sciences. *Nature communications*, 10(1):1–13, 2019.

Karen Sachs, Omar Perez, Dana Pe'er, Douglas A Lauffenburger, and Garry P Nolan. Causal protein-signaling networks derived from multiparameter single-cell data. *Science*, 308(5721):523–529, 2005.

Ruben Sanchez-Romero, Joseph D Ramsey, Kun Zhang, Madelyn RK Glymour, Biwei Huang, and Clark Glymour. Estimating feedforward and feedback effective connections from fmri time series: Assessments of statistical methods. *Network Neuroscience*, 3(2):274–306, 2019.

Patrick Schwab, August DuMont Schütte, Benedikt Dietz, and Stefan Bauer. predcovid-19: A systematic study of clinical predictive models for coronavirus disease 2019. *arXiv preprint arXiv:2005.08302*, 2020.

Rajen D Shah and Jonas Peters. The hardness of conditional independence testing and the generalised covariance measure. *The Annals of Statistics*, 48(3):1514–1538, 2020.

Shohei Shimizu, Patrik O Hoyer, Aapo Hyvärinen, and Antti Kerminen. A linear non-gaussian acyclic model for causal discovery. *Journal of Machine Learning Research*, 7(Oct):2003–2030, 2006.

Patrick E Shrout and Niall Bolger. Mediation in experimental and nonexperimental studies: new procedures and recommendations. *Psychological methods*, 7(4), 2002.

Ezequiel Smucler, Andrea Rotnitzky, and James M Robins. A unifying approach for doubly-robust ℓ_1 regularized estimation of causal contrasts. Technical report, 2019.

Peter Spirtes, Clark N Glymour, Richard Scheines, and David Heckerman. *Causation, prediction, and search*. MIT press, 2000.

Robert Tibshirani. Regression shrinkage and others. *Journal of the Royal Statistical Society: Series B (Methodological)*, 58(1):267–288, 1996.

Ryan Tibshirani and Larry Wasserman. Sparsity, the lasso, and friends, 2017.

Ioannis Tsamardinos, Laura Brown, and Constantin Aliferis. The max-min hill-climbing bayesian network structure learning algorithm. *Machine Learning*, 65:31–78, 10 2006. doi: 10.1007/s10994-006-6889-7.

Benito Van der Zander and Maciej Liskiewicz. On searching for generalized instrumental variables. In *AISTATS*, pp. 1214–1222, 2016.

Jonathan Warrell and Mark Gerstein. Cyclic and multilevel causation in evolutionary processes. *Biology & Philosophy*, 35(5):1–36, 2020.

Shun Yao, Shinjae Yoo, and Dantong Yu. Prior knowledge driven granger causality analysis on gene regulatory network discovery. *BMC bioinformatics*, 16(1):1–18, 2015.

Kui Yu, Lin Liu, and Jiuyong Li. A unified view of causal and non-causal feature selection. *arXiv preprint arXiv:1802.05844*, 2018.

Cun-Hui Zhang and Stephanie S Zhang. Confidence intervals for low dimensional parameters in high dimensional linear models. *Journal of the Royal Statistical Society: Series B (Statistical Methodology)*, 76(1), 2014.

Kun Zhang, Jonas Peters, Dominik Janzing, and Bernhard Schölkopf. Kernel-based conditional independence test and application in causal discovery. *arXiv preprint arXiv:1202.3775*, 2012.

Xun Zheng, Bryon Aragam, Pradeep K Ravikumar, and Eric P Xing. Dags with no tears: Continuous optimization for structure learning. In *Advances in Neural Information Processing Systems*, pp. 9472–9483, 2018.

A Causal Discovery via Orthogonalization

A.1 Example 1

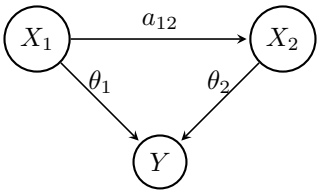

Figure A.1: An example with linear structural equations.

Proof of Example 1 . Let us start from the easier case first (See Figure A.1) . Let us first try to estimate the coefficient of interaction between X_2 and Y but it is also very clear that the estimation of θ_2 will be unbiased as the given setting precisely match with the double machine learning setting. However, we will see in this example that given the population, θ_1 can be approximated as well. Let us write down the structural equation model first:

$$\begin{aligned} Y &:= \theta_1 X_1 + \theta_2 X_2 + \varepsilon_3 \\ X_2 &:= a_{12} X_1 + \varepsilon_2 \\ X_1 &:= \varepsilon_1. \end{aligned} \tag{13}$$

From the set of equations we have:

$$X_1 = a_{12}^{-1} X_2 - a_{12}^{-1} \varepsilon_2.$$

Let also denote $\mathbb{E}[\varepsilon_1^2] = \sigma_1^2$ and $\mathbb{E}[\varepsilon_2^2] = \sigma_2^2$. Hence, $\mathbb{E}[X_1^2] = \sigma_1^2$, $\mathbb{E}[X_1 X_2] = a_{12}\sigma_1^2$ and $\mathbb{E}[X_2^2] = a_{12}\mathbb{E}[X_1 X_2] + \mathbb{E}[\varepsilon_2 X_2] = a_{12}^2\sigma_1^2 + \sigma_2^2$.. Let us first try to find the regression co-efficient of fitting X_2 on Y.

$$Y = \hat{\theta}_2 X_2 + \eta_1.$$

Hence, $\hat{\theta}_2 = \frac{\mathbb{E}[X_2 Y]}{\mathbb{E}[X_2^2]}$ if η is independent of X_2.

$$\hat{\theta}_2 = \frac{\mathbb{E}[X_2 Y]}{\mathbb{E}[X_2^2]} = \frac{\mathbb{E}[X_2(\theta_1 X_1 + \theta_2 X_2 + \varepsilon_3)]}{\mathbb{E}[X_2^2]} = \theta_2 + \theta_1 a_{12} \frac{\sigma_1^2}{\sigma_2^2 + a_{12}^2 \sigma_1^2}. \tag{14}$$

Similarly, if we fit X_2 on X_1 then

$$X_1 = \hat{a}_{12}^{-1} X_2 + \eta_2,$$

then $\hat{a}_{12}^{-1} = \frac{\mathbb{E}[X_1 X_2]}{\mathbb{E}[X_2^2]}$. However $\mathbb{E}[X_1 X_2]$ can also be written as following:

$$\mathbb{E}[X_1 X_2] = a_{12}^{-1}\mathbb{E}[X_2^2] - a_{12}^{-1}\mathbb{E}[\varepsilon_2 X_2].$$

Hence,

$$\hat{a}_{12}^{-1} = a_{12}^{-1}\left(1 - \frac{\sigma_2^2}{\sigma_2^2 + a_{12}^2\sigma_1^2}\right) = a_{12}^{-1}\left(\frac{a_{12}^2\sigma_1^2}{\sigma_2^2 + a_{12}^2\sigma_1^2}\right).$$

Residual $\hat{V} = X_1 - \hat{a}_{12}^{-1} X_2$. Hence we can have

$$\mathbb{E}(\hat{V} X_1) = \mathbb{E}[X_1^2] - \hat{a}_{12}^{-1}\mathbb{E}[X_1 X_2] = \mathbb{E}[\varepsilon_1^2] - \hat{a}_{12}^{-1} a_{12}\mathbb{E}[\varepsilon_1^2] = \frac{\sigma_1^2\sigma_2^2}{\sigma_2^2 + a_{12}^2\sigma_1^2}.$$

We now calculate,

$$\begin{aligned}\mathbb{E}\left[\hat{V}(Y-\hat{\theta}_2 X_2)\right] &= \mathbb{E}\left[(X_1-\hat{a}_{12}^{-1}X_2)(Y-\hat{\theta}_2 X_2)\right] \\ &= \mathbb{E}\left[(X_1-\hat{a}_{12}^{-1}X_2)\big((\theta_2-\hat{\theta}_2)X_2+\theta_1 X_1+\varepsilon_3\big)\right] \\ &= (\theta_2-\hat{\theta}_2)a_{12}\sigma_1^2+\theta_1\sigma_1^2-\hat{a}_{12}^{-1}(\theta_2-\hat{\theta}_2)(\sigma_2^2+a_{12}^2\sigma_1^2)-\hat{a}_{12}^{-1}\theta_1 a_{12}\sigma_1^2 \\ &= \frac{\theta_1\sigma_1^2\sigma_2^2}{\sigma_2^2+a_{12}^2\sigma_1^2}.\end{aligned}$$

Last equation was written after a step of minor calculation. Since the estimator is

$$\hat{\theta}_1 = \left[\mathbb{E}(\hat{V}X_1)\right]^{-1}\mathbb{E}\left[\hat{V}(Y-\hat{\theta}_2 X_2)\right] = \theta_1.$$

□

A.2 Influence of the interactions between parents

In this section, we use a generic example shown in Figure 2 which we show again in Figure A.2 to illustrate the role of interactions between the covariates on the proposed causal discovery algorithm.

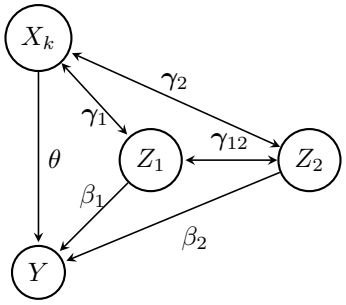

Figure A.2: A generic example of identification of a causal effect θ in the presence of causal and anti-causal interactions between the causal predictor and other putative parents, and possibly arbitrary cyclic and nonlinear assignments for all nodes except Y (see Proposition 2). We have $X_{-k} = Z_1 \cup Z_2$.

The estimator discussed can simply be derived from the Neyman orthogonality condition. We now provide the below the proof for Proposition 2. For the sake of completeness, we also rewrite the statement of the proposition again.

Proposition 4 (**Restatement of Proposition 2**). *Assume the partially linear Gaussian model of Fig. A.2, denote $X_{-k} = [Z_1^\top, Z_2^\top]^\top$ the control variables, $\boldsymbol{\gamma} = (\boldsymbol{\gamma}_1, \boldsymbol{\gamma}_2, \boldsymbol{\gamma}_{12})$ the parameter vector of the (possibly non-linear) assignments between putative parents of Y, and $\boldsymbol{\beta} = (\boldsymbol{\beta}_1, \boldsymbol{\beta}_2)$ the vector of causal coefficients for encoding linear effects of X_{-k} on outcome Y. Then, independently from the $\boldsymbol{\gamma}$ parameters and of the functional form of the associated assignments between parents of Y, the score*

$$\psi(W;\theta,\boldsymbol{\beta}) = (Y - X_k\theta - X_{-k}^\top\boldsymbol{\beta})(X_k - r_{XX_{-k}}X_{-k})\,, \tag{15}$$

with $r_{XX_{-k}} = \mathbb{E}[X_k {X_{-k}}^\top]\mathbb{E}[X_{-k}{X_{-k}}^\top]^{-1}$, follows the Neyman orthogonality condition for the estimation of θ with nuisance parameters $\boldsymbol{\eta} = (\beta, \boldsymbol{\gamma})$ which reads

$$\mathbb{E}\left[(Y - X_k\theta - {X_{-k}}^\top\boldsymbol{\beta})(X_k - \mathbb{E}[X_k {X_{-k}}^\top]\mathbb{E}[X_{-k}{X_{-k}}^\top]^{-1}X_{-k})\right] = 0\,. \tag{16}$$

Proof of Proposition 2. Using the global Markov factorization for simple SCMs[4] (Forré & Mooij, 2017; Bongers et al., 2021),

$$P(W;\theta,\boldsymbol{\eta}) = P(Y|X_{-k},X_K;\theta,\boldsymbol{\beta})P(X_{-k},X_K;\boldsymbol{\gamma}),$$

[4]The necessary condition for this statement to be true is uniquely solvability which is equivalent to not having self-cycles in the causal structure.

due to linearity and gaussianity of the assignment of Y, we obtain a negative log likelihood of the form (up to additive constants)

$$\ell(W;\theta,\boldsymbol{\eta}) = \frac{1}{2\sigma_Y^2}(Y - X_k\theta - {X_{-k}}^\top\boldsymbol{\beta})(Y - X_k\theta - {X_{-k}}^\top\boldsymbol{\beta}) + f(X_k, X_{-k};\boldsymbol{\gamma}).$$

where f stands for the negative log likelihood of the second factor. Following Chernozhukov et al. (2018a) [eq. (2.7)], this leads to the Neyman orthogonal score

$$\begin{aligned}\psi(W;\theta,\boldsymbol{\eta}) = \partial_\theta\ell(W;(\theta,\boldsymbol{\eta})) - \boldsymbol{\mu}\partial_\eta\ell(W;(\theta,\boldsymbol{\eta})) = -\frac{1}{\sigma_Y^2}(Y - X_k\theta - {X_{-k}}^\top\boldsymbol{\beta})X_k \\ - \boldsymbol{\mu}\left(-\frac{1}{\sigma_Y^2}(Y - X_k\theta - {X_{-k}}^\top\boldsymbol{\beta})X_{-k} + \partial_\gamma f(X_k, X_{-k};\gamma)\right).\end{aligned}$$

Following eq. (2.8) of the same paper, we derive the expression of $\boldsymbol{\mu}$ as

$$\boldsymbol{\mu} = J_{\theta,\eta}J_{\eta,\eta}^{-1},$$

with

$$J_{\eta,\eta} = \partial_{\eta^\top}\mathbb{E}\left[\partial_\eta\ell(W,\theta,\boldsymbol{\eta})\right] = \begin{bmatrix} \sigma_Y^{-2}\mathbb{E}\left[X_{-k}^\top X_{-k}\right] & 0 \\ 0 & \partial_{\gamma^\top}\mathbb{E}\left[\partial_\gamma f(X_k, X_{-k};\boldsymbol{\gamma})\right] \end{bmatrix},$$

and

$$J_{\theta,\eta} = \partial_{\eta^\top}\mathbb{E}\left[\partial_\theta\ell(W,\theta,\boldsymbol{\eta})\right] = \sigma_Y^{-2}\begin{bmatrix} \mathbb{E}\left[X_k^\top X_{-k}\right] & 0 \end{bmatrix},$$

resulting in

$$\boldsymbol{\mu} = \mathbb{E}\left[X_k^\top X_{-k}\right]\mathbb{E}\left[X_{-k}^\top X_{-k}\right]^{-1}.$$

Reintroducing $\boldsymbol{\mu}$ in the expression of ψ leads to the result. □

B Examples

The result discussed in Proposition 2 is not directly intuitive. In simple words, there are two takeaways from Proposition 2: (i) the orthogonality condition remains invariant irrespective of the causal direction between X_k and Z, and (ii) the second term in Equation (16) suggests to use a linear estimator for modeling all the relations, given that the relation between Z and Y is linear.
To generate more intuition, we provide a few examples. Let us go back again to the three variable interaction assuming the following structural equation model:

$$\begin{aligned} Y &:= \theta_1 X_1 + \theta_2 X_2 + \varepsilon_3 \\ X_2 &:= f(X_1) + \varepsilon_2 \\ X_1 &:= \varepsilon_1, \end{aligned} \tag{17}$$

where f is a nonlinear function and $\varepsilon_1, \varepsilon_2$ and ε_3 are zero mean Gaussian noises.

- Consider the case when $f(x) = x^2$. The goal is to estimate the parameter θ_1 which we call $\hat{\theta}_1$. We follow the standard double ML procedure assuming policy variable X_1 and control X_2, although the ground truth causal dependency $X_1 \to X_2$ in contradiction with such setting (see Equation (2)). The estimate of θ_2 following the double ML procedure, which we call $\hat{\theta}_2 = \frac{\mathbb{E}[X_2 Y]}{\mathbb{E}[X_2^2]} = \theta_2 + \theta_1\frac{\mathbb{E}[X_1 X_2]}{\mathbb{E}[X_2^2]}$. Similarly, we want to estimate $X_1 = \alpha X_2 + \eta$ from which we get, $\alpha = \frac{\mathbb{E}[X_1 X_2]}{\mathbb{E}[X_2]^2}$. It is easy to see that $\mathbb{E}[X_1 X_2] = \mathbb{E}[X_1^3] = 0$. Hence, $\alpha = 0$ and it is easy to see $\hat{\theta}_1 = \theta_1$.

- Consider now the more general case where f is any nonlinear function. As in the previously discussed example, the goal is to estimate θ_1. We have $\hat{\theta}_2 = \frac{\mathbb{E}[X_2 Y]}{\mathbb{E}[X_2^2]} = \theta_2 + \theta_1 \frac{\mathbb{E}[X_1 X_2]}{\mathbb{E}[X_2^2]}$. Similarly, $\alpha = \frac{\mathbb{E}[X_1 X_2]}{E[X_2^2]}$. We substitute these estimates into the orthogonality condition in Equation (16):

$$
\begin{aligned}
& \mathbb{E}\left[(Y - X_1\hat{\theta}_1 - X_2\hat{\theta_2})(X_1 - \alpha X_2)\right] = 0\,. \\
\Rightarrow\ & \mathbb{E}\left[\left(Y - X_1\hat{\theta}_1 - X_2\hat{\theta_2}\right)\left(X_1 - \frac{\mathbb{E}[X_1X_2]}{E[X_2^2]}X_2\right)\right] = 0\,. \\
\Rightarrow\ & \mathbb{E}\left[\left(X_1(\theta_1 - \hat{\theta}_1) + (a_2 - \hat{\theta}_2)X_2 + \varepsilon_3\right)\right. \\
& \qquad\qquad \left.\left(X_1 - \frac{\mathbb{E}[X_1X_2]}{E[X_2^2]}X_2\right)\right] = 0\,. \\
\Rightarrow\ & \hat{\theta}_1 = \theta_1.
\end{aligned}
$$

From the above two examples, it is clear that even though the internal relations between the variables are nonlinear, all we need is an unbiased linear estimate to estimate the causal parameter.

C Data Generation and Evaluation Metric

C.1 Data Generation

For every combination of number of nodes (#nodes), connectivity (p_s), noise level (σ^2), number of observation (z), and non-linear probability (p_n) (look at Table C.1), 100 examples (DAGs) are generated and stored as csv files (altogether 72.000 DAGs are simulated, comprising a dataset of overall >10GB). For each DAG, z number of samples are generated by sampling noise (ϵ in Equation (18)) with variance σ^2 starting from root of the DAG. For future benchmarking, the generated files will be made available with the code later on.

We generate DAGs (Direct Acyclic Graphs) in multiple steps: i) a random permutation of nodes is chosen as a topological order of a DAG. ii) Based on this order, directed edges are added to this DAG from each node to its followers with a certain probability p_s (connectivity). iii) For each observation, values are assigned to nodes according to the topological order of the DAG in such a way that each node's value is determined by summing over transformations (linear or nonlinear with a certain nonlinear probability p_n) of values of its direct causes with the addition of Gaussian distributed noise. The non-linear transformation used is $\alpha \tanh(\beta x)$[5], with $\alpha = 0.5$ and $\beta = 1.5$. If the set of parents for the node X' is denoted as $PA_{X'}$ as before then value assignment for a node X' is as follow:

$$
X' = \varepsilon + \sum_{X \in PA_{X'}} \iota_\ell(p_n)\theta X + (1 - \iota_\ell(p_n))\alpha \tanh(\beta X), \tag{18}
$$

[5]The resulting values in the experiments are not concentrated around zero, and they are even up to 10ks for large graphs ($\sim$ 50 nodes). With the nonlinearity feature of $\alpha \tanh(\beta x)$ for relatively large values taken into account, this is a good representer of nonlinear relationships.

connectivity (p_s)	# nodes	nonlinear probability (p_n)	# observ. z	noise level (σ^2)
0.1	5	0	100	0.01
0.3	10	0.3	500	0.1
0.5	20	0.5	1.000	0.3
	50	1		0.5
				1

Table C.1: Experimental Setup: In the experiments we vary the connectivity parameter, the number of nodes in the graph, the non-linear probability, the number of observations and the noise level and generate 100 graphs for each setting.

where $\varepsilon \sim N(0, \sigma^2)$ in which σ^2 represents noise level. $\iota_\ell(X)$ is an indicator functions which decides between linear or non-linear contribution of X in X'. We decide the value of $\iota_\ell(p_n)$ by generating a binary randon number which is 1 with probablity p_n and 0 with probability $1 - p_n$. The value of θ is set to 2 for the small DAGs (number of nodes equal to 5 or 10) and 0.5 for large DAGs (number of nodes equal to 20 or 50) due to the value exploitation that might happen in large graphs.

We vary and investigate the effect of non-linear relationships, the number of nodes, number of observations, effect of connectivity and noise level while simulating the data. We summarize the factors in the data generation in Table C.1.

C.2 Evaluation Metric

Correctly and incorrectly inferred direct causes are considered true and false. Let the total number of true positives, false positives, true negatives ,and false negatives denoted by TP, FP, TN, and FN, we evaluate our method using following metrics:

- Recall (true positive rate):
$$TPR = \frac{TP}{TP + FN}$$
- Fall-out (false positive rate):
$$FPR = \frac{FP}{FP + TN}$$
- Critical Success Index (CSI): also known as Threat Score.
$$CSI = \frac{TP}{TP + FN + FP}$$
- Accuracy:
$$ACC = \frac{TP + TN}{P + N}$$
- F1 Score: harmonic mean of precision and sensitivity.
$$F_1 = \frac{2TP}{2TP + FP + FN}$$
- Matthews correlation coefficient (MCC): a metric for evaluating quality of binary classification introduced in (Matthews, 1975).
$$MCC = \frac{TP \times TN - FP \times FN}{\sqrt{(TP + FP)(TP + FN)(TN + FP)(TN + FN)}}$$

In some rare cases, we encountered zero-divided-by-zero and divided-by-zero cases for some of these metrics. In these situations, scores are reported 1 and 0 respectively while Fall-out is reported 0 and 1.

C.3 Supplementary Tables for Performance in Inferring Direct Causes

In this section, supplementary tables supporting superior performance of CORTH Features compared to well-established methods are provided (See Tables C.2 to C.6). This superiority is consistent w.r.t. connectivity (Table C.2), number of nodes (Table C.3), number of observations (Table C.6), nonlinearity (Table C.4), and noise (Table C.5) using different evaluation metrics.

Table C.2: Performance across all the settings for different connectivities. Each single entry in the table is averaged over 24000 simulations. Our method is almost state of the art in every case.

Method	Connectivity											
	0.1				0.3				0.5			
	ACC	CSI	F1	MCC	ACC	CSI	F1	MCC	ACC	CSI	F1	MCC
GES	0.961	0.786	0.825	0.857	0.815	0.539	0.598	0.522	0.646	0.405	0.482	0.315
rankGES	0.954	0.746	0.790	0.840	0.809	0.522	0.584	0.511	0.642	0.398	0.475	0.308
ARGES	0.965	0.794	0.828	0.876	0.805	0.456	0.501	0.726	0.612	0.286	0.330	0.720
rankARGES	0.959	0.763	0.801	0.863	0.802	0.447	0.494	0.721	0.611	0.282	0.328	0.716
FCI+	0.974	0.819	0.853	0.910	0.866	0.631	0.714	0.674	0.734	0.524	0.629	0.521
LINGAM	0.966	0.763	0.796	0.889	0.896	0.710	0.753	0.761	0.827	0.682	0.727	0.715
PC	0.975	0.819	0.849	0.921	0.861	0.609	0.689	0.676	0.718	0.486	0.588	0.516
rankPC	0.971	0.797	0.831	0.912	0.852	0.587	0.670	0.653	0.701	0.458	0.560	0.470
MMHC	0.978	0.834	0.867	0.901	0.830	0.497	0.561	0.574	0.639	0.321	0.397	0.385
PCI	0.986	0.902	0.920	0.954	0.906	0.716	0.759	**0.838**	0.783	0.600	0.661	0.720
Lasso	0.976	0.886	0.925	0.926	0.876	0.725	0.811	0.737	0.800	0.682	0.778	0.622
`CORTH Features (Ours)`	**0.988**	**0.915**	**0.934**	**0.959**	**0.926**	**0.813**	**0.858**	0.833	**0.847**	**0.747**	**0.814**	**0.724**

Table C.3: Performance across all the settings for different number of nodes. Each single entry in the table is averaged over 18000 simulations. Our method is almost state of the art in every case.

Method	Number of Nodes											
	5			10			20			50		
	ACC	CSI	F1	ACC	CSI	F1	ACC	CSI	F1	ACC	CSI	F1
GES	0.935	0.890	0.911	0.854	0.730	0.779	0.743	0.442	0.526	0.698	0.245	0.323
rankGES	0.923	0.857	0.883	0.846	0.700	0.753	0.740	0.428	0.514	0.697	0.237	0.316
ARGES	0.922	0.864	0.885	0.797	0.551	0.584	0.752	0.447	0.524	0.705	0.186	0.221
rankARGES	0.914	0.838	0.861	0.793	0.537	0.572	0.750	0.435	0.514	0.705	0.181	0.216
FCI+	0.963	0.918	0.932	0.873	0.744	0.808	0.830	0.602	0.703	0.766	0.368	0.486
LINGAM	**0.991**	**0.978**	**0.982**	**0.953**	0.865	0.889	0.891	0.712	0.778	0.750	0.318	0.385
PC	0.957	0.913	0.929	0.864	0.723	0.786	0.823	0.569	0.664	0.763	0.348	0.457
rankPC	0.946	0.891	0.912	0.854	0.701	0.768	0.813	0.541	0.638	0.754	0.324	0.431
MMHC	0.929	0.878	0.905	0.841	0.675	0.739	0.767	0.432	0.507	0.725	0.218	0.281
PCI	0.984	0.965	0.972	0.922	0.844	0.875	0.888	0.734	0.782	0.773	0.414	0.491
Lasso	0.965	0.948	0.968	0.905	0.834	0.892	0.894	0.786	0.866	0.773	0.489	0.627
`CORTH Features (Ours)`	0.988	0.968	0.973	0.949	**0.908**	**0.934**	**0.949**	**0.865**	**0.905**	**0.795**	**0.559**	**0.663**

Method	Number of Nodes											
	5			10			20			50		
	TPR	FPR	MCC	TPR	FPR	MCC	TPR	FPR	MCC	TPR	FPR	MCC
GES	0.934	0.056	0.891	0.790	0.090	0.711	0.502	0.088	0.436	0.304	0.083	0.221
rankGES	0.924	0.068	0.877	0.780	0.098	0.695	0.493	0.089	0.425	0.297	0.083	0.215
ARGES	0.903	0.046	0.906	0.590	0.041	0.841	0.500	0.073	0.557	0.220	0.020	0.794
rankARGES	0.897	0.054	0.896	0.584	0.044	0.832	0.495	0.075	0.549	0.216	0.020	0.789
FCI+	0.969	0.029	0.948	0.797	0.054	0.759	0.642	0.042	0.645	0.389	0.030	0.454
LINGAM	0.991	0.007	**0.988**	0.886	0.008	**0.934**	0.770	0.055	0.759	0.391	0.072	0.471
PC	0.950	0.024	0.941	0.759	0.041	0.759	0.600	0.032	0.650	0.363	0.021	0.468
rankPC	0.944	0.039	0.925	0.750	0.053	0.734	0.580	0.034	0.629	0.341	0.024	0.427
MMHC	0.895	0.011	0.903	0.691	0.015	0.724	0.444	0.009	0.523	0.219	0.005	0.330
PCI	0.992	0.017	0.981	0.875	0.028	0.890	0.754	0.016	0.839	0.430	0.030	**0.638**
Lasso	0.999	0.074	0.949	0.944	0.119	0.817	0.954	0.147	0.794	0.681	0.148	0.488
`CORTH Features (Ours)`	0.999	0.016	0.986	0.952	0.044	0.906	0.884	0.011	**0.894**	0.609	0.101	0.567

Table C.4: Performance across all the settings for different number of nonlinear probabilities. Each single entry in the table is averaged over 18000 simulations. Our method is almost state of the art in every case.

Method	Nonlinear Probability 0			0.3			0.5			1		
	ACC	CSI	F1	ACC	CSI	F1	ACC	CSI	F1	ACC	CSI	F1
GES	0.803	0.583	0.646	0.806	0.566	0.622	0.811	0.577	0.632	0.810	0.581	0.641
rankGES	0.796	0.559	0.625	0.801	0.546	0.605	0.805	0.556	0.613	0.805	0.561	0.623
ARGES	0.781	0.476	0.515	0.786	0.486	0.525	0.792	0.506	0.546	0.818	0.581	0.628
rankARGES	0.778	0.461	0.503	0.782	0.474	0.515	0.788	0.490	0.531	0.814	0.564	0.615
FCI+	0.827	0.599	0.674	0.860	0.663	0.745	0.872	0.685	0.764	0.873	0.685	0.746
LINGAM	**0.907**	0.738	0.778	0.886	0.689	0.725	0.880	0.684	0.724	0.911	0.762	0.808
PC	0.818	0.574	0.641	0.854	0.641	0.720	0.864	0.665	0.7430	0.869	0.672	0.731
rankPC	0.813	0.560	0.630	0.841	0.614	0.694	0.848	0.627	0.704	0.864	0.656	0.720
MMHC	0.797	0.516	0.578	0.815	0.549	0.610	0.823	0.566	0.625	0.826	0.571	0.620
PCI	0.853	0.674	0.720	0.897	0.746	0.789	0.905	0.763	0.806	0.911	0.774	0.805
Lasso	0.847	0.694	0.773	0.891	0.776	0.853	0.902	0.797	0.869	0.896	0.790	0.857
`CORTH Features (Ours)`	0.871	**0.768**	**0.824**	**0.934**	**0.830**	**0.873**	**0.943**	**0.851**	**0.891**	**0.933**	**0.852**	**0.887**

Method	Nonlinear Probability 0			0.3			0.5			1		
	TPR	FPR	MCC	TPR	FPR	MCC	TPR	FPR	MCC	TPR	FPR	MCC
GES	0.643	0.093	0.564	0.620	0.074	0.557	0.629	0.071	0.568	0.637	0.079	0.570
rankGES	0.633	0.100	0.550	0.612	0.080	0.546	0.620	0.076	0.557	0.628	0.083	0.559
ARGES	0.514	0.041	0.789	0.526	0.041	0.793	0.547	0.043	0.791	0.626	0.055	0.725
rankARGES	0.509	0.044	0.780	0.522	0.044	0.788	0.540	0.046	0.783	0.620	0.059	0.715
FCI+	0.638	0.045	0.637	0.704	0.037	0.708	0.728	0.035	0.731	0.728	0.037	0.730
LINGAM	0.775	0.025	**0.832**	0.723	0.028	0.759	0.722	0.034	0.741	0.819	0.053	0.822
PC	0.605	0.037	0.649	0.672	0.027	0.707	0.695	0.025	0.728	0.702	0.029	0.734
rankPC	0.597	0.043	0.626	0.656	0.040	0.680	0.668	0.036	0.695	0.692	0.031	0.714
MMHC	0.528	0.017	0.581	0.561	0.008	0.623	0.578	0.007	0.636	0.582	0.008	0.639
PCI	0.712	0.057	0.792	0.765	0.011	0.848	0.781	0.010	0.845	0.794	0.013	**0.864**
Lasso	0.823	0.130	0.684	0.907	0.120	0.778	0.926	0.116	0.800	0.921	0.122	0.787
`CORTH Features (Ours)`	0.840	0.119	0.730	0.849	0.007	**0.872**	0.870	0.008	**0.888**	0.885	0.038	0.863

Table C.5: Performance across all the settings for different noise levels. Each single entry in the table is averaged over 14400 simulations. Our method is almost state of the art in every case.

Method	Noise Level 0.01				0.5				1			
	ACC	CSI	F1	MCC	ACC	CSI	F1	MCC	ACC	CSI	F1	MCC
GES	0.804	0.579	0.639	0.559	0.808	0.571	0.629	0.562	0.818	0.586	0.644	0.589
rankGES	0.797	0.557	0.619	0.548	0.802	0.552	0.613	0.551	0.812	0.565	0.625	0.577
ARGES	0.810	0.572	0.625	0.653	0.789	0.496	0.534	0.814	0.774	0.434	0.460	0.897
rankARGES	0.804	0.549	0.605	0.643	0.786	0.483	0.523	0.806	0.774	0.433	0.459	0.895
FCI+	0.843	0.617	0.691	0.674	0.865	0.678	0.753	0.717	0.874	0.697	0.766	0.740
LINGAM	0.888	0.703	0.744	0.763	0.899	0.723	0.763	0.797	0.903	0.732	0.773	0.803
PC	0.837	0.595	0.664	0.683	0.859	0.659	0.731	0.716	0.870	0.686	0.752	0.745
rankPC	0.831	0.584	0.657	0.653	0.845	0.626	0.699	0.688	0.856	0.655	0.724	0.714
MMHC	0.806	0.526	0.585	0.605	0.818	0.557	0.615	0.626	0.829	0.586	0.639	0.652
PCI	0.873	0.690	0.730	**0.819**	0.901	0.760	0.801	0.846	0.906	0.777	0.815	0.854
Lasso	0.868	0.728	0.807	0.725	0.891	0.780	0.852	0.779	0.898	0.794	0.861	0.793
`CORTH Features (Ours)`	**0.899**	**0.789**	**0.839**	0.795	**0.929**	**0.842**	**0.883**	**0.858**	**0.934**	**0.854**	**0.891**	**0.866**

Table C.6: Performance across all the settings for different number of observations. Each single entry in the table is averaged over 24000 simulations. Our method is almost state of the art in every case.

Method	Number of Observations											
	100				500				1000			
	ACC	CSI	F1	MCC	ACC	CSI	F1	MCC	ACC	CSI	F1	MCC
GES	0.797	0.524	0.588	0.539	0.811	0.593	0.650	0.572	0.815	0.612	0.666	0.583
rankGES	0.788	0.495	0.561	0.522	0.806	0.576	0.636	0.564	0.810	0.595	0.652	0.573
ARGES	0.780	0.446	0.489	0.786	0.799	0.535	0.576	0.773	0.803	0.555	0.595	0.764
rankARGES	0.776	0.428	0.473	0.778	0.795	0.523	0.566	0.766	0.800	0.542	0.584	0.757
FCI+	0.837	0.589	0.671	0.652	0.865	0.684	0.755	0.720	0.871	0.702	0.771	0.732
LINGAM	0.840	0.578	0.650	0.678	0.908	0.719	0.743	0.825	0.941	0.858	0.883	0.862
PC	0.830	0.568	0.642	0.661	0.858	0.662	0.732	0.719	0.866	0.684	0.752	0.733
rankPC	0.821	0.544	0.617	0.632	0.849	0.639	0.711	0.696	0.855	0.660	0.733	0.707
MMHC	0.800	0.495	0.557	0.579	0.820	0.570	0.625	0.633	0.826	0.587	0.642	0.647
PCI	0.829	0.551	0.594	**0.804**	0.914	0.812	0.853	0.842	0.931	0.855	0.893	0.866
Lasso	0.870	**0.729**	**0.812**	0.732	0.889	0.778	0.848	0.773	0.893	0.786	0.854	0.780
`CORTH Features (Ours)`	**0.883**	0.710	0.780	0.754	**0.935**	**0.874**	**0.906**	**0.874**	**0.942**	**0.891**	**0.920**	**0.887**

D Real-World Data Experiment-Covid19

D.1 Preprocessing

The preprocessing stage for this dataset is the same as (Schwab et al., 2020) except that, for each target variable upsampling is used to resolve data imbalance.

D.2 Results

The results obtained by leveraging CORTH Features is suprisingly consistent with (Schwab et al., 2020) which demonstrates the ability of this method in feature selection. The selected features are indicated in Tables D.1 to D.4

Table D.1: Ranks of the features based on the times being predicted as direct causes of **SARS-Cov-2 exam result** out of 1000 different runs of our propsal approach. Not mentiond features were not predicted even once, note that preprocessed dataset has 331 features.

Rank	Feature	Rate of being Predicted as a Direct Cause
1	Patient age quantile Arterial Lactic Acid Promyelocytes Base excess venous blood gas analysis	1
5	pH venous blood gas analysis	0.999
6	MISSING Mean platelet volume	0.992
7	MISSING Lactic Dehydrogenase	0.966
8	Segmented	0.934
9	Myelocytes	0.904
10	Eosinophils	0.794
11	Leukocytes	0.784
12	Total CO2 arterial blood gas analysis	0.450
13	Potassium	0.340
14	MISSING International normalized ratio INR	0.289
15	Metapneumovirus not detected	0.234
16	Arteiral Fio2	0.092
17	HCO3 arterial blood gas analysis.	0.046
18	Creatinine	0.035
19	MISSING.Magnesium	0.034
20	pO2 arterial blood gas analysis	0.031
21	MISSING Arteiral Fio2	0.024
22	Direct Bilirubin	0.016
23	MISSING Ferritin Respiratory Syncytial Virus detected	0.014
25	MISSING Albumin Creatine phosphokinase CPK	0.010
27	Strepto A positive	0.008
28	Neutrophils Red blood cell distribution width RDW Coronavirus HKU1 detected Influenza A rapid test positive	0.004
32	Hb saturation venous blood gas analysis	0.002
33	Urine pH Inf A H1N1 2009 detected MISSING Serum Glucose Aspartate transaminase Urine Esterase nan	0.001

Table D.2: Ranks of the features based on the times being predicted as direct causes of **Patient addmited to regular ward** out of 1000 different runs of our propsal approach. Not mentiond features were not predicted even once, note that preprocessed dataset has 331 features.

Rank	Feature	Rate of being Predicted as a Direct Cause
1	Patient age quantile HCO3 venous blood gas analysis Total CO2 venous blood gas analysis Gamma glutamyltransferase	1
5	MISSING Lactic Dehydrogenase	0.987
6	Alanine transaminase	0.845
7	MISSING International normalized ratio INR	0.804
8	Serum Glucose	0.652
9	pH venous blood gas analysis	0.631
10	Base.excess venous blood gas analysis	0.341
11	MISSING Arteiral Fio2	0.334
12	Urine Density	0.334
13	Magnesium	0.323
14	Metapneumovirus not detected	0.261
15	MISSING Mean platelet volume	0.118
16	Creatine phosphokinase CPK	0.086
17	Creatinine	0.058
18	International normalized ratio INR	0.049
19	MISSING Ferritin	0.046
20	Urea	0.044
21	Respiratory Syncytial Virus detected	0.032
22	MISSING Magnesium	0.021
23	MISSING Albumin	0.018
24	MISSING Potassium	0.016
25	Inf A H1N1 2009 detected	0.014
26	Coronavirus HKU1 detected	0.010
27	Strepto A positive	0.008
28	Influenza A rapid test positive	0.007
29	MISSING Sodium Urine Protein nan	0.002
31	ctO2 arterial blood gas analysis Influenza A detected Influenza B detected	0.001

Table D.3: Ranks of the features based on the times being predicted as direct causes of **Patient addmited to semi-intensive unit** out of 1000 different runs of our propsal approach. Not mentiond features were not predicted even once, note that preprocessed dataset has 331 features.

Rank	Feature	Rate of being Predicted as a Direct Cause
1	Patient age quantile Creatinine MISSING Lactic Dehydrogenase Total CO2 venous blood gas analysis Magnesium Gamma glutamyltransferase Alanine transaminase	1
8	ctO2 arterial blood gas analysis HCO3 venous blood gas analysis	0.999
10	Relationship Patient Normal	0.786
11	MISSING Arteiral Fio2	0.595
12	Base excess venous blood gas analysis	0.578
13	pO2 venous blood gas analysis	0.449
14	MISSING International normalized ratio INR	0.435
15	Mean platelet volume	0.366
16	Metapneumovirus not detected	0.308
17	Proteina C reativa mg dL	0.235
18	Sodium	0.212
19	Phosphor	0.164
20	Urine Density	0.085
21	Respiratory Syncytial Virus detected	0.068
22	MISSING Mean platelet volume	0.056
23	MISSING Ferritin	0.054
24	pH venous blood gas analysis	0.021
25	Strepto A positive	0.018
26	Inf A H1N1 2009 detected	0.016
27	Influenza A rapid test positive	0.014
28	MISSING Albumin Coronavirus HKU1 detected	0.012
30	MISSING Magnesium	0.008
31	Aspartate transaminase	0.004
32	Urine Ketone Bodies absent Red blood cell distribution width RDW Influenza A detected Urine Esterase absent Urine Protein nan	0.001

Table D.4: Ranks of the features based on the times being predicted as direct causes of **Patient addmited to intensive care unit** out of 1000 different runs of our propsal approach. Not mentiond features were not predicted even once, note that preprocessed dataset has 331 features.

Rank	Feature	Rate of being Predicted as a Direct Cause
1	Patient age quantile MISSING Mean platelet volume Total CO2 venous blood gas analysis HCO3 venous blood gas analysis Alanine transaminase Gamma glutamyltransferase Magnesium MISSING Lactic Dehydrogenase Creatinine	1
10	pO2 venous blood gas analysis	0.982
11	ctO2 arterial blood gas analysis	0.962
12	pH venous blood gas analysis	0.938
13	MISSING Arteiral Fio2	0.667
14	MISSING International normalized ratio INR	0.586
15	Red blood cell distribution width RDW	0.503
16	Urine Density	0.414
17	Creatine phosphokinase CPK	0.380
18	Base excess venous blood gas analysis	0.352
19	Potassium	0.234
20	Promyelocytes	0.221
21	MISSING Ferritin	0.174
22	Metapneumovirus not detected	0.132
23	Phosphor	0.082
24	Sodium	0.036
25	MISSING Magnesium	0.032
26	Proteina C reativa mg dL	0.016
27	Aspartate transaminase	0.015
28	Respiratory Syncytial Virus detected	0.010
29	Relationship Patient Normal	0.007
30	MISSING Albumin Arterial Lactic Acid	0.006
32	Coronavirus HKU1 detected Eosinophils	0.005
34	Inf A H1N1 2009 detected	0.004
35	Influenza A rapid test positive International normalized ratio INR	0.002
37	Urine Crystals Ausentes Leukocytes Strepto A positive	0.001

E Supplementary Figures for Parameter Estimation

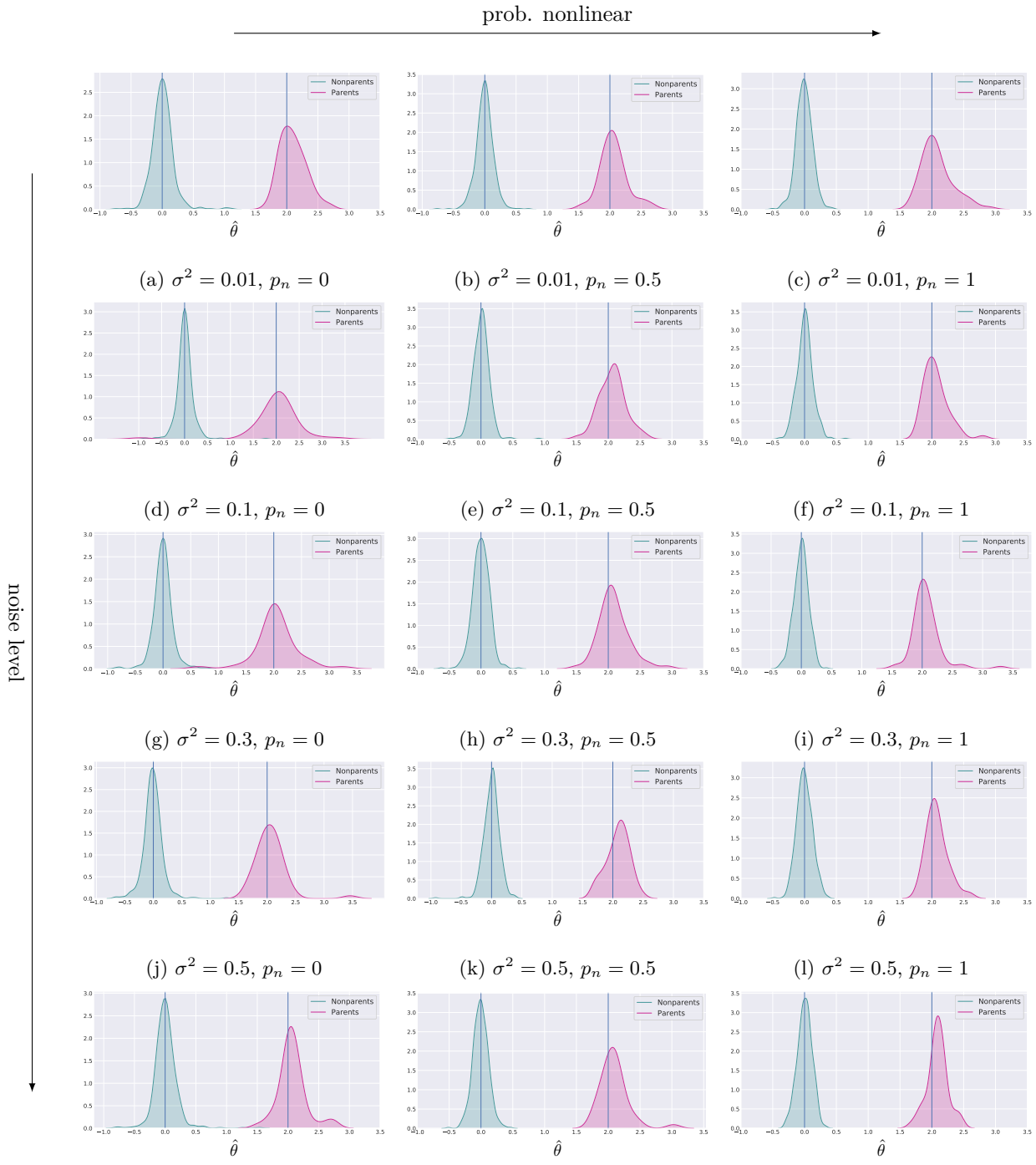

(a) $\sigma^2 = 0.01$, $p_n = 0$ (b) $\sigma^2 = 0.01$, $p_n = 0.5$ (c) $\sigma^2 = 0.01$, $p_n = 1$

(d) $\sigma^2 = 0.1$, $p_n = 0$ (e) $\sigma^2 = 0.1$, $p_n = 0.5$ (f) $\sigma^2 = 0.1$, $p_n = 1$

(g) $\sigma^2 = 0.3$, $p_n = 0$ (h) $\sigma^2 = 0.3$, $p_n = 0.5$ (i) $\sigma^2 = 0.3$, $p_n = 1$

(j) $\sigma^2 = 0.5$, $p_n = 0$ (k) $\sigma^2 = 0.5$, $p_n = 0.5$ (l) $\sigma^2 = 0.5$, $p_n = 1$

(m) $\sigma^2 = 1$, $p_n = 0$ (n) $\sigma^2 = 1$, $p_n = 1$ (o) $\sigma^2 = 1$, $p_n = 1$

Figure E.1: 0.1 connectivity, 5 nodes, 100 observations, 100 simulations. Distribution of the estimated θ values for the true and false causal parents in 100 simulations. The vertical lines indicate the ground truth values for the causal parents linear coefficients. In general we observe that in all settings with enough observations the parameter estimation works reliably.

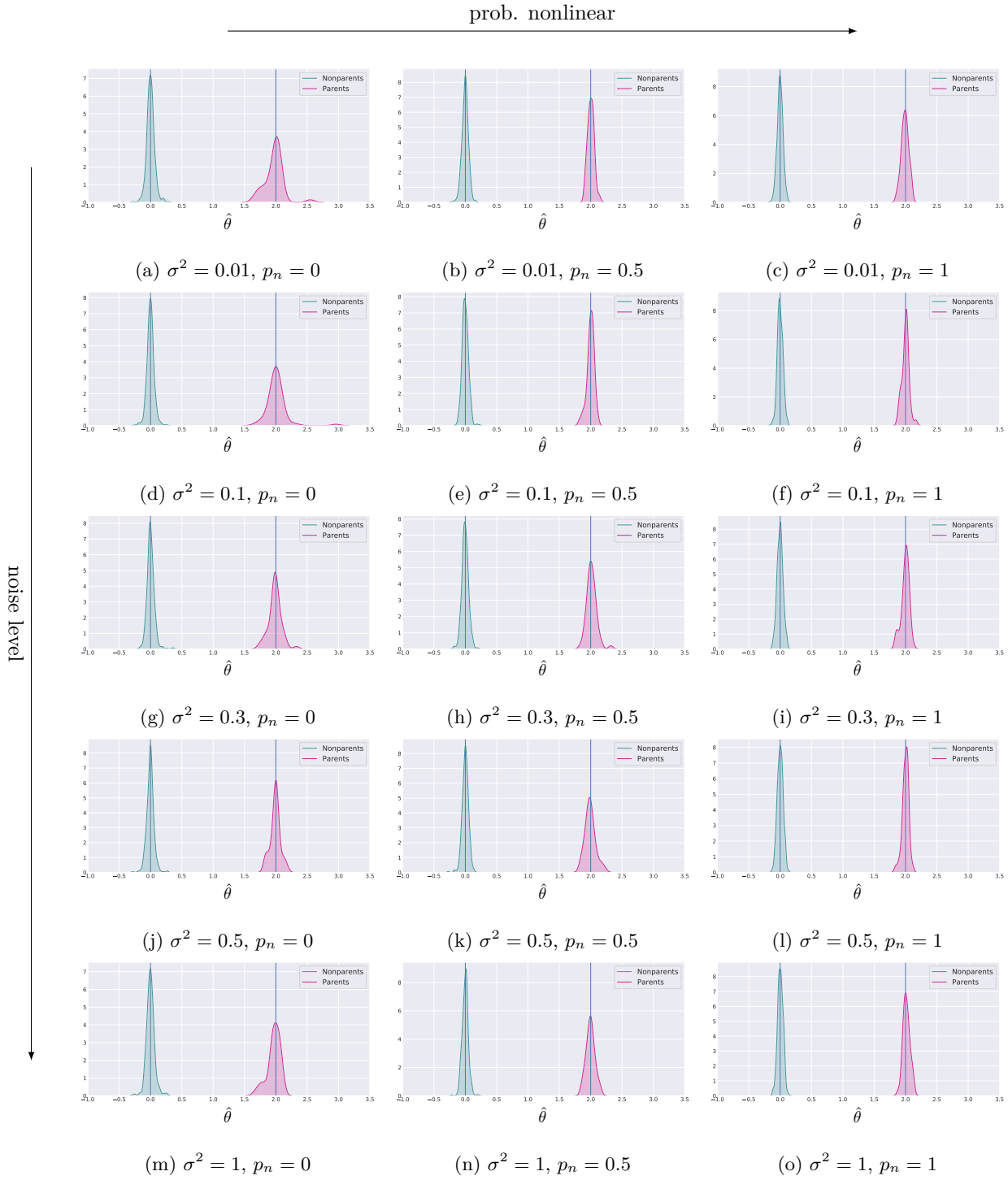

(a) $\sigma^2 = 0.01$, $p_n = 0$ (b) $\sigma^2 = 0.01$, $p_n = 0.5$ (c) $\sigma^2 = 0.01$, $p_n = 1$

(d) $\sigma^2 = 0.1$, $p_n = 0$ (e) $\sigma^2 = 0.1$, $p_n = 0.5$ (f) $\sigma^2 = 0.1$, $p_n = 1$

(g) $\sigma^2 = 0.3$, $p_n = 0$ (h) $\sigma^2 = 0.3$, $p_n = 0.5$ (i) $\sigma^2 = 0.3$, $p_n = 1$

(j) $\sigma^2 = 0.5$, $p_n = 0$ (k) $\sigma^2 = 0.5$, $p_n = 0.5$ (l) $\sigma^2 = 0.5$, $p_n = 1$

(m) $\sigma^2 = 1$, $p_n = 0$ (n) $\sigma^2 = 1$, $p_n = 0.5$ (o) $\sigma^2 = 1$, $p_n = 1$

Figure E.2: 0.1 connectivity, 5 nodes, 500 observations, 100 simulations. Distribution of the estimated θ values for the true and false causal parents in 100 simulations. The vertical lines indicate the ground truth values for the causal parents linear coefficients. In general we observe that in all settings with enough observations the parameter estimation works reliably.

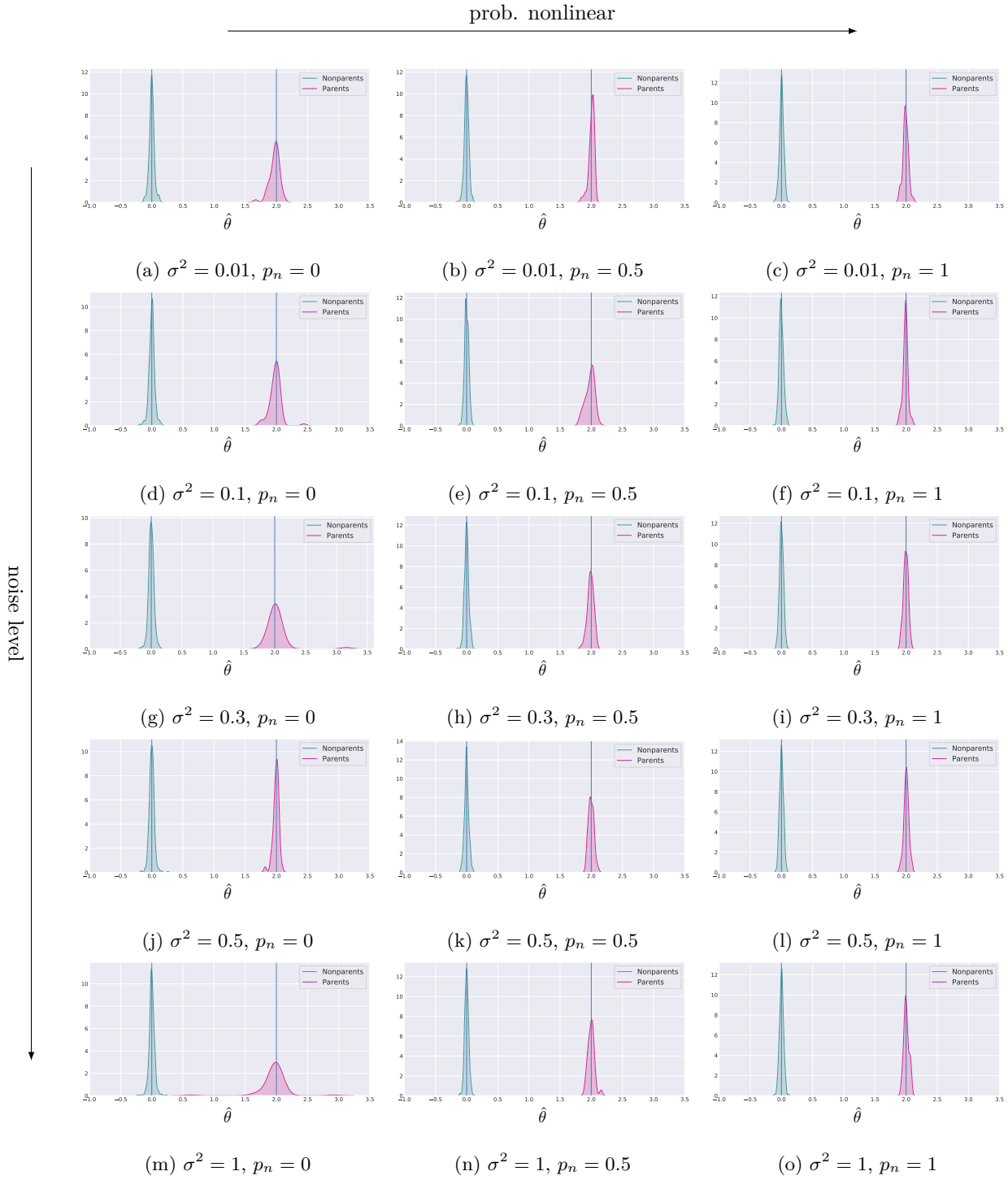

(a) $\sigma^2 = 0.01$, $p_n = 0$ (b) $\sigma^2 = 0.01$, $p_n = 0.5$ (c) $\sigma^2 = 0.01$, $p_n = 1$

(d) $\sigma^2 = 0.1$, $p_n = 0$ (e) $\sigma^2 = 0.1$, $p_n = 0.5$ (f) $\sigma^2 = 0.1$, $p_n = 1$

(g) $\sigma^2 = 0.3$, $p_n = 0$ (h) $\sigma^2 = 0.3$, $p_n = 0.5$ (i) $\sigma^2 = 0.3$, $p_n = 1$

(j) $\sigma^2 = 0.5$, $p_n = 0$ (k) $\sigma^2 = 0.5$, $p_n = 0.5$ (l) $\sigma^2 = 0.5$, $p_n = 1$

(m) $\sigma^2 = 1$, $p_n = 0$ (n) $\sigma^2 = 1$, $p_n = 0.5$ (o) $\sigma^2 = 1$, $p_n = 1$

Figure E.3: 0.1 connectivity, 5 nodes, 1000 observations, 100 simulations. Distribution of the estimated θ values for the true and false causal parents in 100 simulations. The vertical lines indicate the ground truth values for the causal parents linear coefficients. In general we observe that in all settings with enough observations the parameter estimation works reliably.

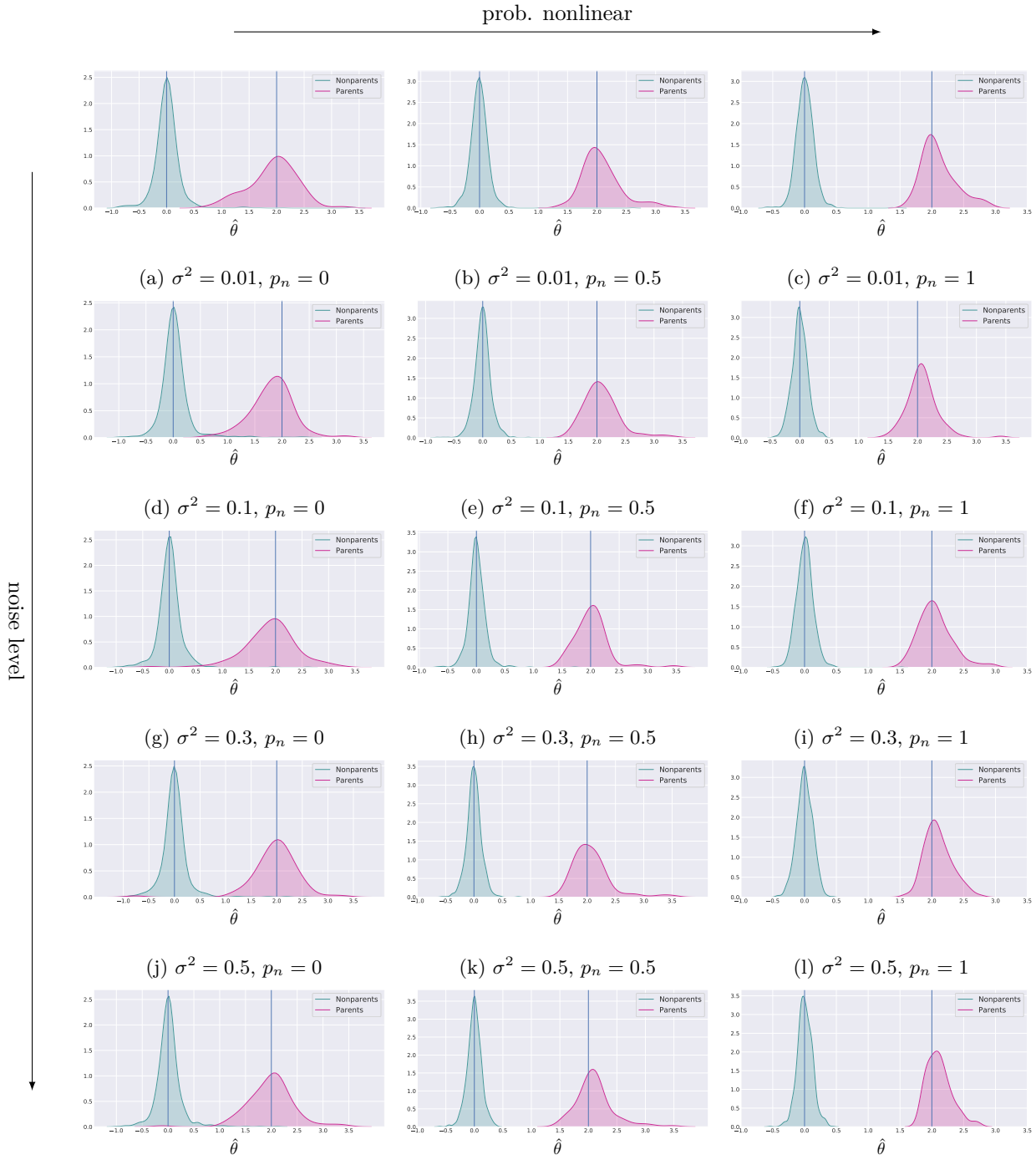

(a) $\sigma^2 = 0.01$, $p_n = 0$ (b) $\sigma^2 = 0.01$, $p_n = 0.5$ (c) $\sigma^2 = 0.01$, $p_n = 1$

(d) $\sigma^2 = 0.1$, $p_n = 0$ (e) $\sigma^2 = 0.1$, $p_n = 0.5$ (f) $\sigma^2 = 0.1$, $p_n = 1$

(g) $\sigma^2 = 0.3$, $p_n = 0$ (h) $\sigma^2 = 0.3$, $p_n = 0.5$ (i) $\sigma^2 = 0.3$, $p_n = 1$

(j) $\sigma^2 = 0.5$, $p_n = 0$ (k) $\sigma^2 = 0.5$, $p_n = 0.5$ (l) $\sigma^2 = 0.5$, $p_n = 1$

(m) $\sigma^2 = 1$, $p_n = 0$ (n) $\sigma^2 = 1$, $p_n = 0.5$ (o) $\sigma^2 = 1$, $p_n = 1$

Figure E.4: 0.1 connectivity, 10 nodes, 100 observations, 100 simulations. Distribution of the estimated θ values for the true and false causal parents in 100 simulations. The vertical lines indicate the ground truth values for the causal parents linear coefficients. In general we observe that in all settings with enough observations the parameter estimation works reliably.

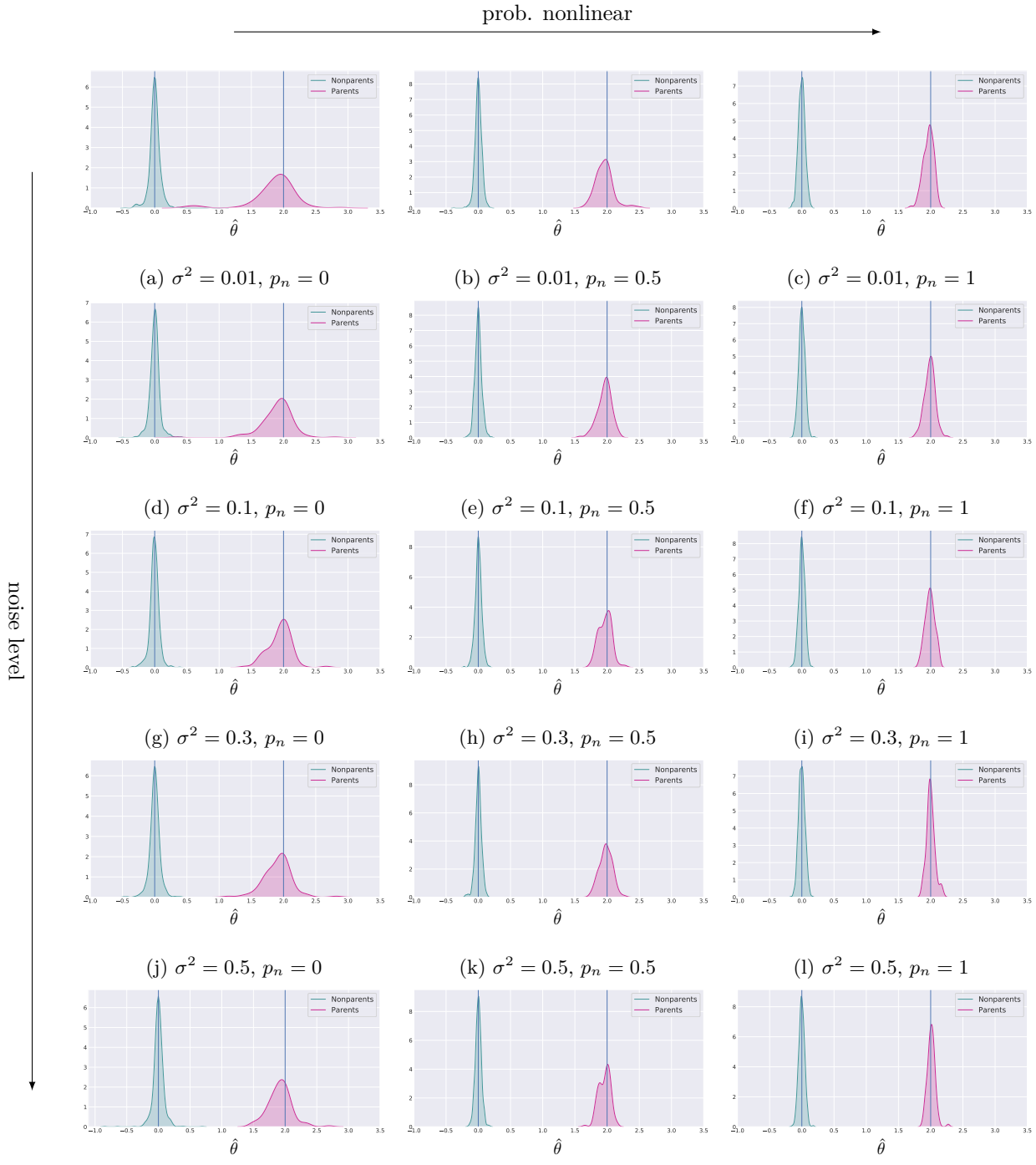

(a) $\sigma^2 = 0.01$, $p_n = 0$ (b) $\sigma^2 = 0.01$, $p_n = 0.5$ (c) $\sigma^2 = 0.01$, $p_n = 1$

(d) $\sigma^2 = 0.1$, $p_n = 0$ (e) $\sigma^2 = 0.1$, $p_n = 0.5$ (f) $\sigma^2 = 0.1$, $p_n = 1$

(g) $\sigma^2 = 0.3$, $p_n = 0$ (h) $\sigma^2 = 0.3$, $p_n = 0.5$ (i) $\sigma^2 = 0.3$, $p_n = 1$

(j) $\sigma^2 = 0.5$, $p_n = 0$ (k) $\sigma^2 = 0.5$, $p_n = 0.5$ (l) $\sigma^2 = 0.5$, $p_n = 1$

(m) $\sigma^2 = 1$, $p_n = 0$ (n) $\sigma^2 = 1$, $p_n = 0.5$ (o) $\sigma^2 = 1$, $p_n = 1$

Figure E.5: connectivity 0.1, 10 nodes, 500 observations, 100 simulations. Distribution of the estimated θ values for the true and false causal parents in 100 simulations. The vertical lines indicate the ground truth values for the causal parents linear coefficients. In general we observe that in all settings with enough observations the parameter estimation works reliably.

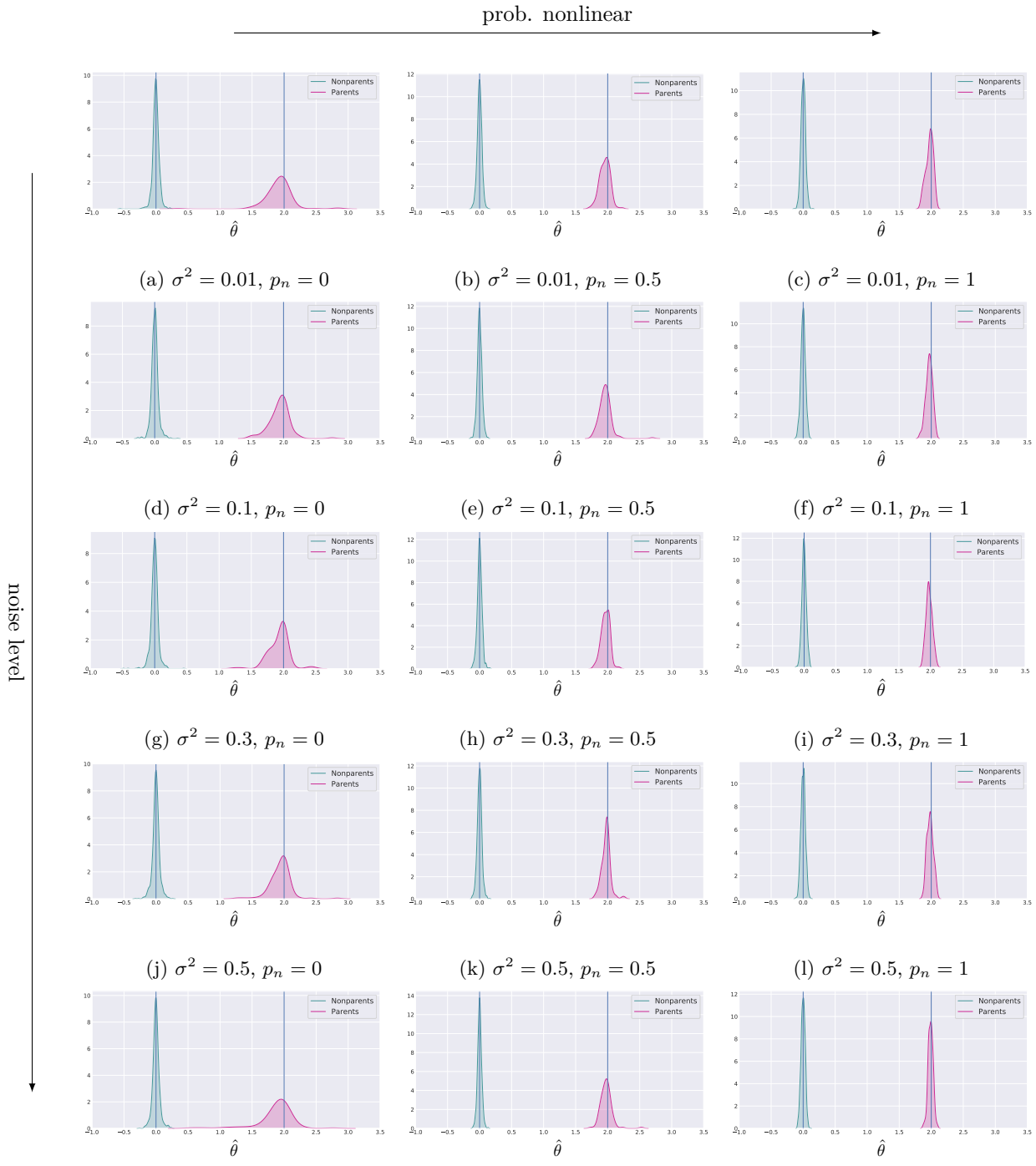

(a) $\sigma^2 = 0.01$, $p_n = 0$ (b) $\sigma^2 = 0.01$, $p_n = 0.5$ (c) $\sigma^2 = 0.01$, $p_n = 1$

(d) $\sigma^2 = 0.1$, $p_n = 0$ (e) $\sigma^2 = 0.1$, $p_n = 0.5$ (f) $\sigma^2 = 0.1$, $p_n = 1$

(g) $\sigma^2 = 0.3$, $p_n = 0$ (h) $\sigma^2 = 0.3$, $p_n = 0.5$ (i) $\sigma^2 = 0.3$, $p_n = 1$

(j) $\sigma^2 = 0.5$, $p_n = 0$ (k) $\sigma^2 = 0.5$, $p_n = 0.5$ (l) $\sigma^2 = 0.5$, $p_n = 1$

(m) $\sigma^2 = 1$, $p_n = 0$ (n) $\sigma^2 = 1$, $p_n = 0.5$ (o) $\sigma^2 = 1$, $p_n = 1$

Figure E.6: connectivity 0.1, 10 nodes, 1000 observations, 100 simulations. Distribution of the estimated θ values for the true and false causal parents in 100 simulations. The vertical lines indicate the ground truth values for the causal parents linear coefficients. In general we observe that in all settings with enough observations the parameter estimation works reliably.

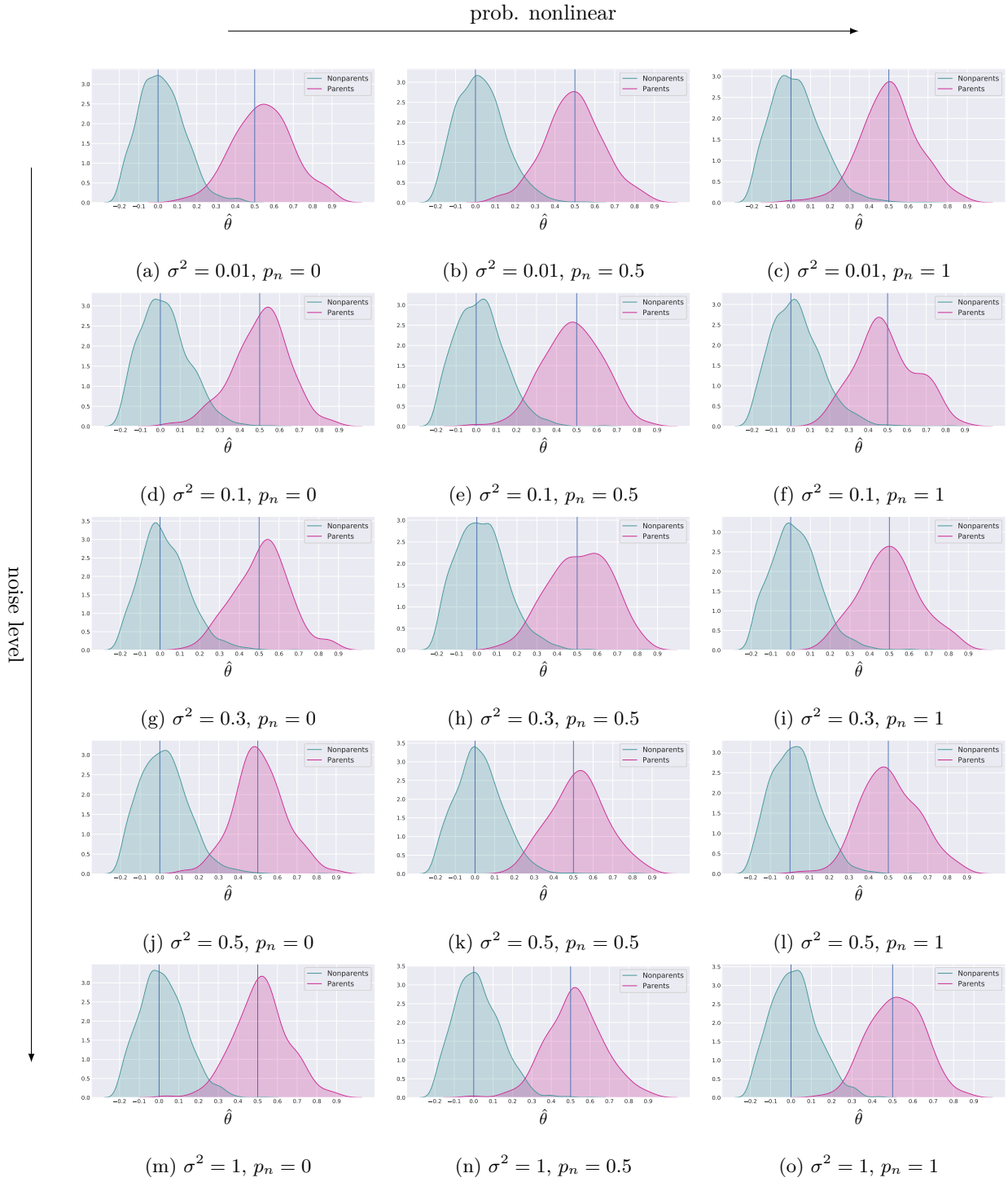

(a) $\sigma^2 = 0.01$, $p_n = 0$ (b) $\sigma^2 = 0.01$, $p_n = 0.5$ (c) $\sigma^2 = 0.01$, $p_n = 1$

(d) $\sigma^2 = 0.1$, $p_n = 0$ (e) $\sigma^2 = 0.1$, $p_n = 0.5$ (f) $\sigma^2 = 0.1$, $p_n = 1$

(g) $\sigma^2 = 0.3$, $p_n = 0$ (h) $\sigma^2 = 0.3$, $p_n = 0.5$ (i) $\sigma^2 = 0.3$, $p_n = 1$

(j) $\sigma^2 = 0.5$, $p_n = 0$ (k) $\sigma^2 = 0.5$, $p_n = 0.5$ (l) $\sigma^2 = 0.5$, $p_n = 1$

(m) $\sigma^2 = 1$, $p_n = 0$ (n) $\sigma^2 = 1$, $p_n = 0.5$ (o) $\sigma^2 = 1$, $p_n = 1$

Figure E.7: connectivity 0.1, 20 nodes, 100 observations, 100 simulations. Distribution of the estimated θ values for the true and false causal parents in 100 simulations. The vertical lines indicate the ground truth values for the causal parents linear coefficients. In general we observe that in all settings with enough observations the parameter estimation works reliably.

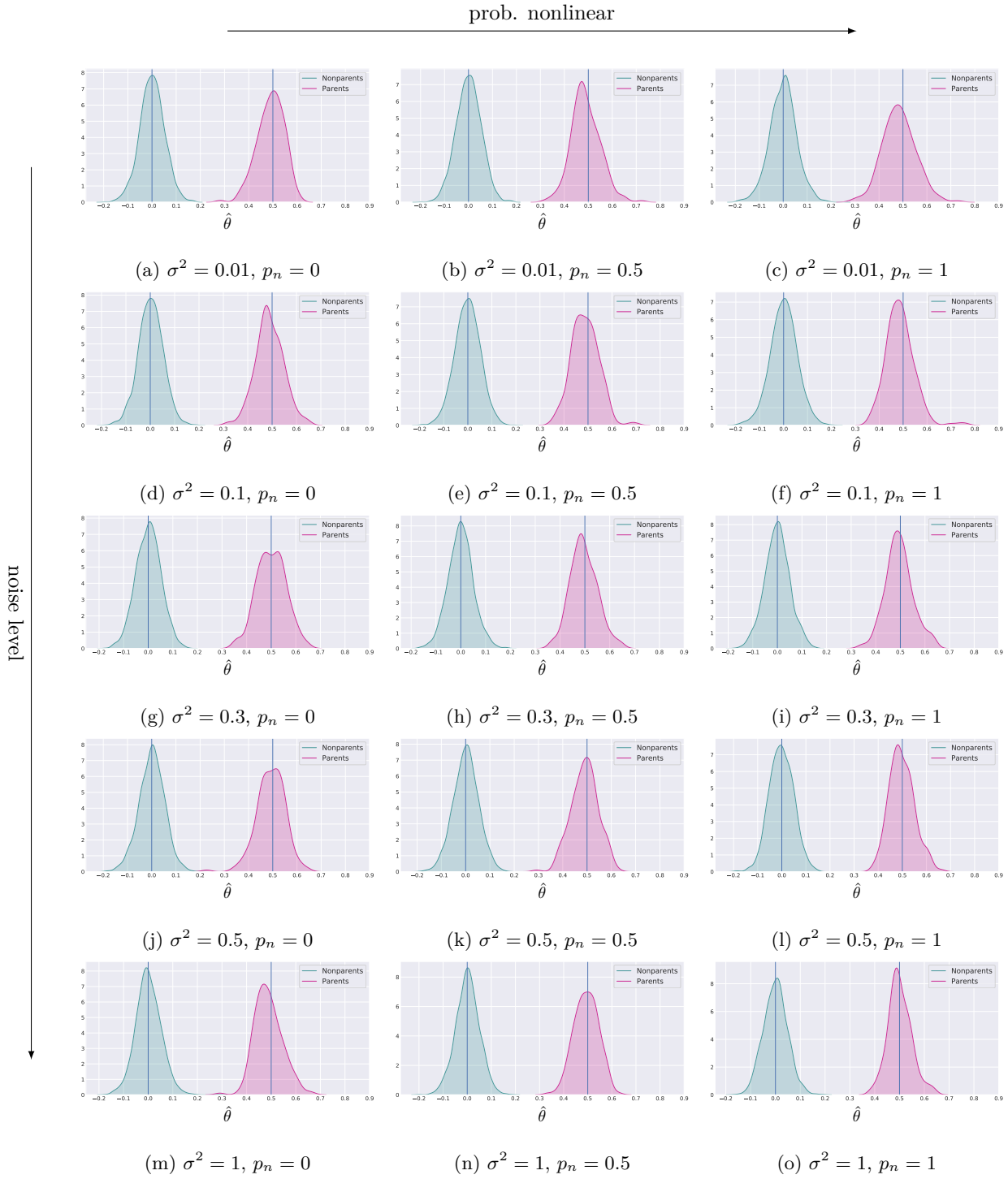

(a) $\sigma^2 = 0.01$, $p_n = 0$ (b) $\sigma^2 = 0.01$, $p_n = 0.5$ (c) $\sigma^2 = 0.01$, $p_n = 1$

(d) $\sigma^2 = 0.1$, $p_n = 0$ (e) $\sigma^2 = 0.1$, $p_n = 0.5$ (f) $\sigma^2 = 0.1$, $p_n = 1$

(g) $\sigma^2 = 0.3$, $p_n = 0$ (h) $\sigma^2 = 0.3$, $p_n = 0.5$ (i) $\sigma^2 = 0.3$, $p_n = 1$

(j) $\sigma^2 = 0.5$, $p_n = 0$ (k) $\sigma^2 = 0.5$, $p_n = 0.5$ (l) $\sigma^2 = 0.5$, $p_n = 1$

(m) $\sigma^2 = 1$, $p_n = 0$ (n) $\sigma^2 = 1$, $p_n = 0.5$ (o) $\sigma^2 = 1$, $p_n = 1$

Figure E.8: connectivity 0.1, 20 nodes, 500 observations, 100 simulations. Distribution of the estimated θ values for the true and false causal parents in 100 simulations. The vertical lines indicate the ground truth values for the causal parents linear coefficients. In general we observe that in all settings with enough observations the parameter estimation works reliably.

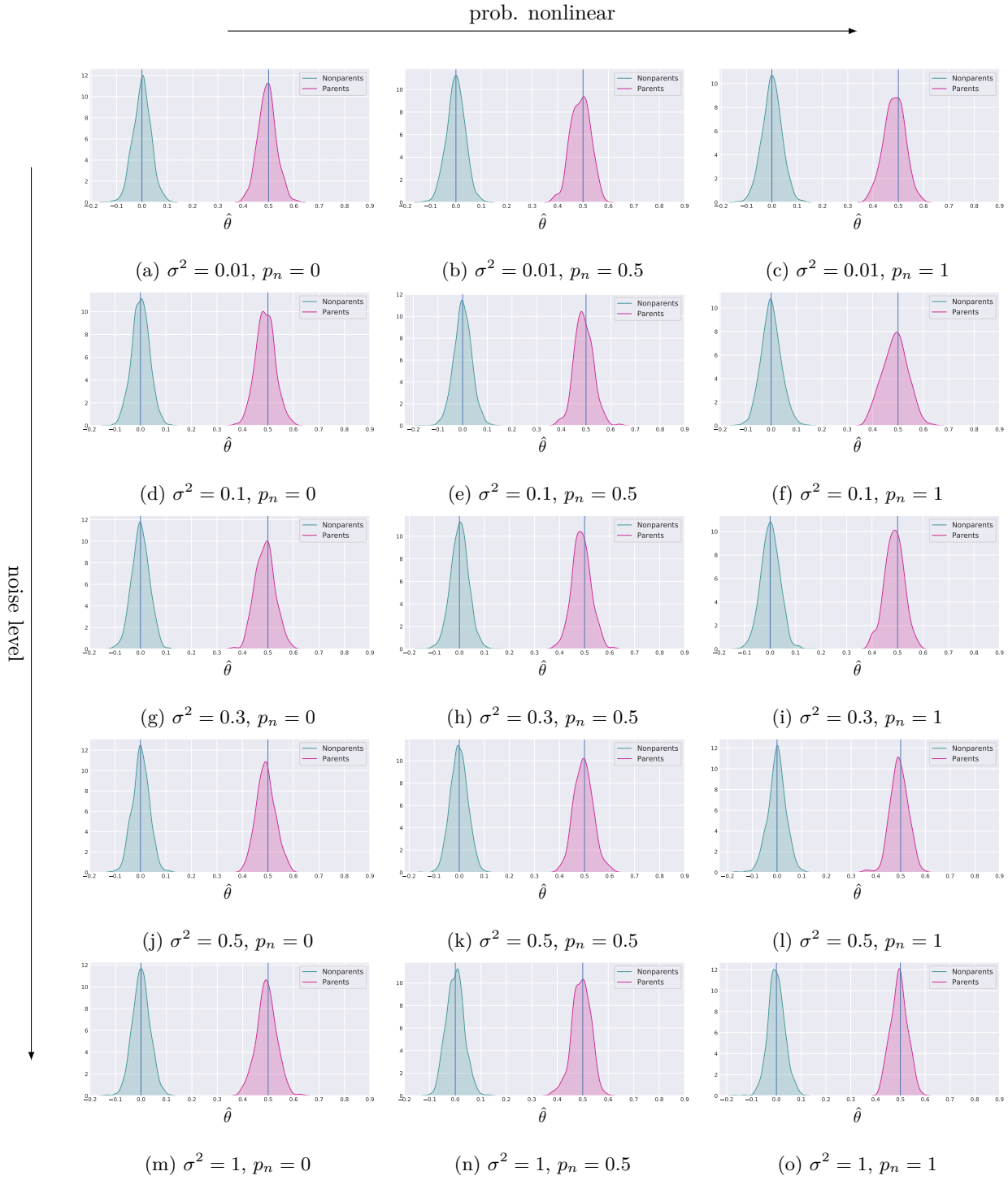

(a) $\sigma^2 = 0.01$, $p_n = 0$ (b) $\sigma^2 = 0.01$, $p_n = 0.5$ (c) $\sigma^2 = 0.01$, $p_n = 1$

(d) $\sigma^2 = 0.1$, $p_n = 0$ (e) $\sigma^2 = 0.1$, $p_n = 0.5$ (f) $\sigma^2 = 0.1$, $p_n = 1$

(g) $\sigma^2 = 0.3$, $p_n = 0$ (h) $\sigma^2 = 0.3$, $p_n = 0.5$ (i) $\sigma^2 = 0.3$, $p_n = 1$

(j) $\sigma^2 = 0.5$, $p_n = 0$ (k) $\sigma^2 = 0.5$, $p_n = 0.5$ (l) $\sigma^2 = 0.5$, $p_n = 1$

(m) $\sigma^2 = 1$, $p_n = 0$ (n) $\sigma^2 = 1$, $p_n = 0.5$ (o) $\sigma^2 = 1$, $p_n = 1$

Figure E.9: connectivity 0.1, 20 nodes, 1000 observations, 100 simulations. Distribution of the estimated θ values for the true and false causal parents in 100 simulations. The vertical lines indicate the ground truth values for the causal parents linear coefficients. In general we observe that in all settings with enough observations the parameter estimation works reliably.

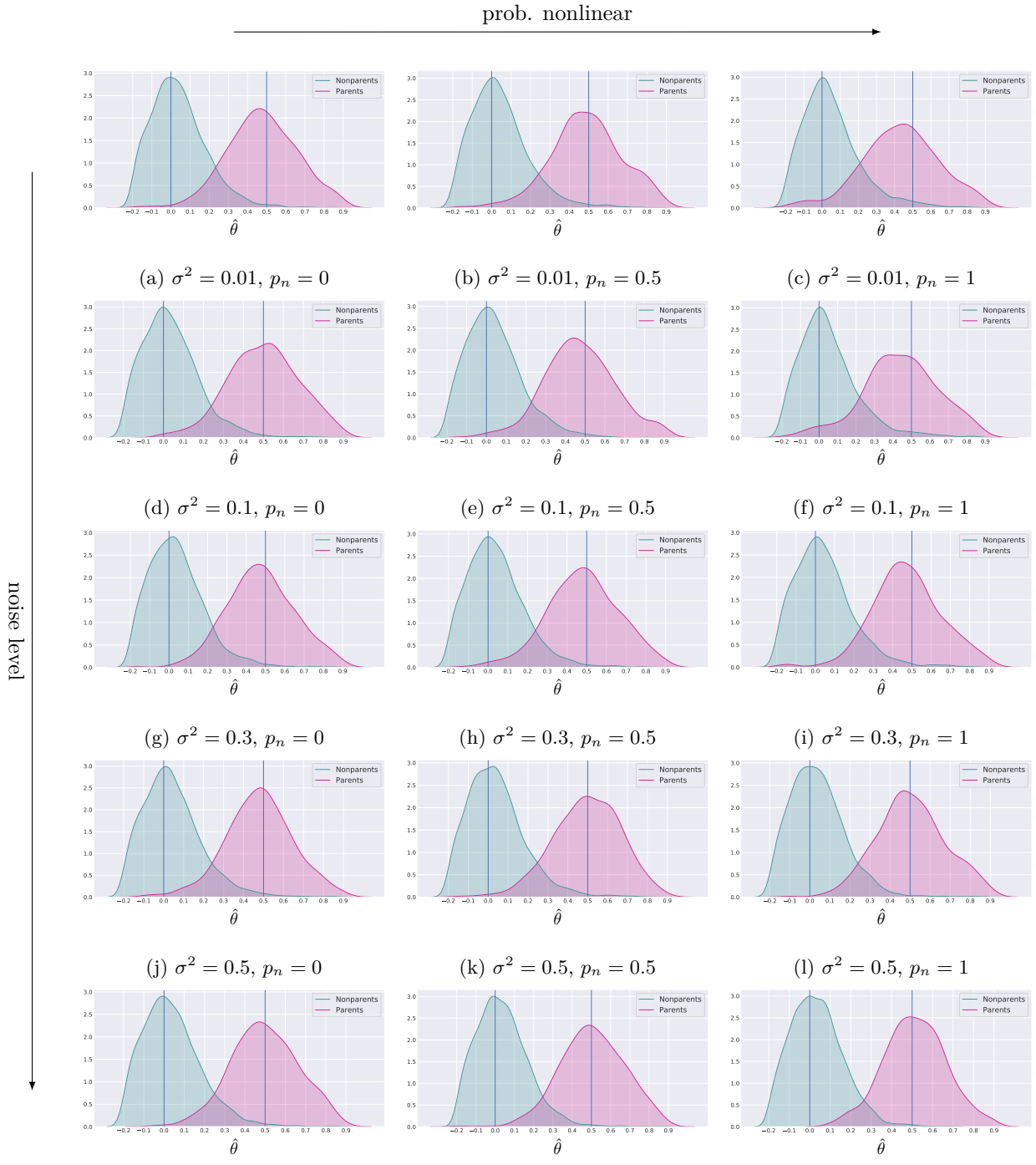

(a) $\sigma^2 = 0.01$, $p_n = 0$ (b) $\sigma^2 = 0.01$, $p_n = 0.5$ (c) $\sigma^2 = 0.01$, $p_n = 1$

(d) $\sigma^2 = 0.1$, $p_n = 0$ (e) $\sigma^2 = 0.1$, $p_n = 0.5$ (f) $\sigma^2 = 0.1$, $p_n = 1$

(g) $\sigma^2 = 0.3$, $p_n = 0$ (h) $\sigma^2 = 0.3$, $p_n = 0.5$ (i) $\sigma^2 = 0.3$, $p_n = 1$

(j) $\sigma^2 = 0.5$, $p_n = 0$ (k) $\sigma^2 = 0.5$, $p_n = 0.5$ (l) $\sigma^2 = 0.5$, $p_n = 1$

(m) $\sigma^2 = 1$, $p_n = 0$ (n) $\sigma^2 = 1$, $p_n = 0.5$ (o) $\sigma^2 = 1$, $p_n = 1$

Figure E.10: connectivity 0.1, 50 nodes, 100 observations, 100 simulations. Distribution of the estimated θ values for the true and false causal parents in 100 simulations. The vertical lines indicate the ground truth values for the causal parents linear coefficients. In general we observe that in all settings with enough observations the parameter estimation works reliably.

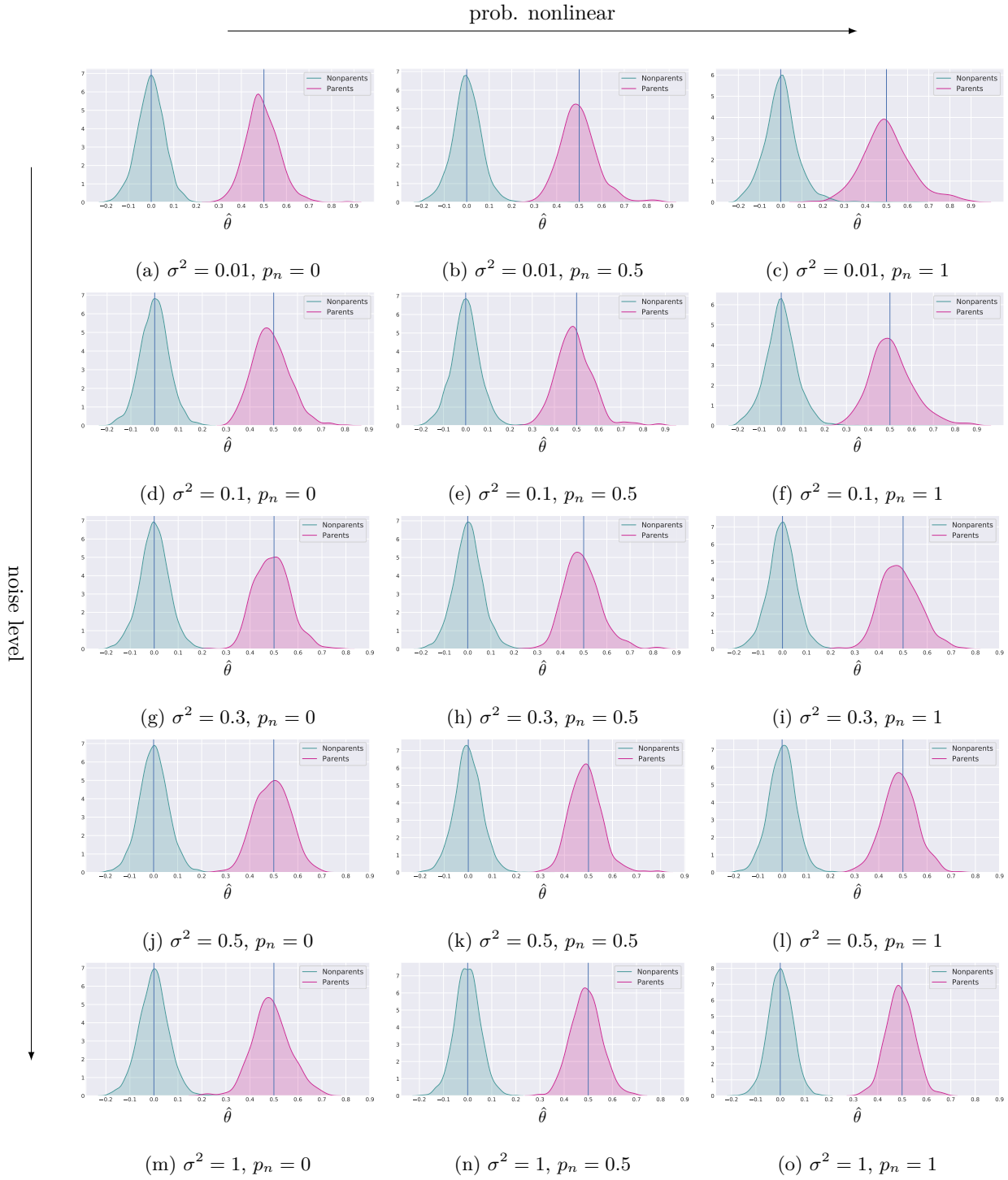

(a) $\sigma^2 = 0.01$, $p_n = 0$ (b) $\sigma^2 = 0.01$, $p_n = 0.5$ (c) $\sigma^2 = 0.01$, $p_n = 1$

(d) $\sigma^2 = 0.1$, $p_n = 0$ (e) $\sigma^2 = 0.1$, $p_n = 0.5$ (f) $\sigma^2 = 0.1$, $p_n = 1$

(g) $\sigma^2 = 0.3$, $p_n = 0$ (h) $\sigma^2 = 0.3$, $p_n = 0.5$ (i) $\sigma^2 = 0.3$, $p_n = 1$

(j) $\sigma^2 = 0.5$, $p_n = 0$ (k) $\sigma^2 = 0.5$, $p_n = 0.5$ (l) $\sigma^2 = 0.5$, $p_n = 1$

(m) $\sigma^2 = 1$, $p_n = 0$ (n) $\sigma^2 = 1$, $p_n = 0.5$ (o) $\sigma^2 = 1$, $p_n = 1$

Figure E.11: connectivity 0.1, 50 nodes, 500 observations, 100 simulations. Distribution of the estimated θ values for the true and false causal parents in 100 simulations. The vertical lines indicate the ground truth values for the causal parents linear coefficients. In general we observe that in all settings with enough observations the parameter estimation works reliably.

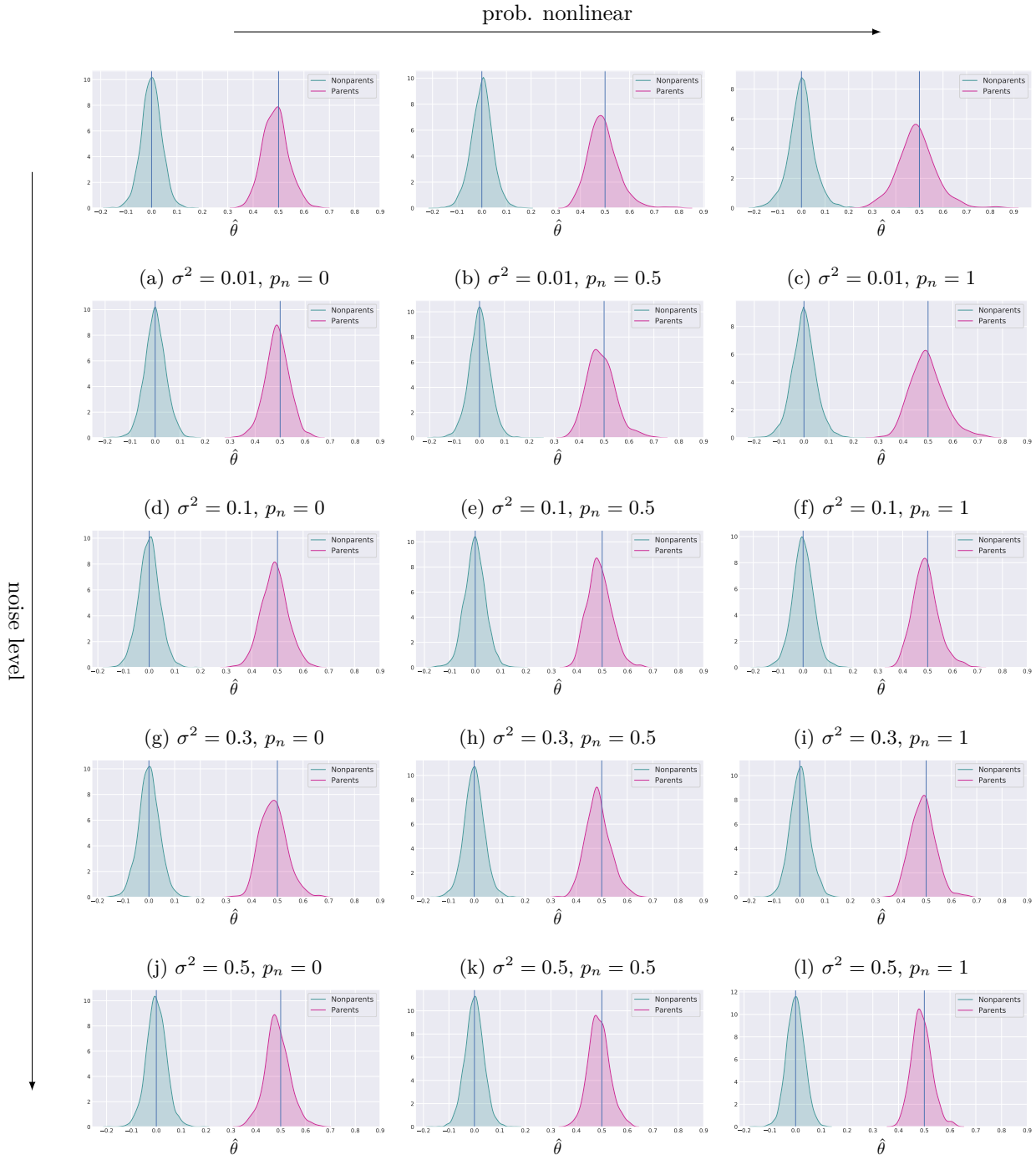

(a) $\sigma^2 = 0.01$, $p_n = 0$ (b) $\sigma^2 = 0.01$, $p_n = 0.5$ (c) $\sigma^2 = 0.01$, $p_n = 1$

(d) $\sigma^2 = 0.1$, $p_n = 0$ (e) $\sigma^2 = 0.1$, $p_n = 0.5$ (f) $\sigma^2 = 0.1$, $p_n = 1$

(g) $\sigma^2 = 0.3$, $p_n = 0$ (h) $\sigma^2 = 0.3$, $p_n = 0.5$ (i) $\sigma^2 = 0.3$, $p_n = 1$

(j) $\sigma^2 = 0.5$, $p_n = 0$ (k) $\sigma^2 = 0.5$, $p_n = 0.5$ (l) $\sigma^2 = 0.5$, $p_n = 1$

(m) $\sigma^2 = 1$, $p_n = 0$ (n) $\sigma^2 = 1$, $p_n = 0.5$ (o) $\sigma^2 = 1$, $p_n = 1$

Figure E.12: connectivity 0.1, 50 nodes, 1000 observations, 100 simulations. Distribution of the estimated θ values for the true and false causal parents in 100 simulations. The vertical lines indicate the ground truth values for the causal parents linear coefficients. In general we observe that in all settings with enough observations the parameter estimation works reliably.

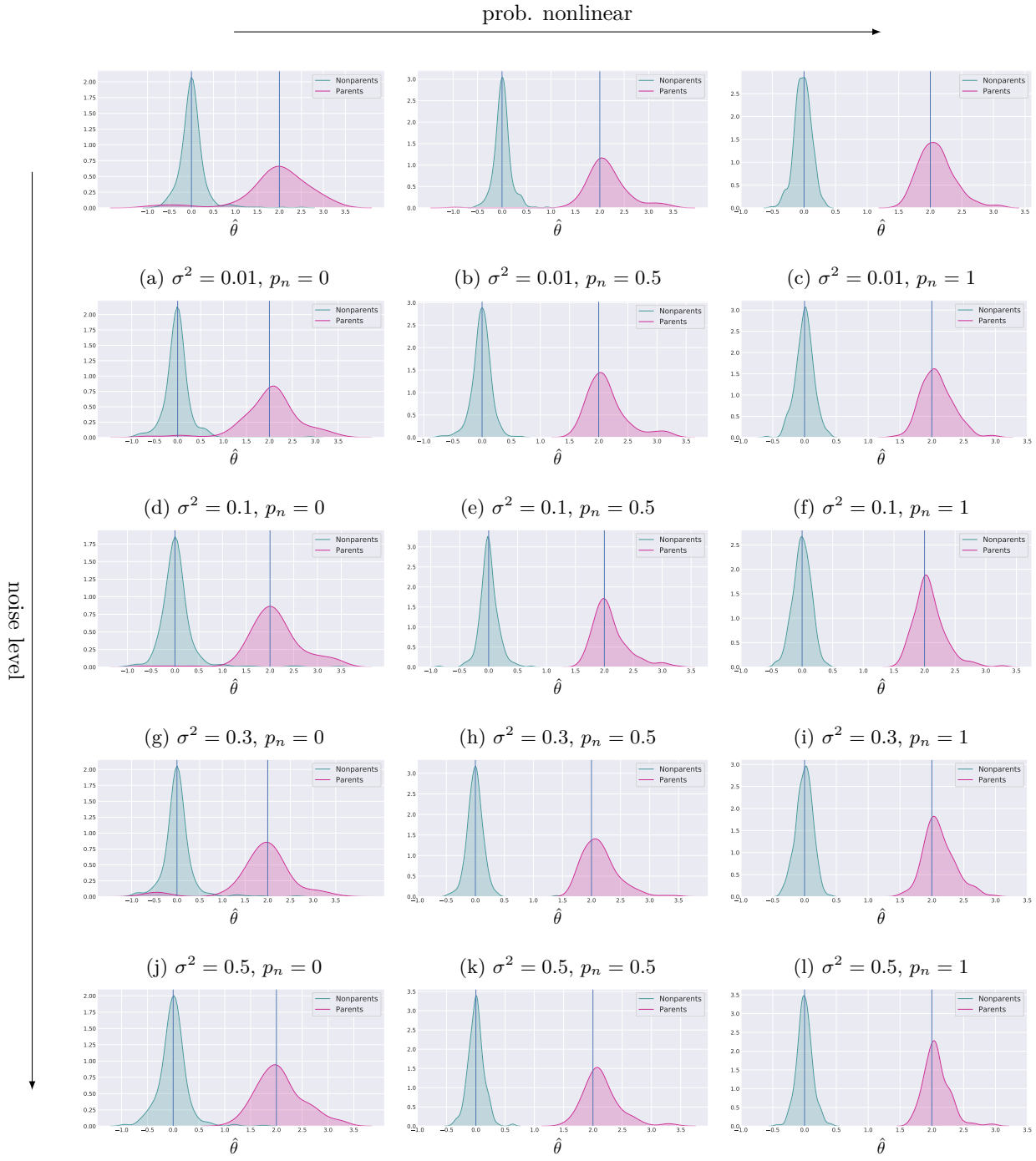

(a) $\sigma^2 = 0.01$, $p_n = 0$ (b) $\sigma^2 = 0.01$, $p_n = 0.5$ (c) $\sigma^2 = 0.01$, $p_n = 1$

(d) $\sigma^2 = 0.1$, $p_n = 0$ (e) $\sigma^2 = 0.1$, $p_n = 0.5$ (f) $\sigma^2 = 0.1$, $p_n = 1$

(g) $\sigma^2 = 0.3$, $p_n = 0$ (h) $\sigma^2 = 0.3$, $p_n = 0.5$ (i) $\sigma^2 = 0.3$, $p_n = 1$

(j) $\sigma^2 = 0.5$, $p_n = 0$ (k) $\sigma^2 = 0.5$, $p_n = 0.5$ (l) $\sigma^2 = 0.5$, $p_n = 1$

(m) $\sigma^2 = 1$, $p_n = 0$ (n) $\sigma^2 = 1$, $p_n = 0.5$ (o) $\sigma^2 = 1$, $p_n = 1$

Figure E.13: 0.3 connectivity, 5 nodes, 100 observations, 100 simulations. Distribution of the estimated θ values for the true and false causal parents in 100 simulations. The vertical lines indicate the ground truth values for the causal parents linear coefficients. In general we observe that in all settings with enough observations the parameter estimation works reliably.

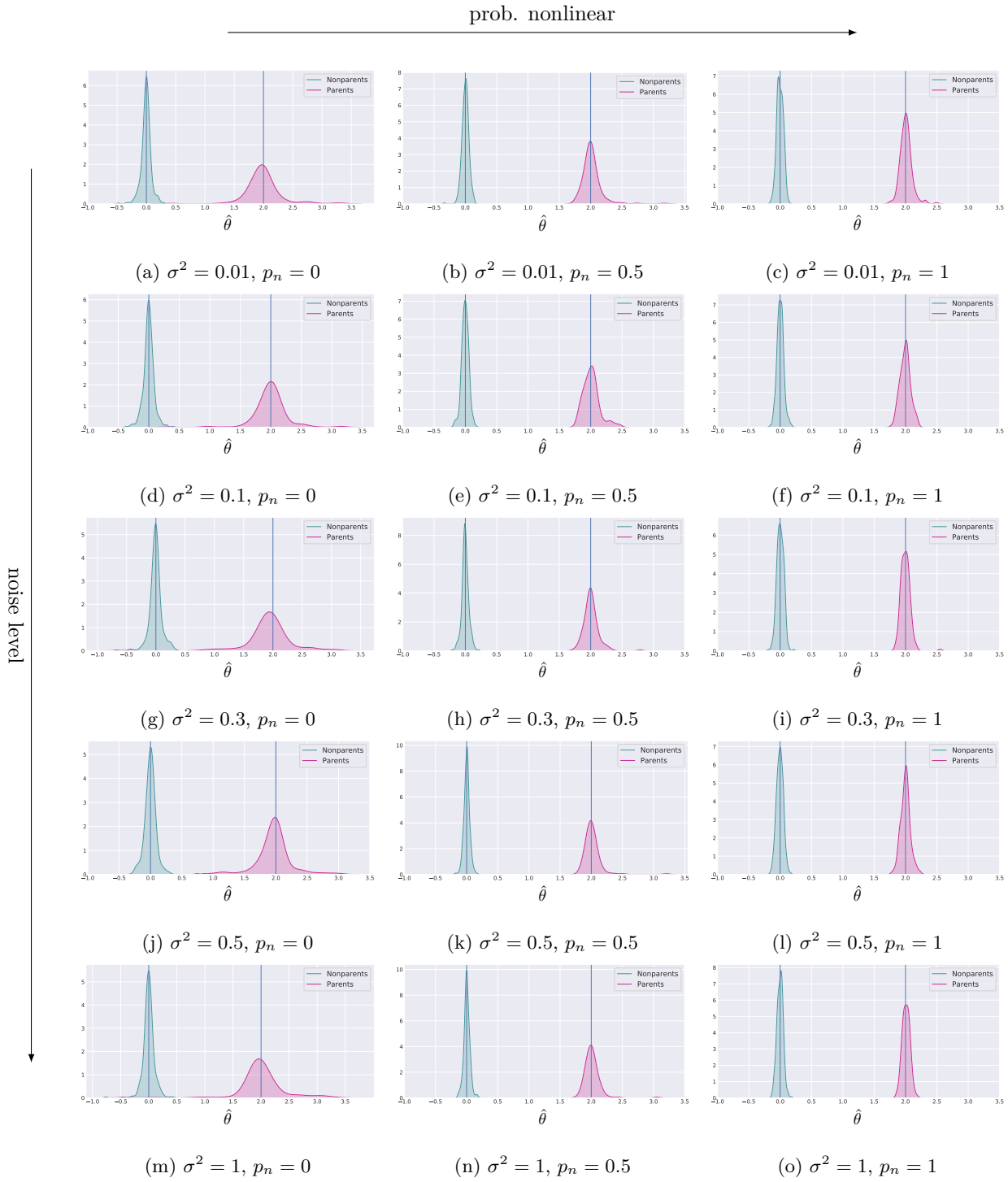

(a) $\sigma^2 = 0.01$, $p_n = 0$ (b) $\sigma^2 = 0.01$, $p_n = 0.5$ (c) $\sigma^2 = 0.01$, $p_n = 1$

(d) $\sigma^2 = 0.1$, $p_n = 0$ (e) $\sigma^2 = 0.1$, $p_n = 0.5$ (f) $\sigma^2 = 0.1$, $p_n = 1$

(g) $\sigma^2 = 0.3$, $p_n = 0$ (h) $\sigma^2 = 0.3$, $p_n = 0.5$ (i) $\sigma^2 = 0.3$, $p_n = 1$

(j) $\sigma^2 = 0.5$, $p_n = 0$ (k) $\sigma^2 = 0.5$, $p_n = 0.5$ (l) $\sigma^2 = 0.5$, $p_n = 1$

(m) $\sigma^2 = 1$, $p_n = 0$ (n) $\sigma^2 = 1$, $p_n = 0.5$ (o) $\sigma^2 = 1$, $p_n = 1$

Figure E.14: 0.3 connectivity, 5 nodes, 500 observations, 100 simulations. Distribution of the estimated θ values for the true and false causal parents in 100 simulations. The vertical lines indicate the ground truth values for the causal parents linear coefficients. In general we observe that in all settings with enough observations the parameter estimation works reliably.

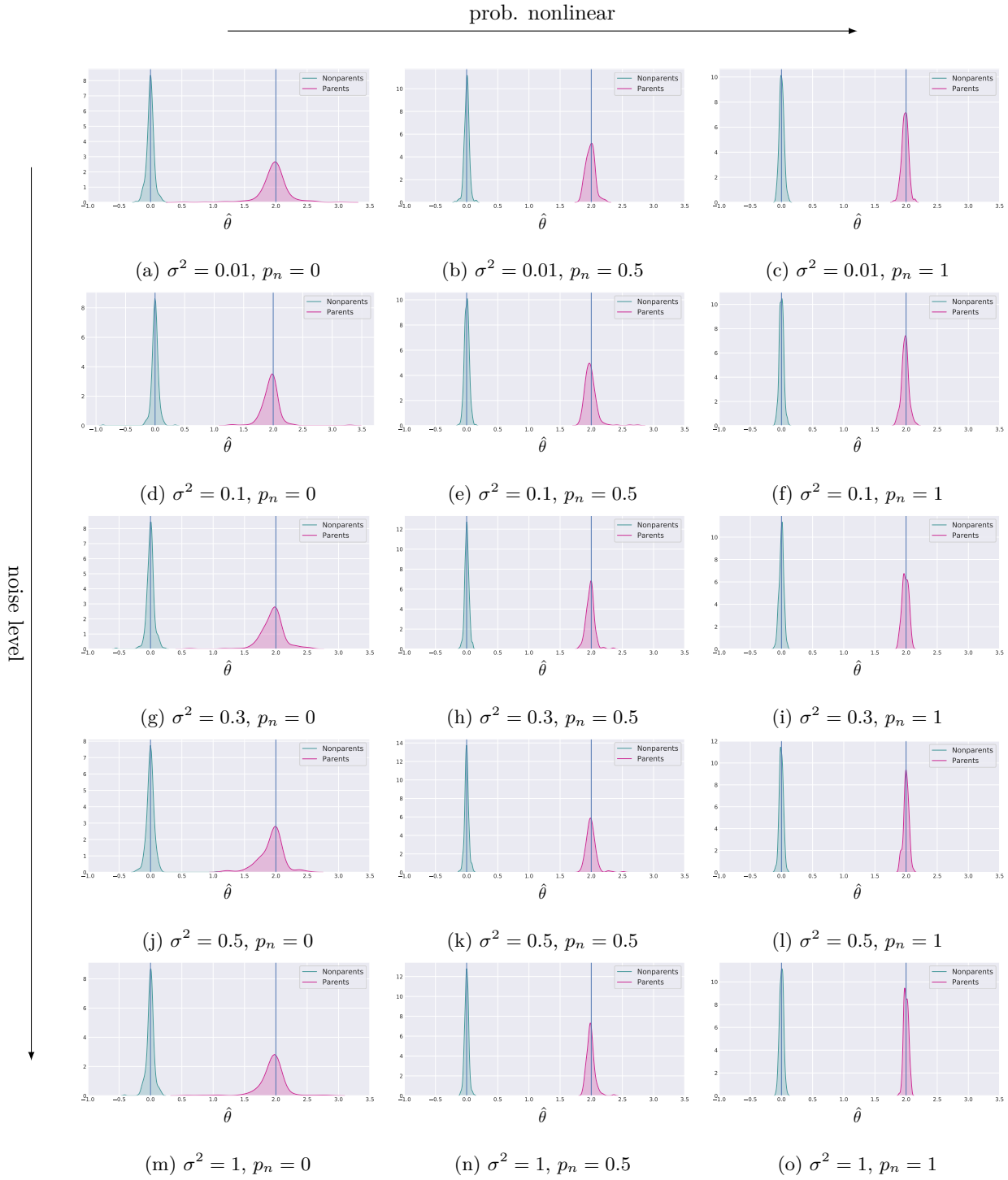

(a) $\sigma^2 = 0.01$, $p_n = 0$ (b) $\sigma^2 = 0.01$, $p_n = 0.5$ (c) $\sigma^2 = 0.01$, $p_n = 1$

(d) $\sigma^2 = 0.1$, $p_n = 0$ (e) $\sigma^2 = 0.1$, $p_n = 0.5$ (f) $\sigma^2 = 0.1$, $p_n = 1$

(g) $\sigma^2 = 0.3$, $p_n = 0$ (h) $\sigma^2 = 0.3$, $p_n = 0.5$ (i) $\sigma^2 = 0.3$, $p_n = 1$

(j) $\sigma^2 = 0.5$, $p_n = 0$ (k) $\sigma^2 = 0.5$, $p_n = 0.5$ (l) $\sigma^2 = 0.5$, $p_n = 1$

(m) $\sigma^2 = 1$, $p_n = 0$ (n) $\sigma^2 = 1$, $p_n = 0.5$ (o) $\sigma^2 = 1$, $p_n = 1$

Figure E.15: 0.3 connectivity, 5 nodes, 1000 observations, 100 simulations. Distribution of the estimated θ values for the true and false causal parents in 100 simulations. The vertical lines indicate the ground truth values for the causal parents linear coefficients. In general we observe that in all settings with enough observations the parameter estimation works reliably.

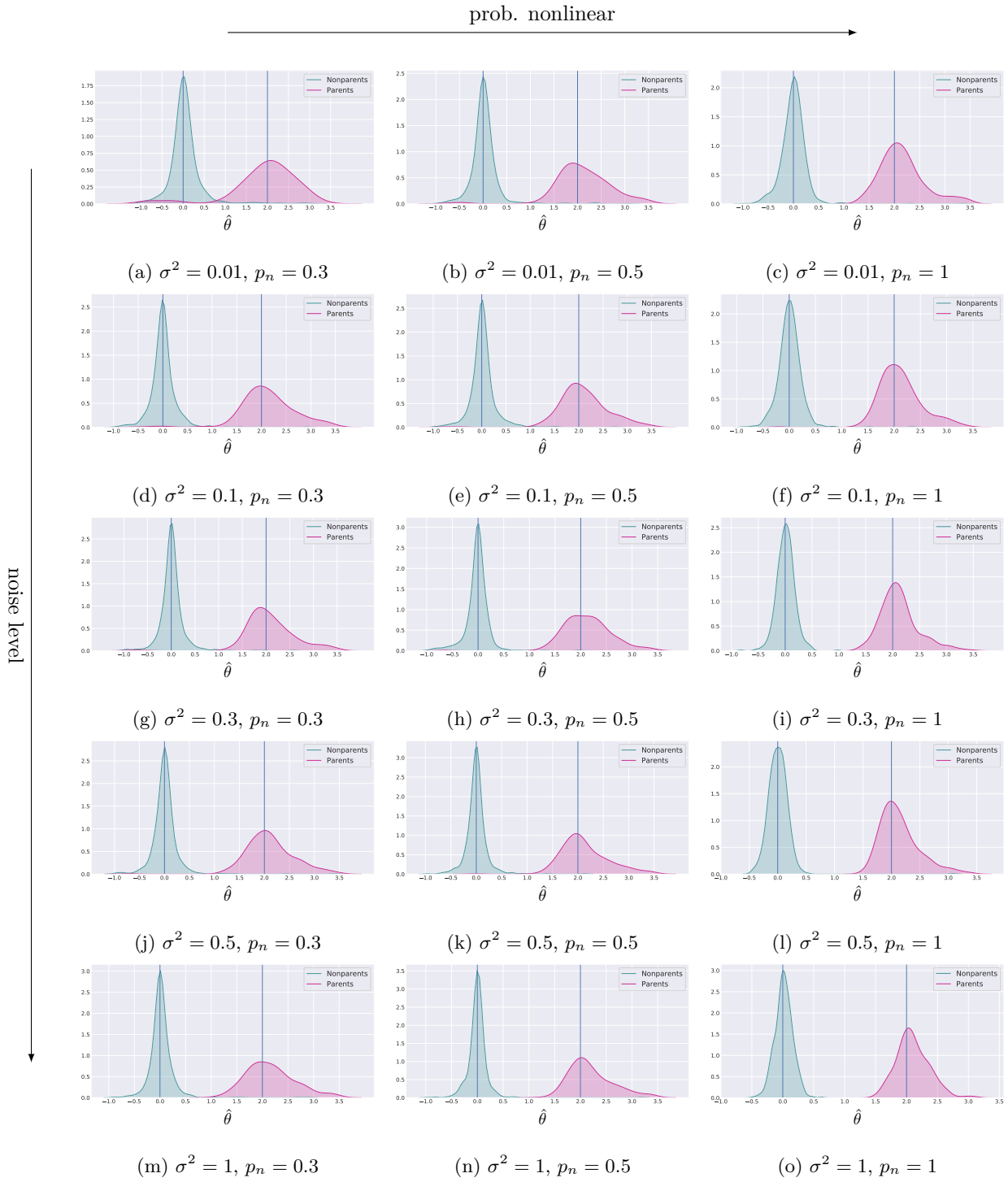

(a) $\sigma^2 = 0.01$, $p_n = 0.3$ (b) $\sigma^2 = 0.01$, $p_n = 0.5$ (c) $\sigma^2 = 0.01$, $p_n = 1$

(d) $\sigma^2 = 0.1$, $p_n = 0.3$ (e) $\sigma^2 = 0.1$, $p_n = 0.5$ (f) $\sigma^2 = 0.1$, $p_n = 1$

(g) $\sigma^2 = 0.3$, $p_n = 0.3$ (h) $\sigma^2 = 0.3$, $p_n = 0.5$ (i) $\sigma^2 = 0.3$, $p_n = 1$

(j) $\sigma^2 = 0.5$, $p_n = 0.3$ (k) $\sigma^2 = 0.5$, $p_n = 0.5$ (l) $\sigma^2 = 0.5$, $p_n = 1$

(m) $\sigma^2 = 1$, $p_n = 0.3$ (n) $\sigma^2 = 1$, $p_n = 0.5$ (o) $\sigma^2 = 1$, $p_n = 1$

Figure E.16: 0.3 connectivity, 10 nodes, 100 observations, 100 simulations. Distribution of the estimated θ values for the true and false causal parents in 100 simulations. The vertical lines indicate the ground truth values for the causal parents linear coefficients. In general we observe that in all settings with enough observations the parameter estimation works reliably.

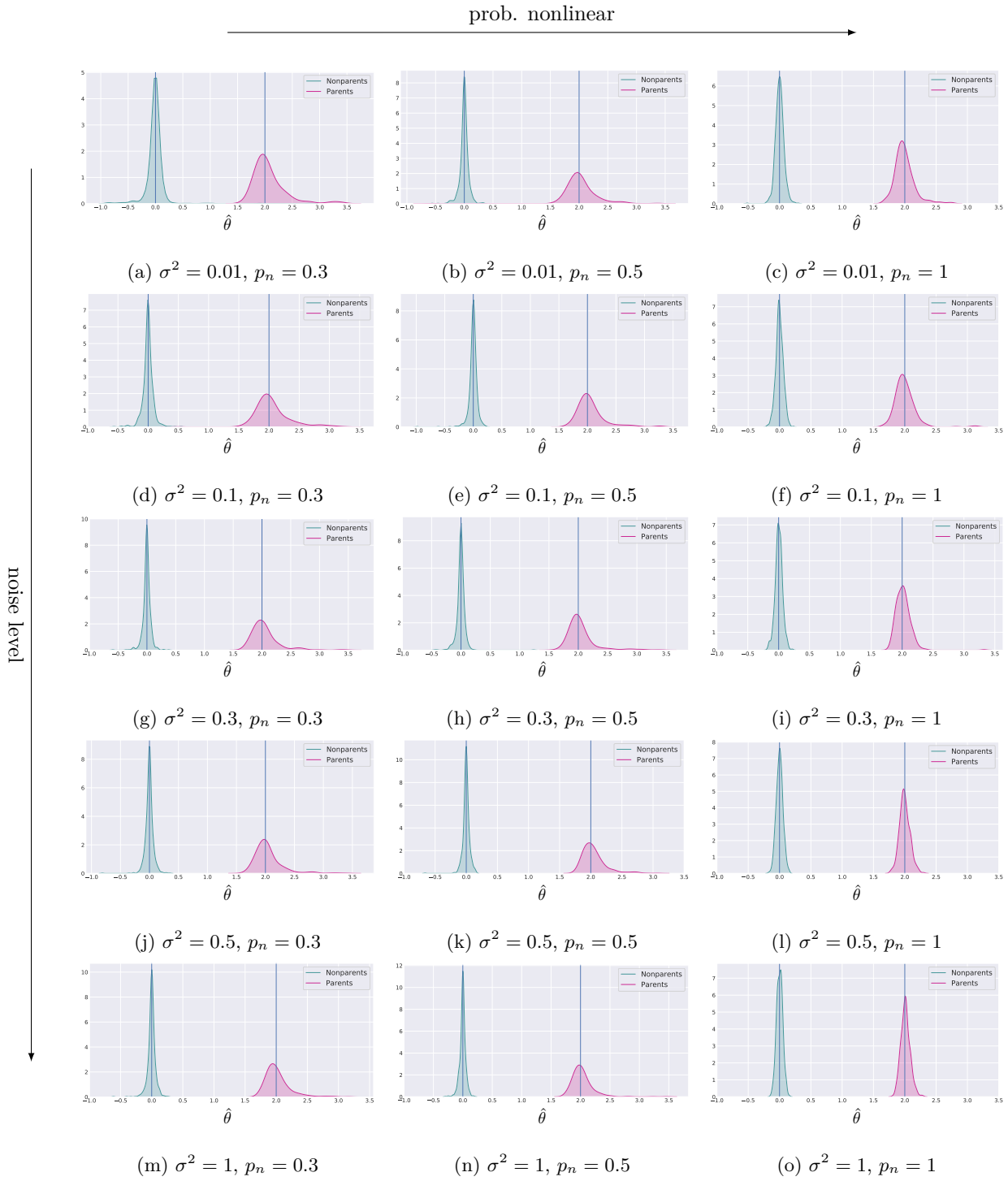

(a) $\sigma^2 = 0.01$, $p_n = 0.3$ (b) $\sigma^2 = 0.01$, $p_n = 0.5$ (c) $\sigma^2 = 0.01$, $p_n = 1$

(d) $\sigma^2 = 0.1$, $p_n = 0.3$ (e) $\sigma^2 = 0.1$, $p_n = 0.5$ (f) $\sigma^2 = 0.1$, $p_n = 1$

(g) $\sigma^2 = 0.3$, $p_n = 0.3$ (h) $\sigma^2 = 0.3$, $p_n = 0.5$ (i) $\sigma^2 = 0.3$, $p_n = 1$

(j) $\sigma^2 = 0.5$, $p_n = 0.3$ (k) $\sigma^2 = 0.5$, $p_n = 0.5$ (l) $\sigma^2 = 0.5$, $p_n = 1$

(m) $\sigma^2 = 1$, $p_n = 0.3$ (n) $\sigma^2 = 1$, $p_n = 0.5$ (o) $\sigma^2 = 1$, $p_n = 1$

Figure E.17: 0.3 connectivity, 10 nodes, 500 observations, 100 simulations. Distribution of the estimated θ values for the true and false causal parents in 100 simulations. The vertical lines indicate the ground truth values for the causal parents linear coefficients. In general we observe that in all settings with enough observations the parameter estimation works reliably.

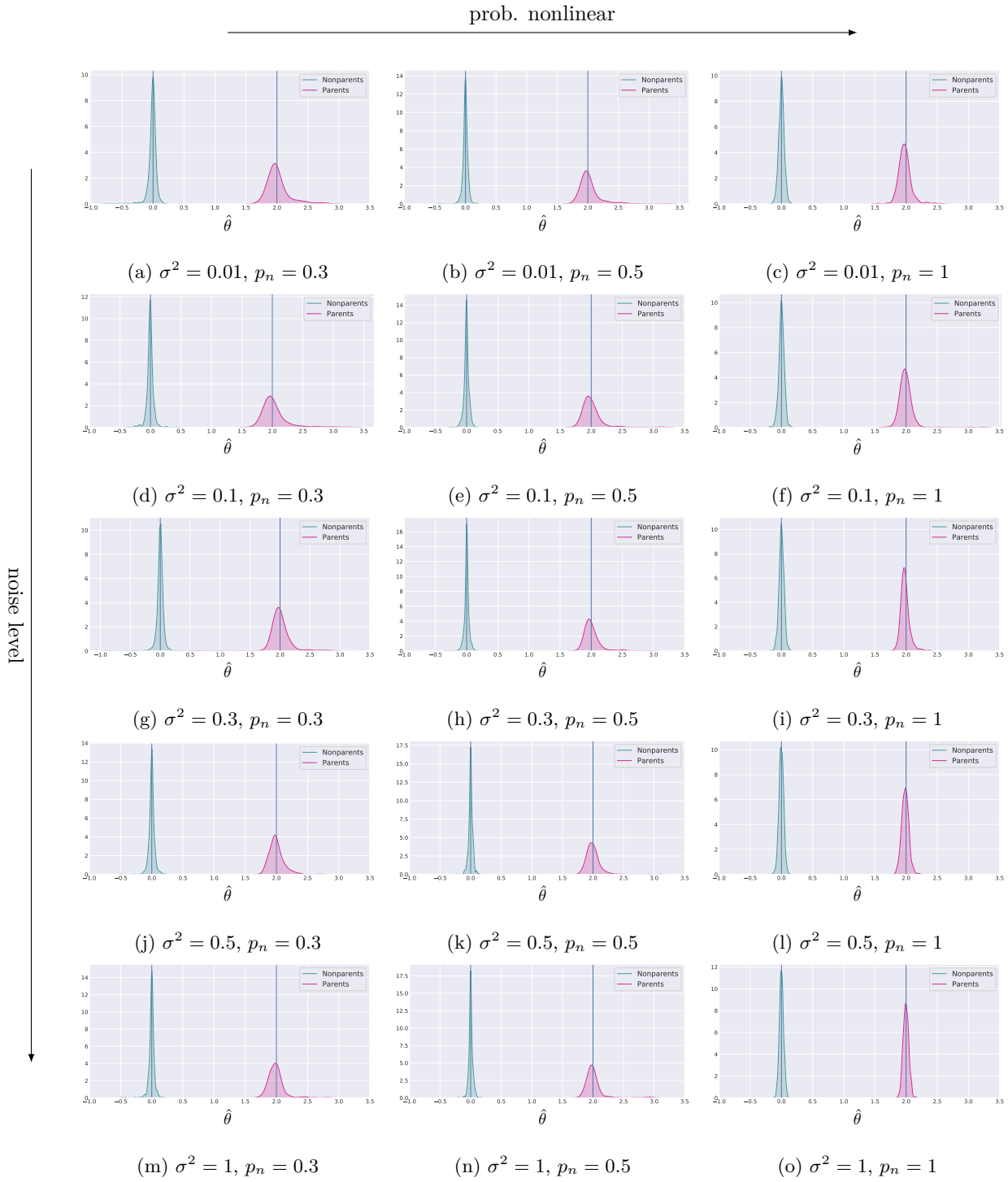

(a) $\sigma^2 = 0.01$, $p_n = 0.3$ (b) $\sigma^2 = 0.01$, $p_n = 0.5$ (c) $\sigma^2 = 0.01$, $p_n = 1$

(d) $\sigma^2 = 0.1$, $p_n = 0.3$ (e) $\sigma^2 = 0.1$, $p_n = 0.5$ (f) $\sigma^2 = 0.1$, $p_n = 1$

(g) $\sigma^2 = 0.3$, $p_n = 0.3$ (h) $\sigma^2 = 0.3$, $p_n = 0.5$ (i) $\sigma^2 = 0.3$, $p_n = 1$

(j) $\sigma^2 = 0.5$, $p_n = 0.3$ (k) $\sigma^2 = 0.5$, $p_n = 0.5$ (l) $\sigma^2 = 0.5$, $p_n = 1$

(m) $\sigma^2 = 1$, $p_n = 0.3$ (n) $\sigma^2 = 1$, $p_n = 0.5$ (o) $\sigma^2 = 1$, $p_n = 1$

Figure E.18: 0.3 connectivity, 10 nodes, 1000 observations, 100 simulations. Distribution of the estimated θ values for the true and false causal parents in 100 simulations. The vertical lines indicate the ground truth values for the causal parents linear coefficients. In general we observe that in all settings with enough observations the parameter estimation works reliably.

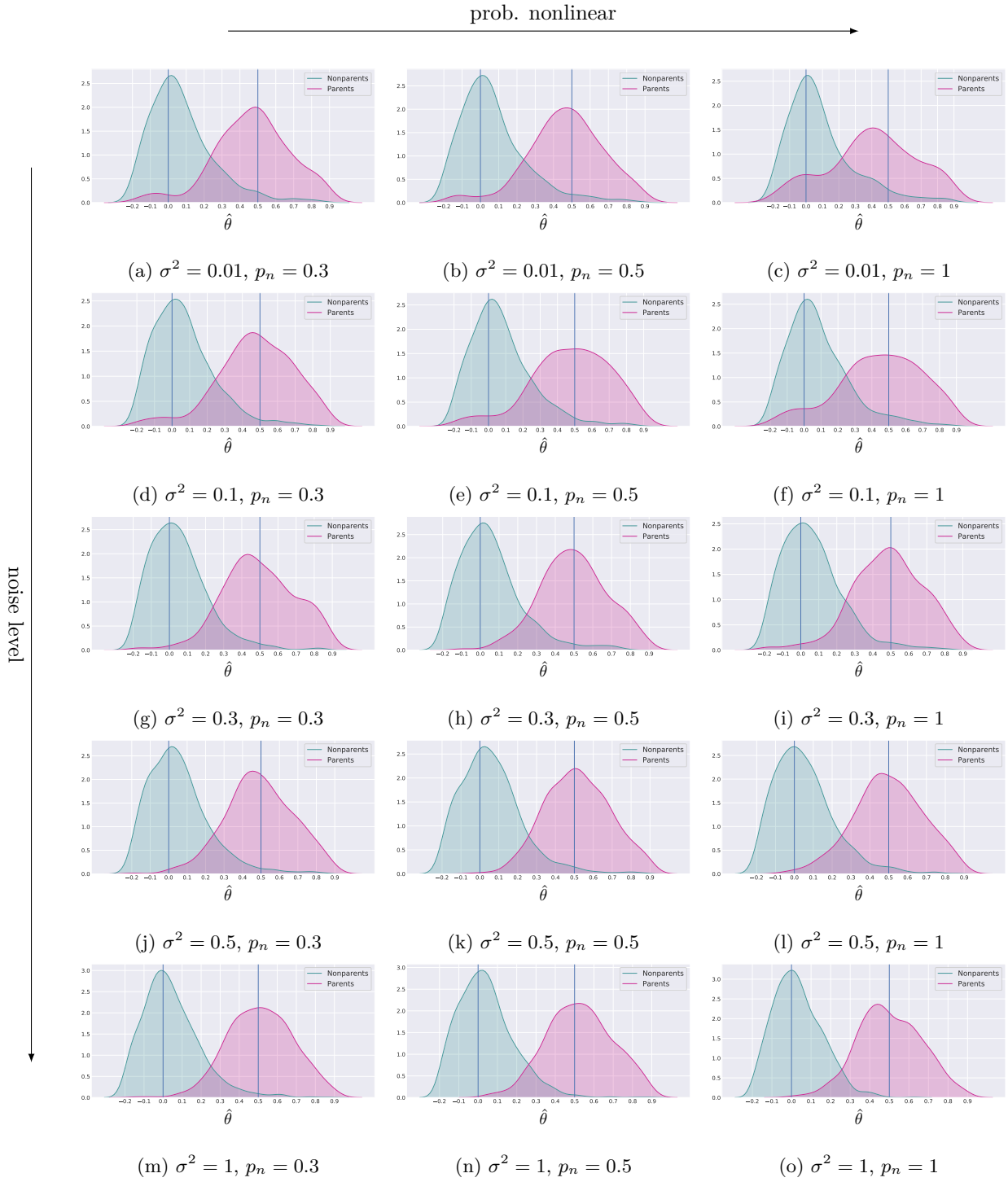

(a) $\sigma^2 = 0.01$, $p_n = 0.3$ (b) $\sigma^2 = 0.01$, $p_n = 0.5$ (c) $\sigma^2 = 0.01$, $p_n = 1$

(d) $\sigma^2 = 0.1$, $p_n = 0.3$ (e) $\sigma^2 = 0.1$, $p_n = 0.5$ (f) $\sigma^2 = 0.1$, $p_n = 1$

(g) $\sigma^2 = 0.3$, $p_n = 0.3$ (h) $\sigma^2 = 0.3$, $p_n = 0.5$ (i) $\sigma^2 = 0.3$, $p_n = 1$

(j) $\sigma^2 = 0.5$, $p_n = 0.3$ (k) $\sigma^2 = 0.5$, $p_n = 0.5$ (l) $\sigma^2 = 0.5$, $p_n = 1$

(m) $\sigma^2 = 1$, $p_n = 0.3$ (n) $\sigma^2 = 1$, $p_n = 0.5$ (o) $\sigma^2 = 1$, $p_n = 1$

Figure E.19: 0.3 connectivity, 20 nodes, 100 observations, 100 simulations. Distribution of the estimated θ values for the true and false causal parents in 100 simulations. The vertical lines indicate the ground truth values for the causal parents linear coefficients. In general we observe that in all settings with enough observations the parameter estimation works reliably.

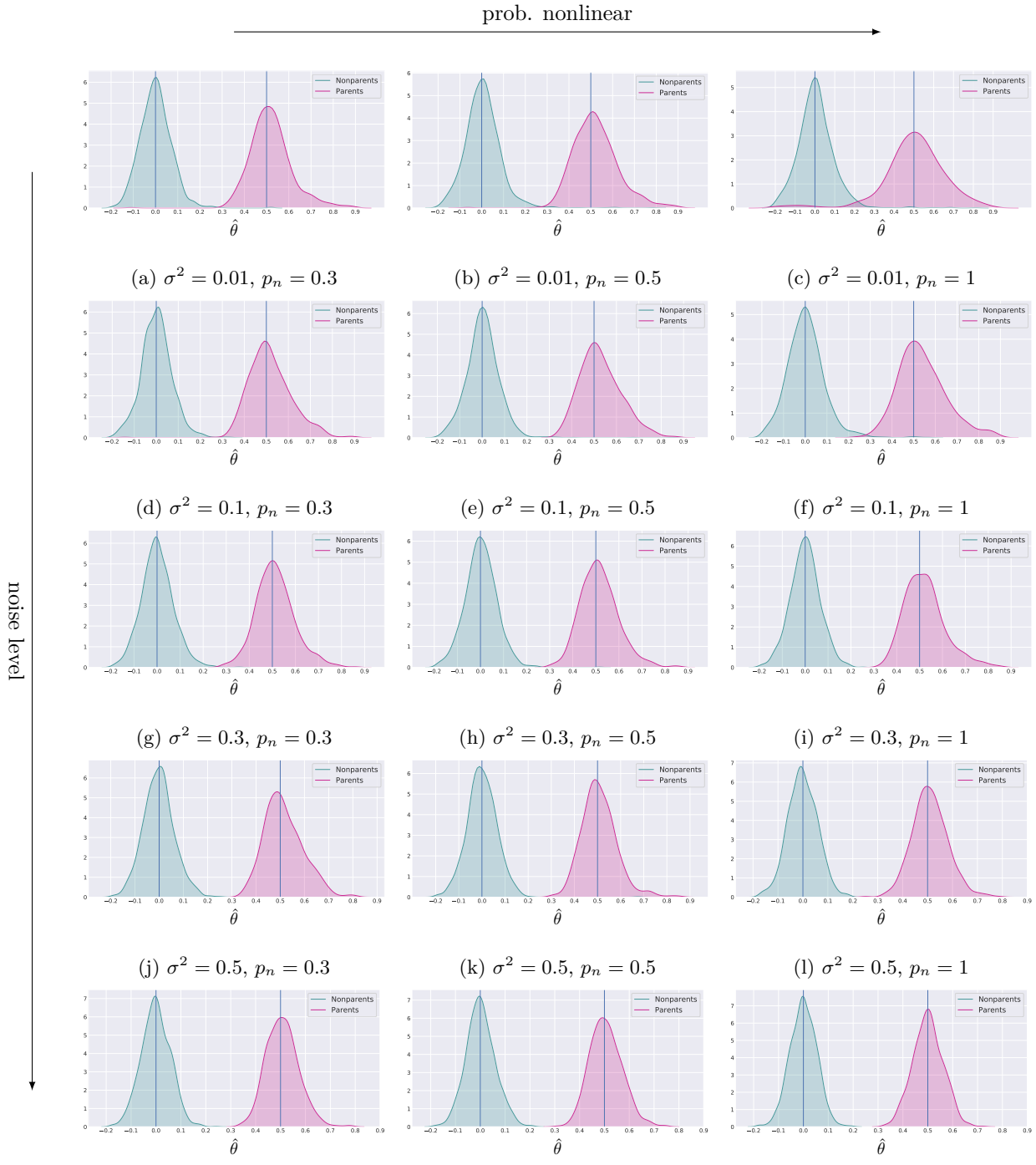

(a) $\sigma^2 = 0.01$, $p_n = 0.3$ (b) $\sigma^2 = 0.01$, $p_n = 0.5$ (c) $\sigma^2 = 0.01$, $p_n = 1$

(d) $\sigma^2 = 0.1$, $p_n = 0.3$ (e) $\sigma^2 = 0.1$, $p_n = 0.5$ (f) $\sigma^2 = 0.1$, $p_n = 1$

(g) $\sigma^2 = 0.3$, $p_n = 0.3$ (h) $\sigma^2 = 0.3$, $p_n = 0.5$ (i) $\sigma^2 = 0.3$, $p_n = 1$

(j) $\sigma^2 = 0.5$, $p_n = 0.3$ (k) $\sigma^2 = 0.5$, $p_n = 0.5$ (l) $\sigma^2 = 0.5$, $p_n = 1$

(m) $\sigma^2 = 1$, $p_n = 0.3$ (n) $\sigma^2 = 1$, $p_n = 0.5$ (o) $\sigma^2 = 1$, $p_n = 1$

Figure E.20: 0.3 connectivity, 20 nodes, 500 observations, 100 simulations. Distribution of the estimated θ values for the true and false causal parents in 100 simulations. The vertical lines indicate the ground truth values for the causal parents linear coefficients. In general we observe that in all settings with enough observations the parameter estimation works reliably.

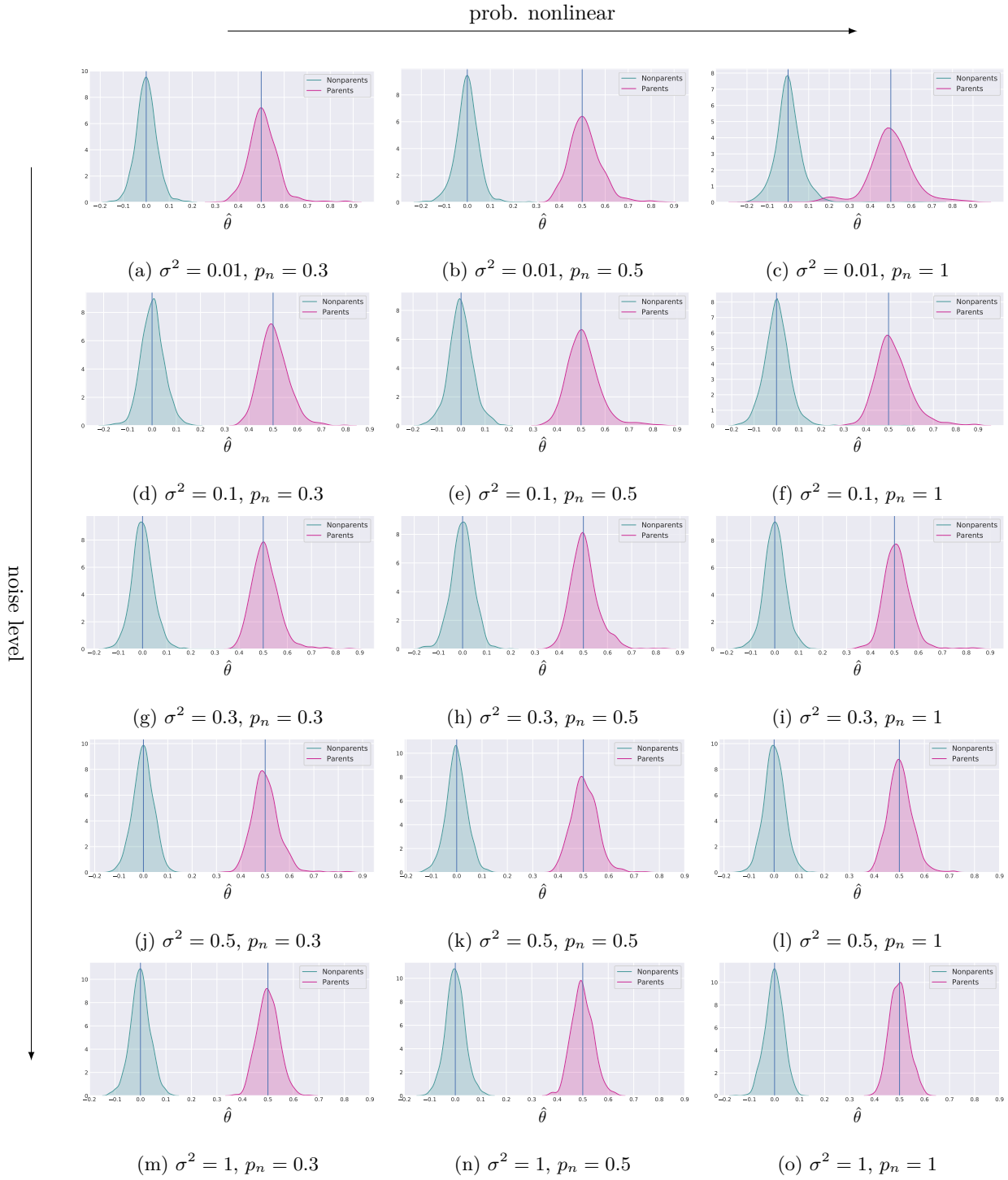

(a) $\sigma^2 = 0.01$, $p_n = 0.3$ (b) $\sigma^2 = 0.01$, $p_n = 0.5$ (c) $\sigma^2 = 0.01$, $p_n = 1$

(d) $\sigma^2 = 0.1$, $p_n = 0.3$ (e) $\sigma^2 = 0.1$, $p_n = 0.5$ (f) $\sigma^2 = 0.1$, $p_n = 1$

(g) $\sigma^2 = 0.3$, $p_n = 0.3$ (h) $\sigma^2 = 0.3$, $p_n = 0.5$ (i) $\sigma^2 = 0.3$, $p_n = 1$

(j) $\sigma^2 = 0.5$, $p_n = 0.3$ (k) $\sigma^2 = 0.5$, $p_n = 0.5$ (l) $\sigma^2 = 0.5$, $p_n = 1$

(m) $\sigma^2 = 1$, $p_n = 0.3$ (n) $\sigma^2 = 1$, $p_n = 0.5$ (o) $\sigma^2 = 1$, $p_n = 1$

Figure E.21: 0.3 connectivity, 20 nodes, 1000 observations, 100 simulations. Distribution of the estimated θ values for the true and false causal parents in 100 simulations. The vertical lines indicate the ground truth values for the causal parents linear coefficients. In general we observe that in all settings with enough observations the parameter estimation works reliably.

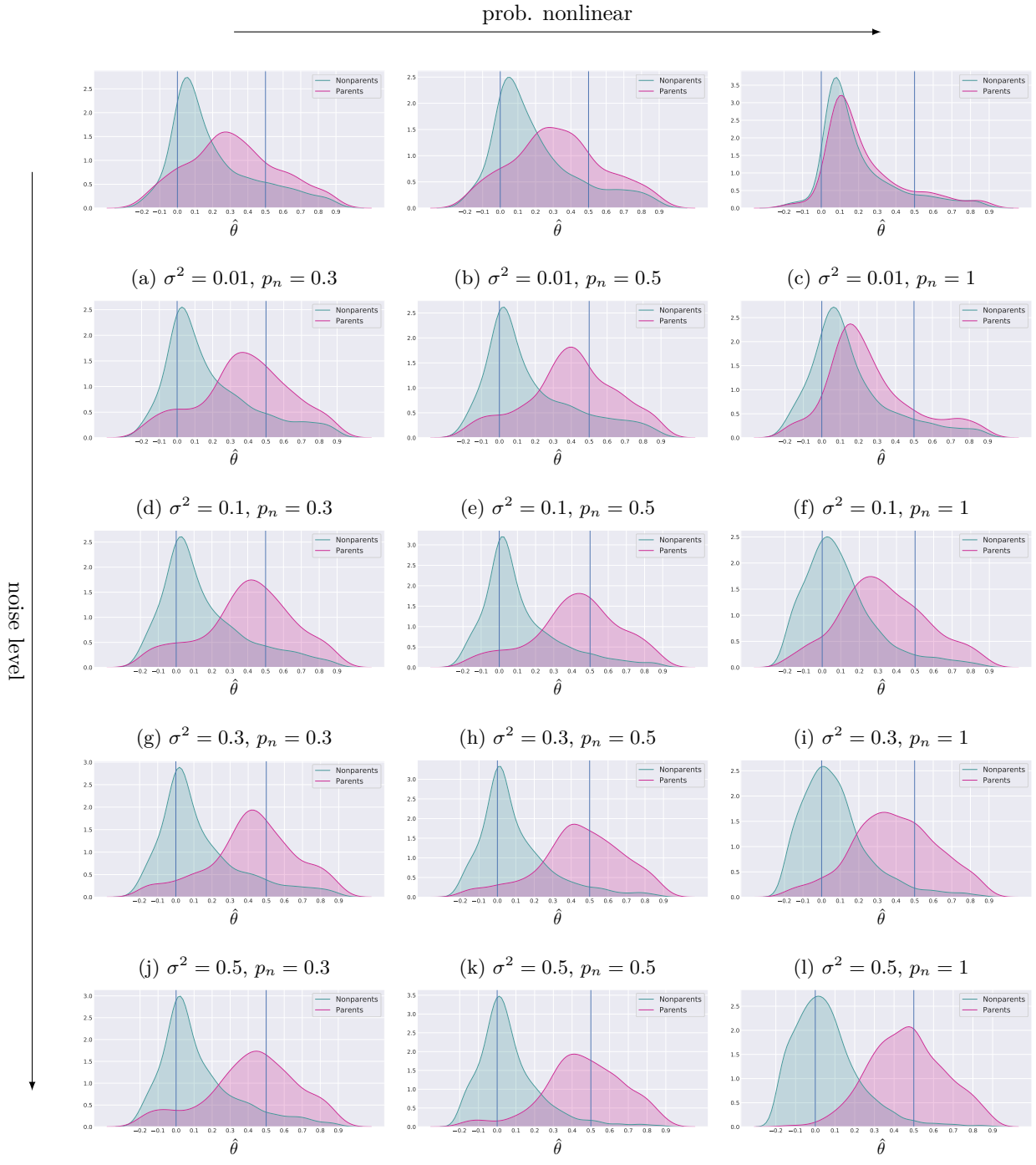

(a) $\sigma^2 = 0.01$, $p_n = 0.3$ (b) $\sigma^2 = 0.01$, $p_n = 0.5$ (c) $\sigma^2 = 0.01$, $p_n = 1$

(d) $\sigma^2 = 0.1$, $p_n = 0.3$ (e) $\sigma^2 = 0.1$, $p_n = 0.5$ (f) $\sigma^2 = 0.1$, $p_n = 1$

(g) $\sigma^2 = 0.3$, $p_n = 0.3$ (h) $\sigma^2 = 0.3$, $p_n = 0.5$ (i) $\sigma^2 = 0.3$, $p_n = 1$

(j) $\sigma^2 = 0.5$, $p_n = 0.3$ (k) $\sigma^2 = 0.5$, $p_n = 0.5$ (l) $\sigma^2 = 0.5$, $p_n = 1$

(m) $\sigma^2 = 1$, $p_n = 0.3$ (n) $\sigma^2 = 1$, $p_n = 0.5$ (o) $\sigma^2 = 1$, $p_n = 1$

Figure E.22: 0.3 connectivity, 50 nodes, 100 observations, 100 simulations. Distribution of the estimated θ values for the true and false causal parents in 100 simulations. The vertical lines indicate the ground truth values for the causal parents linear coefficients. In general we observe that in all settings with enough observations the parameter estimation works reliably.

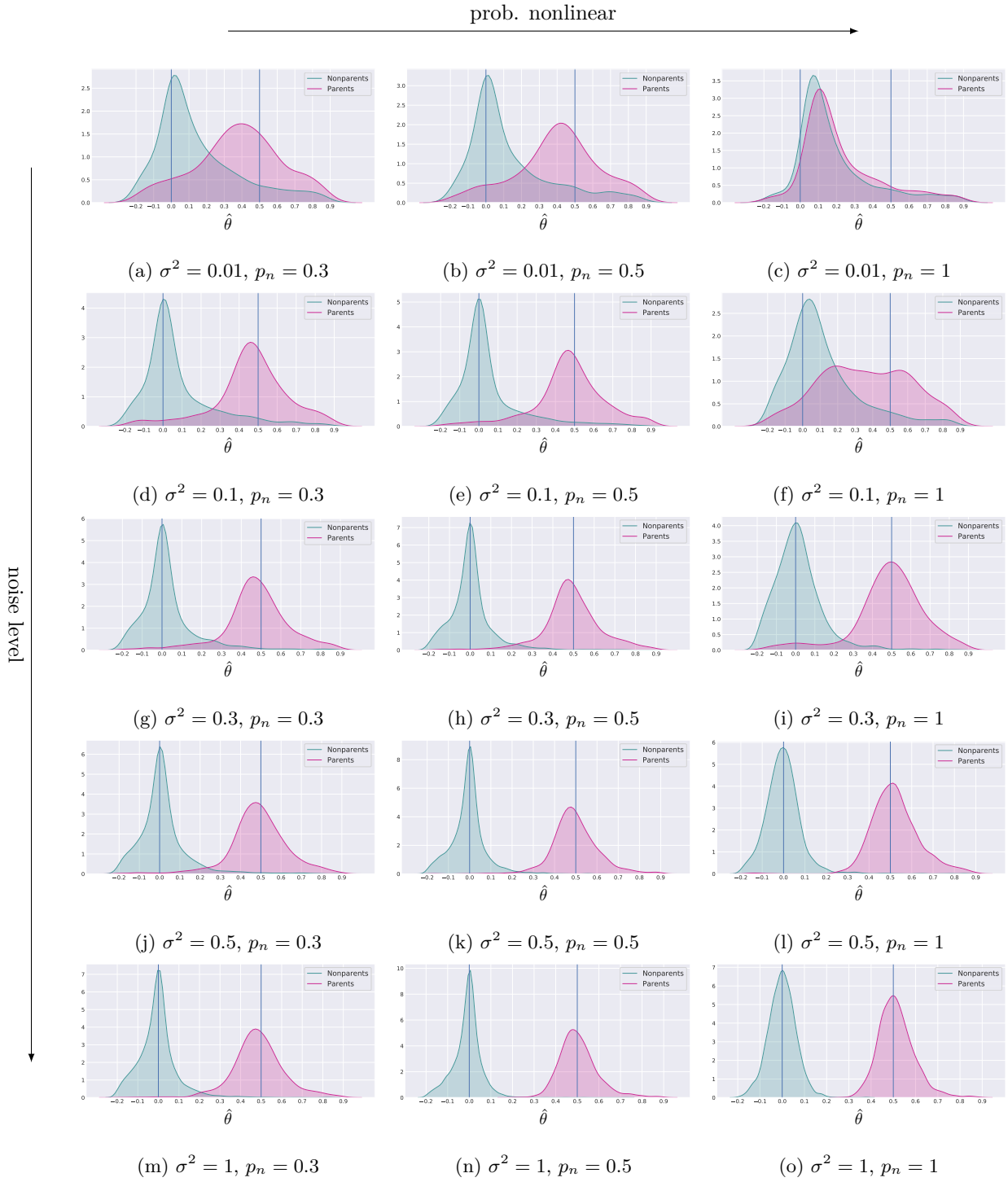

(a) $\sigma^2 = 0.01$, $p_n = 0.3$ (b) $\sigma^2 = 0.01$, $p_n = 0.5$ (c) $\sigma^2 = 0.01$, $p_n = 1$

(d) $\sigma^2 = 0.1$, $p_n = 0.3$ (e) $\sigma^2 = 0.1$, $p_n = 0.5$ (f) $\sigma^2 = 0.1$, $p_n = 1$

(g) $\sigma^2 = 0.3$, $p_n = 0.3$ (h) $\sigma^2 = 0.3$, $p_n = 0.5$ (i) $\sigma^2 = 0.3$, $p_n = 1$

(j) $\sigma^2 = 0.5$, $p_n = 0.3$ (k) $\sigma^2 = 0.5$, $p_n = 0.5$ (l) $\sigma^2 = 0.5$, $p_n = 1$

(m) $\sigma^2 = 1$, $p_n = 0.3$ (n) $\sigma^2 = 1$, $p_n = 0.5$ (o) $\sigma^2 = 1$, $p_n = 1$

Figure E.23: 0.3 connectivity, 50 nodes, 500 observations, 100 simulations. Distribution of the estimated θ values for the true and false causal parents in 100 simulations. The vertical lines indicate the ground truth values for the causal parents linear coefficients. In general we observe that in all settings with enough observations the parameter estimation works reliably.

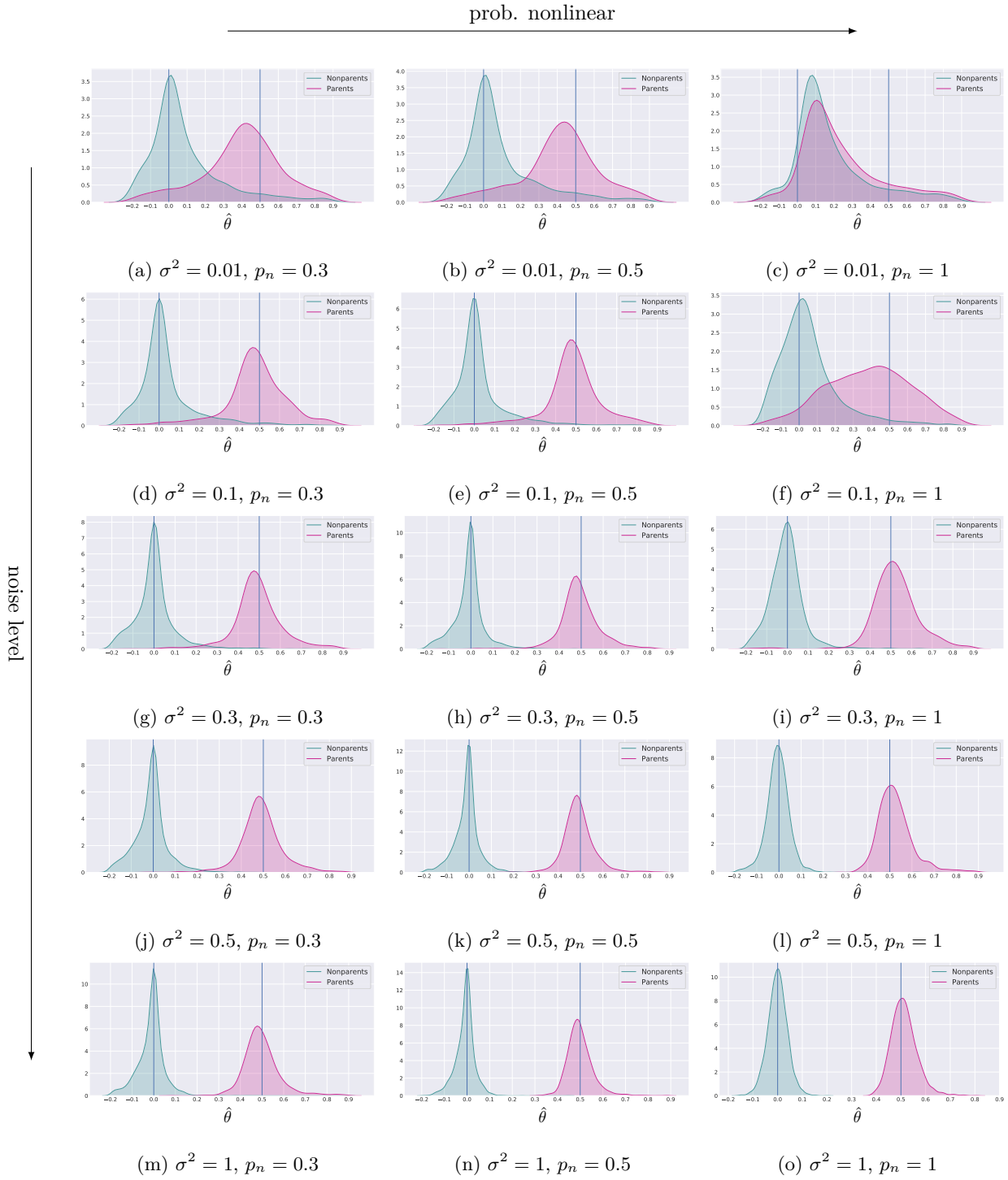

(a) $\sigma^2 = 0.01$, $p_n = 0.3$ (b) $\sigma^2 = 0.01$, $p_n = 0.5$ (c) $\sigma^2 = 0.01$, $p_n = 1$

(d) $\sigma^2 = 0.1$, $p_n = 0.3$ (e) $\sigma^2 = 0.1$, $p_n = 0.5$ (f) $\sigma^2 = 0.1$, $p_n = 1$

(g) $\sigma^2 = 0.3$, $p_n = 0.3$ (h) $\sigma^2 = 0.3$, $p_n = 0.5$ (i) $\sigma^2 = 0.3$, $p_n = 1$

(j) $\sigma^2 = 0.5$, $p_n = 0.3$ (k) $\sigma^2 = 0.5$, $p_n = 0.5$ (l) $\sigma^2 = 0.5$, $p_n = 1$

(m) $\sigma^2 = 1$, $p_n = 0.3$ (n) $\sigma^2 = 1$, $p_n = 0.5$ (o) $\sigma^2 = 1$, $p_n = 1$

Figure E.24: 0.3 connectivity, 50 nodes, 1000 observations, 100 simulations. Distribution of the estimated θ values for the true and false causal parents in 100 simulations. The vertical lines indicate the ground truth values for the causal parents linear coefficients. In general we observe that in all settings with enough observations the parameter estimation works reliably.

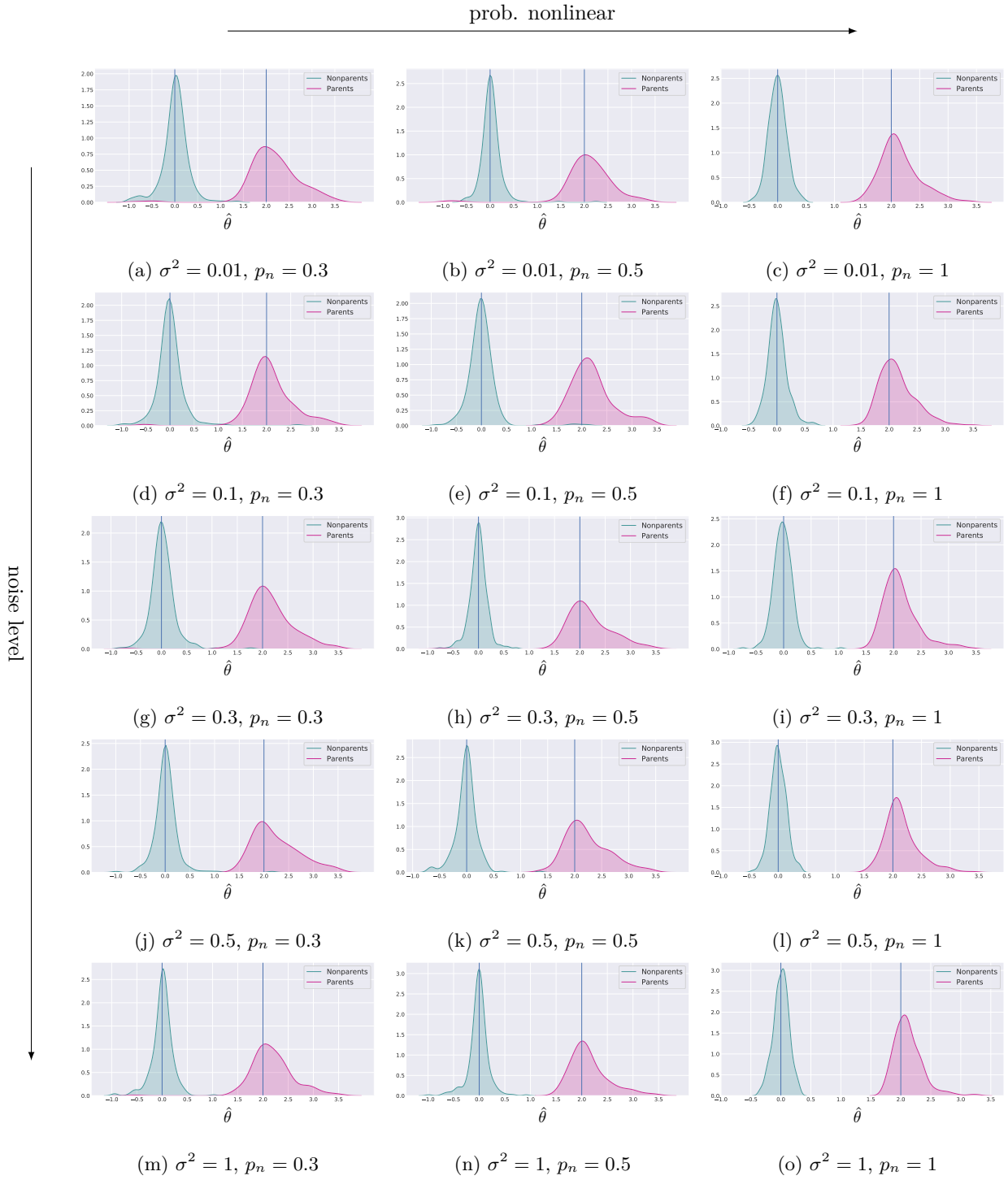

(a) $\sigma^2 = 0.01$, $p_n = 0.3$ (b) $\sigma^2 = 0.01$, $p_n = 0.5$ (c) $\sigma^2 = 0.01$, $p_n = 1$

(d) $\sigma^2 = 0.1$, $p_n = 0.3$ (e) $\sigma^2 = 0.1$, $p_n = 0.5$ (f) $\sigma^2 = 0.1$, $p_n = 1$

(g) $\sigma^2 = 0.3$, $p_n = 0.3$ (h) $\sigma^2 = 0.3$, $p_n = 0.5$ (i) $\sigma^2 = 0.3$, $p_n = 1$

(j) $\sigma^2 = 0.5$, $p_n = 0.3$ (k) $\sigma^2 = 0.5$, $p_n = 0.5$ (l) $\sigma^2 = 0.5$, $p_n = 1$

(m) $\sigma^2 = 1$, $p_n = 0.3$ (n) $\sigma^2 = 1$, $p_n = 0.5$ (o) $\sigma^2 = 1$, $p_n = 1$

Figure E.25: 0.5 connectivity, 5 nodes, 100 observations, 100 simulations. Distribution of the estimated θ values for the true and false causal parents in 100 simulations. The vertical lines indicate the ground truth values for the causal parents linear coefficients. In general we observe that in all settings with enough observations the parameter estimation works reliably.

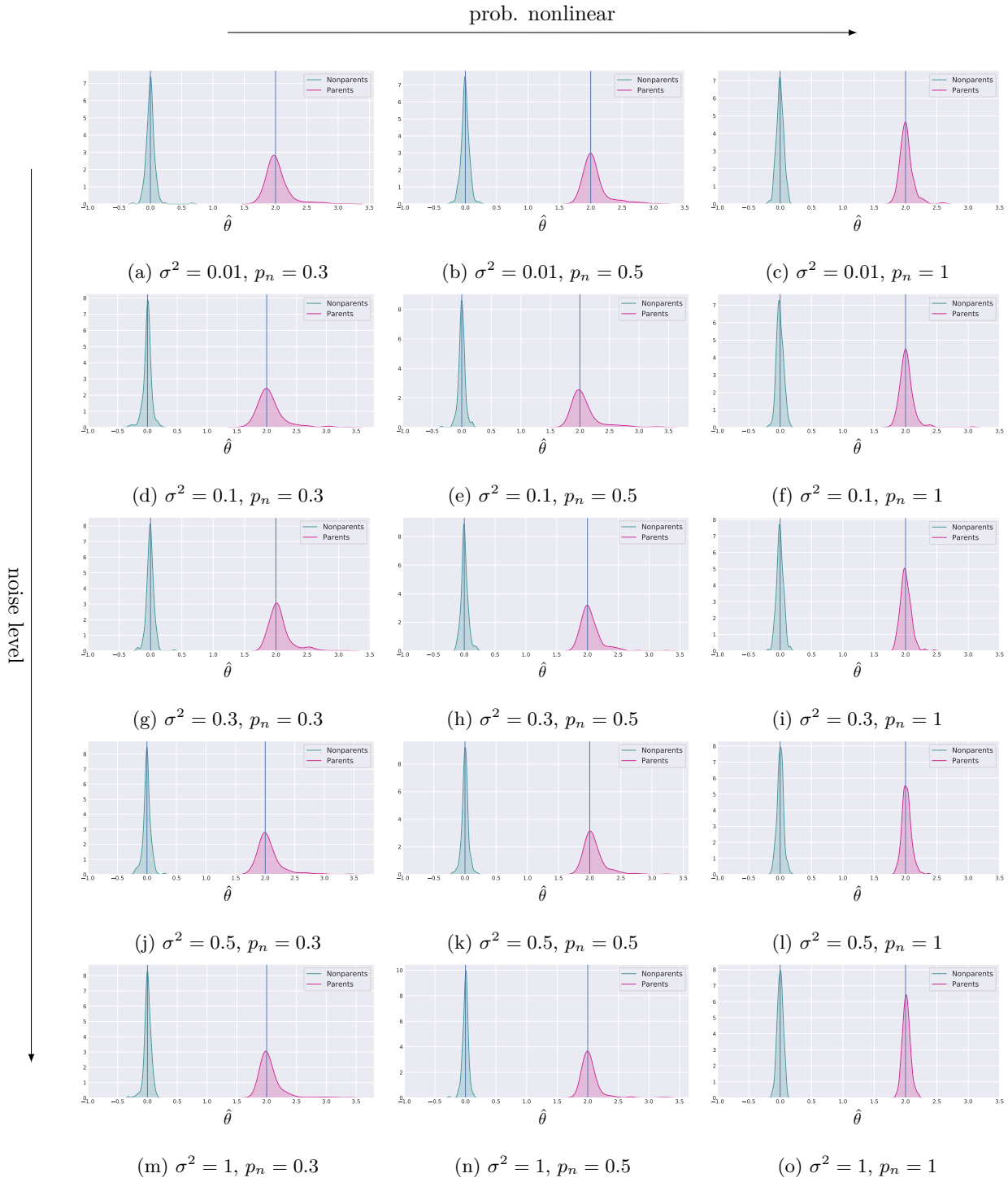

(a) $\sigma^2 = 0.01$, $p_n = 0.3$ (b) $\sigma^2 = 0.01$, $p_n = 0.5$ (c) $\sigma^2 = 0.01$, $p_n = 1$

(d) $\sigma^2 = 0.1$, $p_n = 0.3$ (e) $\sigma^2 = 0.1$, $p_n = 0.5$ (f) $\sigma^2 = 0.1$, $p_n = 1$

(g) $\sigma^2 = 0.3$, $p_n = 0.3$ (h) $\sigma^2 = 0.3$, $p_n = 0.5$ (i) $\sigma^2 = 0.3$, $p_n = 1$

(j) $\sigma^2 = 0.5$, $p_n = 0.3$ (k) $\sigma^2 = 0.5$, $p_n = 0.5$ (l) $\sigma^2 = 0.5$, $p_n = 1$

(m) $\sigma^2 = 1$, $p_n = 0.3$ (n) $\sigma^2 = 1$, $p_n = 0.5$ (o) $\sigma^2 = 1$, $p_n = 1$

Figure E.26: 0.5 connectivity, 5 nodes, 500 observations, 100 simulations. Distribution of the estimated θ values for the true and false causal parents in 100 simulations. The vertical lines indicate the ground truth values for the causal parents linear coefficients. In general we observe that in all settings with enough observations the parameter estimation works reliably.

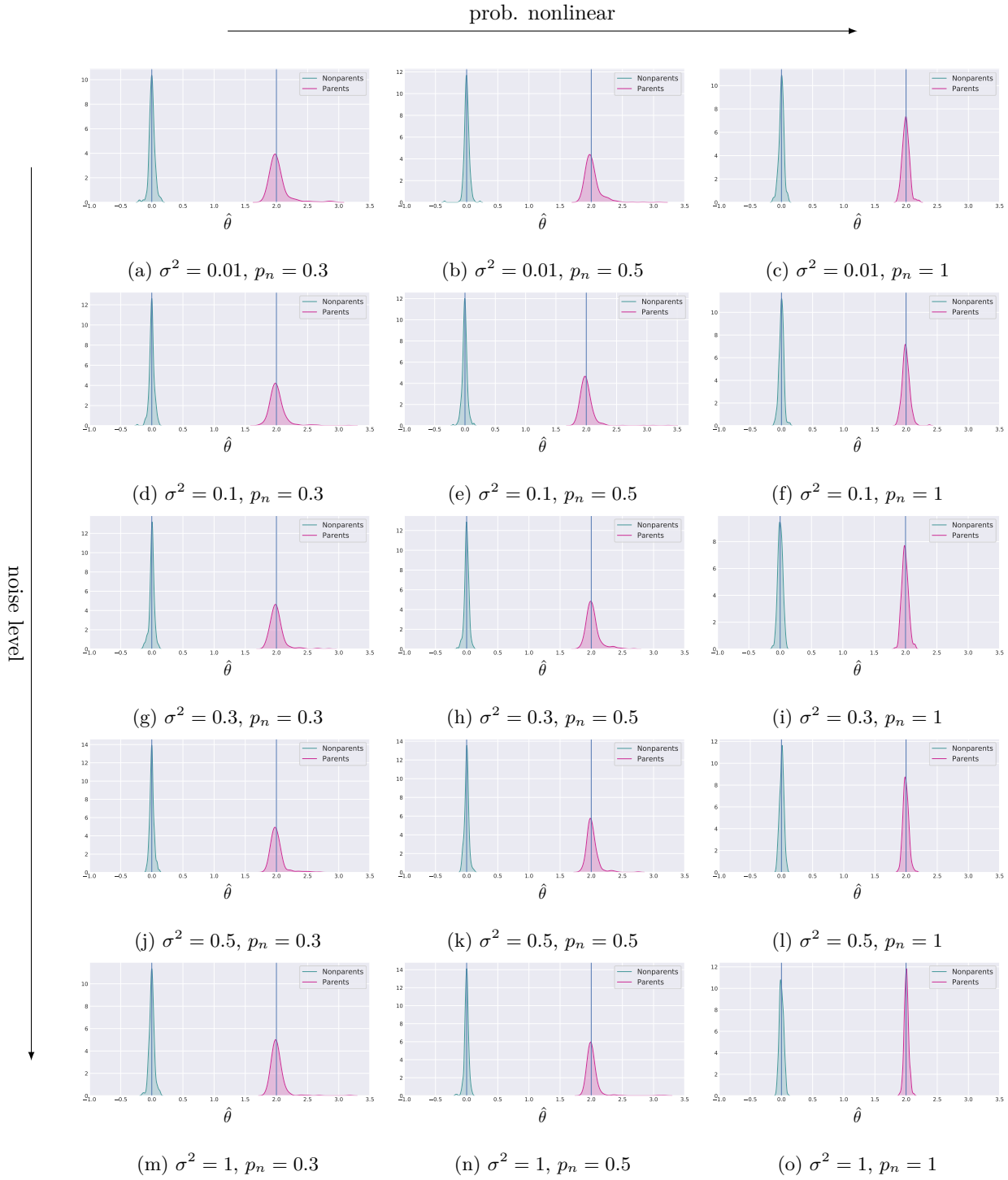

(a) $\sigma^2 = 0.01$, $p_n = 0.3$ (b) $\sigma^2 = 0.01$, $p_n = 0.5$ (c) $\sigma^2 = 0.01$, $p_n = 1$

(d) $\sigma^2 = 0.1$, $p_n = 0.3$ (e) $\sigma^2 = 0.1$, $p_n = 0.5$ (f) $\sigma^2 = 0.1$, $p_n = 1$

(g) $\sigma^2 = 0.3$, $p_n = 0.3$ (h) $\sigma^2 = 0.3$, $p_n = 0.5$ (i) $\sigma^2 = 0.3$, $p_n = 1$

(j) $\sigma^2 = 0.5$, $p_n = 0.3$ (k) $\sigma^2 = 0.5$, $p_n = 0.5$ (l) $\sigma^2 = 0.5$, $p_n = 1$

(m) $\sigma^2 = 1$, $p_n = 0.3$ (n) $\sigma^2 = 1$, $p_n = 0.5$ (o) $\sigma^2 = 1$, $p_n = 1$

Figure E.27: 0.5 connectivity, 5 nodes, 1000 observations, 100 simulations. Distribution of the estimated θ values for the true and false causal parents in 100 simulations. The vertical lines indicate the ground truth values for the causal parents linear coefficients. In general we observe that in all settings with enough observations the parameter estimation works reliably.

(a) $\sigma^2 = 0.01$, $p_n = 0.3$ (b) $\sigma^2 = 0.01$, $p_n = 0.5$ (c) $\sigma^2 = 0.01$, $p_n = 1$

(d) $\sigma^2 = 0.1$, $p_n = 0.3$ (e) $\sigma^2 = 0.1$, $p_n = 0.5$ (f) $\sigma^2 = 0.1$, $p_n = 1$

(g) $\sigma^2 = 0.3$, $p_n = 0.3$ (h) $\sigma^2 = 0.3$, $p_n = 0.5$ (i) $\sigma^2 = 0.3$, $p_n = 1$

(j) $\sigma^2 = 0.5$, $p_n = 0.3$ (k) $\sigma^2 = 0.5$, $p_n = 0.5$ (l) $\sigma^2 = 0.5$, $p_n = 1$

(m) $\sigma^2 = 1$, $p_n = 0.3$ (n) $\sigma^2 = 1$, $p_n = 0.5$ (o) $\sigma^2 = 1$, $p_n = 1$

Figure E.28: 0.5 connectivity, 10 nodes, 100 observations, 100 simulations. Distribution of the estimated θ values for the true and false causal parents in 100 simulations. The vertical lines indicate the ground truth values for the causal parents linear coefficients. In general we observe that in all settings with enough observations the parameter estimation works reliably.

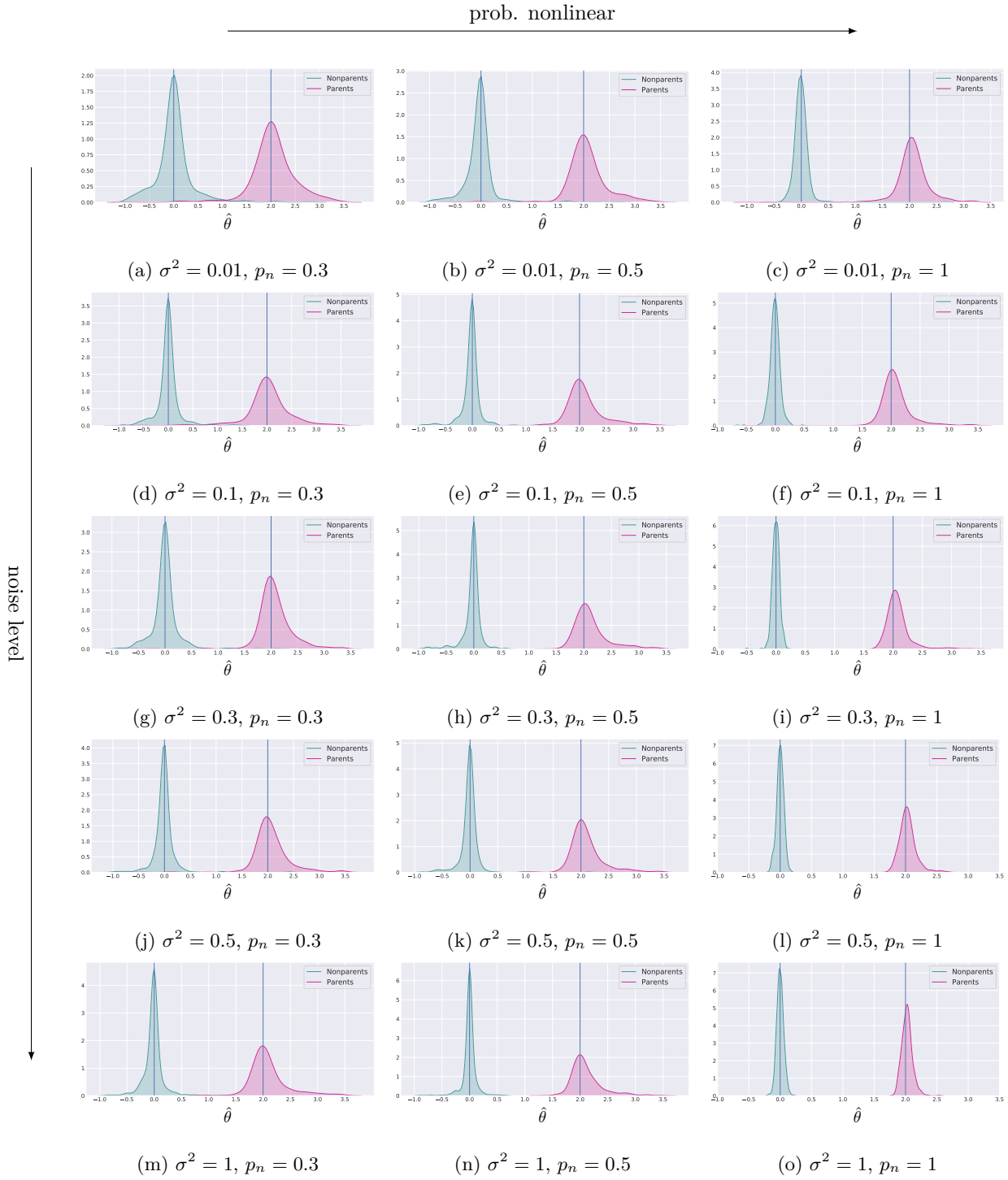

(a) $\sigma^2 = 0.01$, $p_n = 0.3$ (b) $\sigma^2 = 0.01$, $p_n = 0.5$ (c) $\sigma^2 = 0.01$, $p_n = 1$

(d) $\sigma^2 = 0.1$, $p_n = 0.3$ (e) $\sigma^2 = 0.1$, $p_n = 0.5$ (f) $\sigma^2 = 0.1$, $p_n = 1$

(g) $\sigma^2 = 0.3$, $p_n = 0.3$ (h) $\sigma^2 = 0.3$, $p_n = 0.5$ (i) $\sigma^2 = 0.3$, $p_n = 1$

(j) $\sigma^2 = 0.5$, $p_n = 0.3$ (k) $\sigma^2 = 0.5$, $p_n = 0.5$ (l) $\sigma^2 = 0.5$, $p_n = 1$

(m) $\sigma^2 = 1$, $p_n = 0.3$ (n) $\sigma^2 = 1$, $p_n = 0.5$ (o) $\sigma^2 = 1$, $p_n = 1$

Figure E.29: 0.5 connectivity, 10 nodes, 500 observations, 100 simulations. Distribution of the estimated θ values for the true and false causal parents in 100 simulations. The vertical lines indicate the ground truth values for the causal parents linear coefficients. In general we observe that in all settings with enough observations the parameter estimation works reliably.

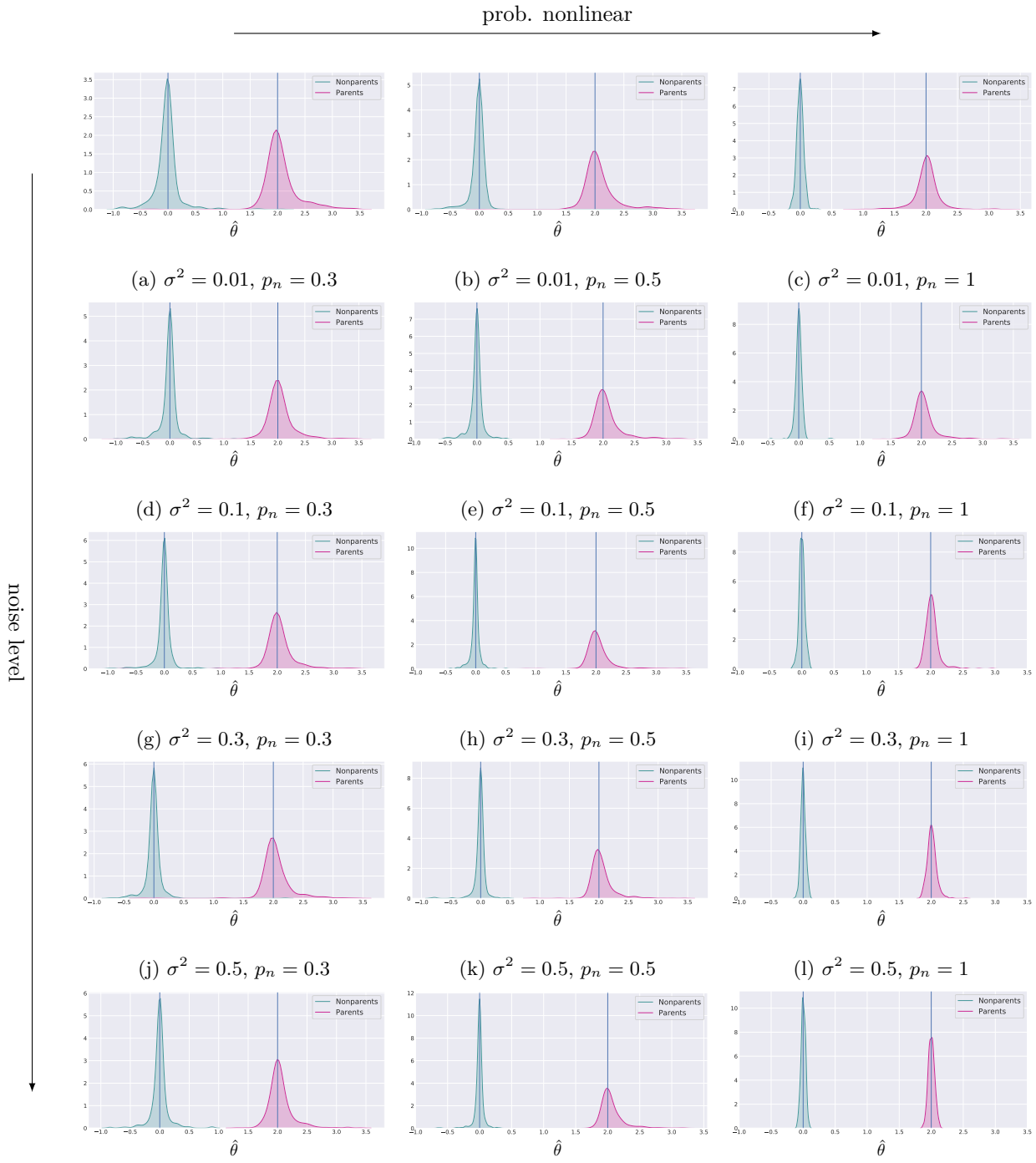

(a) $\sigma^2 = 0.01$, $p_n = 0.3$ (b) $\sigma^2 = 0.01$, $p_n = 0.5$ (c) $\sigma^2 = 0.01$, $p_n = 1$

(d) $\sigma^2 = 0.1$, $p_n = 0.3$ (e) $\sigma^2 = 0.1$, $p_n = 0.5$ (f) $\sigma^2 = 0.1$, $p_n = 1$

(g) $\sigma^2 = 0.3$, $p_n = 0.3$ (h) $\sigma^2 = 0.3$, $p_n = 0.5$ (i) $\sigma^2 = 0.3$, $p_n = 1$

(j) $\sigma^2 = 0.5$, $p_n = 0.3$ (k) $\sigma^2 = 0.5$, $p_n = 0.5$ (l) $\sigma^2 = 0.5$, $p_n = 1$

(m) $\sigma^2 = 1$, $p_n = 0.3$ (n) $\sigma^2 = 1$, $p_n = 0.5$ (o) $\sigma^2 = 1$, $p_n = 1$

Figure E.30: 0.5 connectivity, 10 nodes, 1000 observations, 100 simulations. Distribution of the estimated θ values for the true and false causal parents in 100 simulations. The vertical lines indicate the ground truth values for the causal parents linear coefficients. In general we observe that in all settings with enough observations the parameter estimation works reliably.

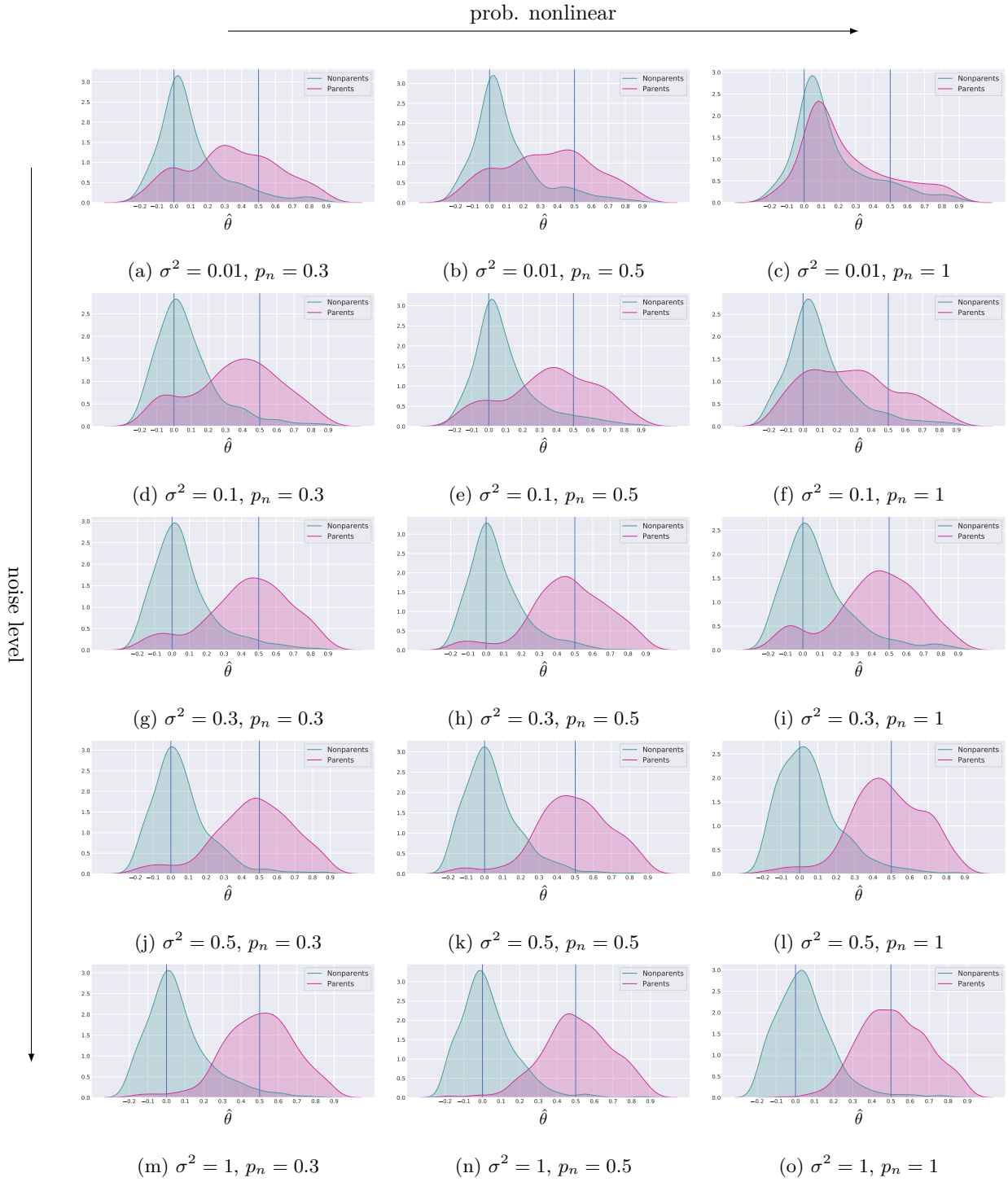

(a) $\sigma^2 = 0.01$, $p_n = 0.3$ (b) $\sigma^2 = 0.01$, $p_n = 0.5$ (c) $\sigma^2 = 0.01$, $p_n = 1$

(d) $\sigma^2 = 0.1$, $p_n = 0.3$ (e) $\sigma^2 = 0.1$, $p_n = 0.5$ (f) $\sigma^2 = 0.1$, $p_n = 1$

(g) $\sigma^2 = 0.3$, $p_n = 0.3$ (h) $\sigma^2 = 0.3$, $p_n = 0.5$ (i) $\sigma^2 = 0.3$, $p_n = 1$

(j) $\sigma^2 = 0.5$, $p_n = 0.3$ (k) $\sigma^2 = 0.5$, $p_n = 0.5$ (l) $\sigma^2 = 0.5$, $p_n = 1$

(m) $\sigma^2 = 1$, $p_n = 0.3$ (n) $\sigma^2 = 1$, $p_n = 0.5$ (o) $\sigma^2 = 1$, $p_n = 1$

Figure E.31: 0.5 connectivity, 20 nodes, 100 observations, 100 simulations. Distribution of the estimated θ values for the true and false causal parents in 100 simulations. The vertical lines indicate the ground truth values for the causal parents linear coefficients. In general we observe that in all settings with enough observations the parameter estimation works reliably.

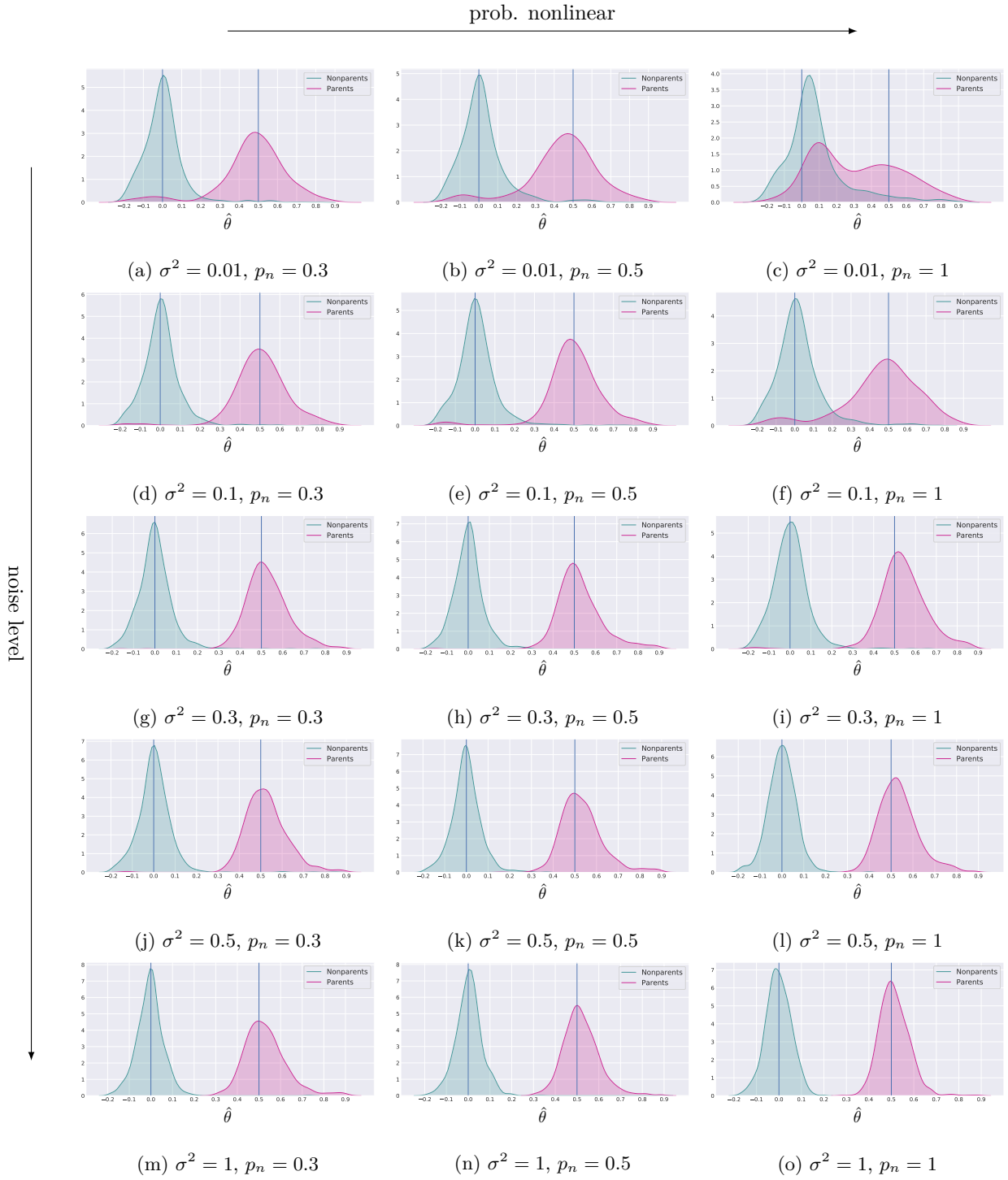

(a) $\sigma^2 = 0.01$, $p_n = 0.3$ (b) $\sigma^2 = 0.01$, $p_n = 0.5$ (c) $\sigma^2 = 0.01$, $p_n = 1$

(d) $\sigma^2 = 0.1$, $p_n = 0.3$ (e) $\sigma^2 = 0.1$, $p_n = 0.5$ (f) $\sigma^2 = 0.1$, $p_n = 1$

(g) $\sigma^2 = 0.3$, $p_n = 0.3$ (h) $\sigma^2 = 0.3$, $p_n = 0.5$ (i) $\sigma^2 = 0.3$, $p_n = 1$

(j) $\sigma^2 = 0.5$, $p_n = 0.3$ (k) $\sigma^2 = 0.5$, $p_n = 0.5$ (l) $\sigma^2 = 0.5$, $p_n = 1$

(m) $\sigma^2 = 1$, $p_n = 0.3$ (n) $\sigma^2 = 1$, $p_n = 0.5$ (o) $\sigma^2 = 1$, $p_n = 1$

Figure E.32: 0.5 connectivity, 20 nodes, 500 observations, 100 simulations. Distribution of the estimated θ values for the true and false causal parents in 100 simulations. The vertical lines indicate the ground truth values for the causal parents linear coefficients. In general we observe that in all settings with enough observations the parameter estimation works reliably.

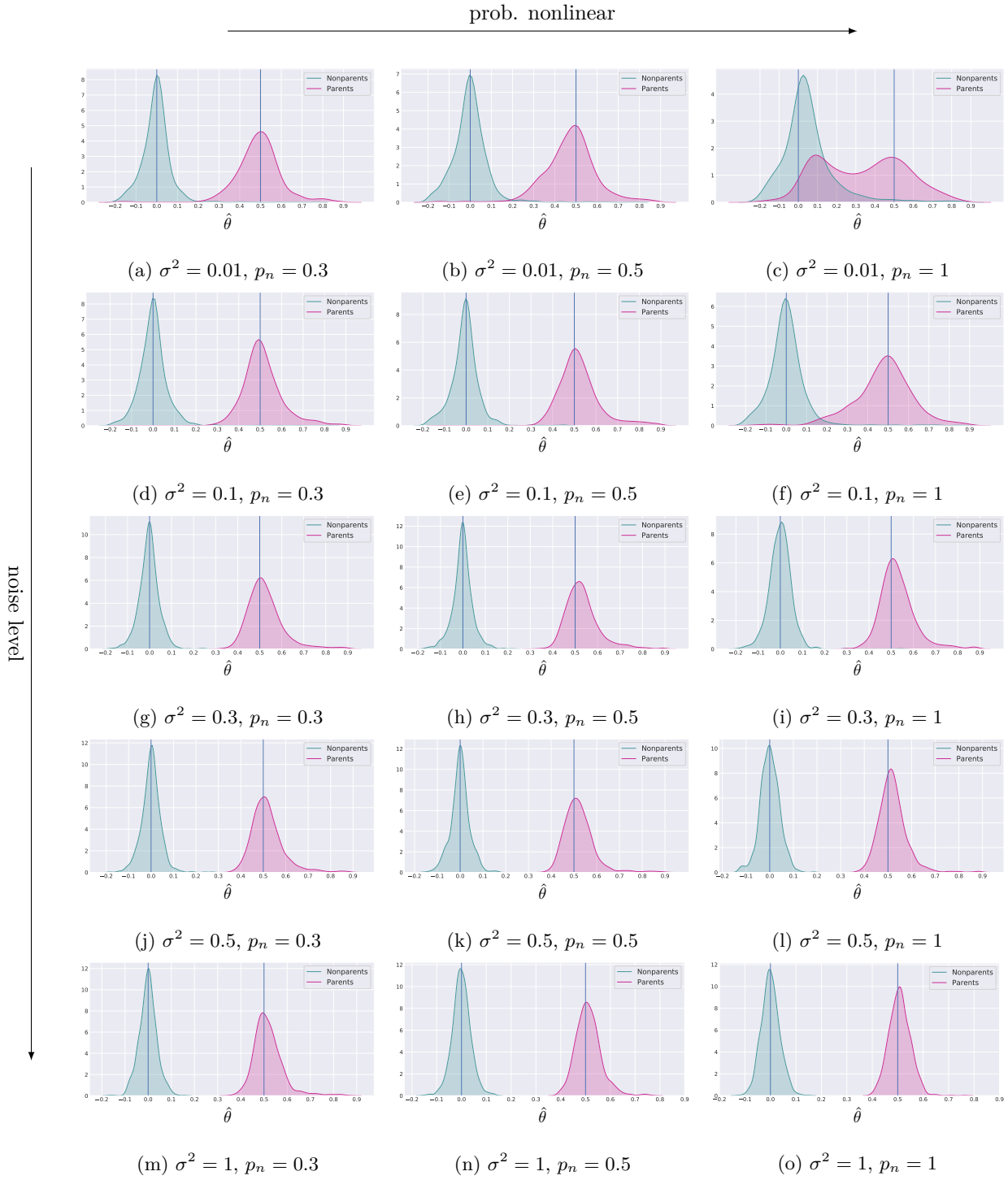

(a) $\sigma^2 = 0.01$, $p_n = 0.3$ (b) $\sigma^2 = 0.01$, $p_n = 0.5$ (c) $\sigma^2 = 0.01$, $p_n = 1$

(d) $\sigma^2 = 0.1$, $p_n = 0.3$ (e) $\sigma^2 = 0.1$, $p_n = 0.5$ (f) $\sigma^2 = 0.1$, $p_n = 1$

(g) $\sigma^2 = 0.3$, $p_n = 0.3$ (h) $\sigma^2 = 0.3$, $p_n = 0.5$ (i) $\sigma^2 = 0.3$, $p_n = 1$

(j) $\sigma^2 = 0.5$, $p_n = 0.3$ (k) $\sigma^2 = 0.5$, $p_n = 0.5$ (l) $\sigma^2 = 0.5$, $p_n = 1$

(m) $\sigma^2 = 1$, $p_n = 0.3$ (n) $\sigma^2 = 1$, $p_n = 0.5$ (o) $\sigma^2 = 1$, $p_n = 1$

Figure E.33: 0.5 connectivity, 20 nodes, 1000 observations, 100 simulations. Distribution of the estimated θ values for the true and false causal parents in 100 simulations. The vertical lines indicate the ground truth values for the causal parents linear coefficients. In general we observe that in all settings with enough observations the parameter estimation works reliably.

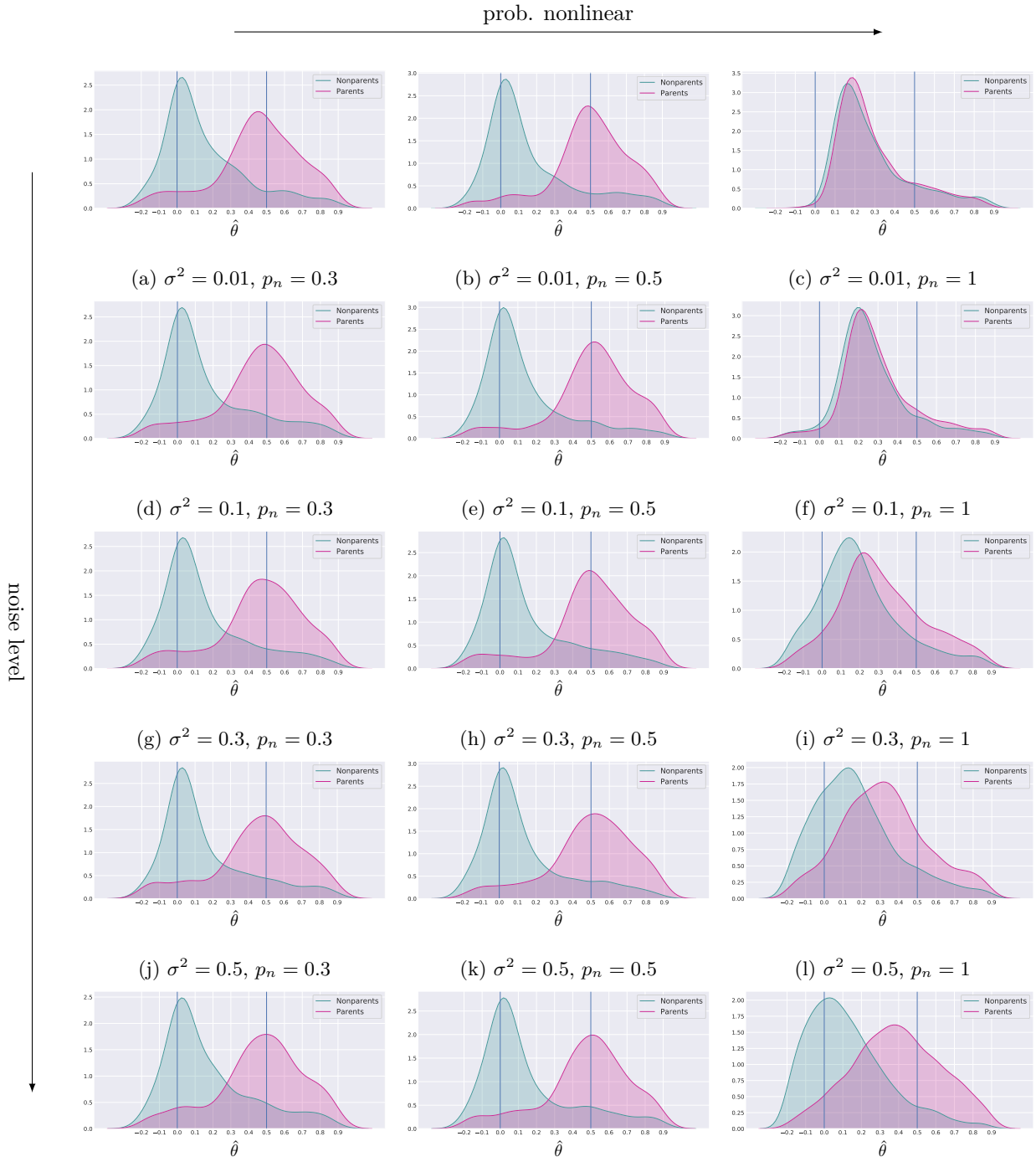

(a) $\sigma^2 = 0.01$, $p_n = 0.3$ (b) $\sigma^2 = 0.01$, $p_n = 0.5$ (c) $\sigma^2 = 0.01$, $p_n = 1$

(d) $\sigma^2 = 0.1$, $p_n = 0.3$ (e) $\sigma^2 = 0.1$, $p_n = 0.5$ (f) $\sigma^2 = 0.1$, $p_n = 1$

(g) $\sigma^2 = 0.3$, $p_n = 0.3$ (h) $\sigma^2 = 0.3$, $p_n = 0.5$ (i) $\sigma^2 = 0.3$, $p_n = 1$

(j) $\sigma^2 = 0.5$, $p_n = 0.3$ (k) $\sigma^2 = 0.5$, $p_n = 0.5$ (l) $\sigma^2 = 0.5$, $p_n = 1$

(m) $\sigma^2 = 1$, $p_n = 0.3$ (n) $\sigma^2 = 1$, $p_n = 0.5$ (o) $\sigma^2 = 1$, $p_n = 1$

Figure E.34: 0.5 connectivity, 50 nodes, 100 observations, 100 simulations. Distribution of the estimated θ values for the true and false causal parents in 100 simulations. The vertical lines indicate the ground truth values for the causal parents linear coefficients. In general we observe that in all settings with enough observations the parameter estimation works reliably.

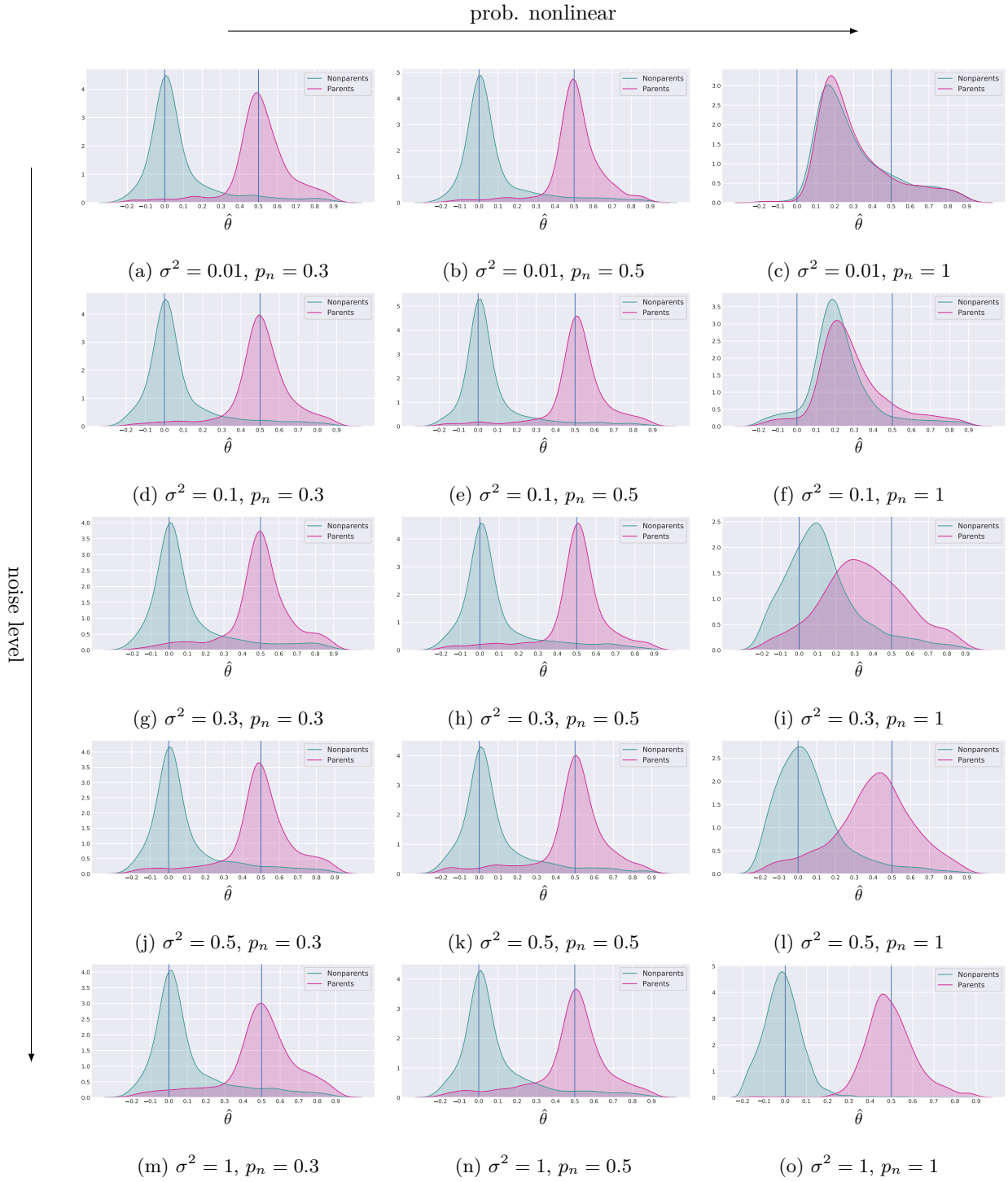

(a) $\sigma^2 = 0.01$, $p_n = 0.3$ (b) $\sigma^2 = 0.01$, $p_n = 0.5$ (c) $\sigma^2 = 0.01$, $p_n = 1$

(d) $\sigma^2 = 0.1$, $p_n = 0.3$ (e) $\sigma^2 = 0.1$, $p_n = 0.5$ (f) $\sigma^2 = 0.1$, $p_n = 1$

(g) $\sigma^2 = 0.3$, $p_n = 0.3$ (h) $\sigma^2 = 0.3$, $p_n = 0.5$ (i) $\sigma^2 = 0.3$, $p_n = 1$

(j) $\sigma^2 = 0.5$, $p_n = 0.3$ (k) $\sigma^2 = 0.5$, $p_n = 0.5$ (l) $\sigma^2 = 0.5$, $p_n = 1$

(m) $\sigma^2 = 1$, $p_n = 0.3$ (n) $\sigma^2 = 1$, $p_n = 0.5$ (o) $\sigma^2 = 1$, $p_n = 1$

Figure E.35: 0.5 connectivity, 50 nodes, 500 observations, 100 simulations. Distribution of the estimated θ values for the true and false causal parents in 100 simulations. The vertical lines indicate the ground truth values for the causal parents linear coefficients. In general we observe that in all settings with enough observations the parameter estimation works reliably.

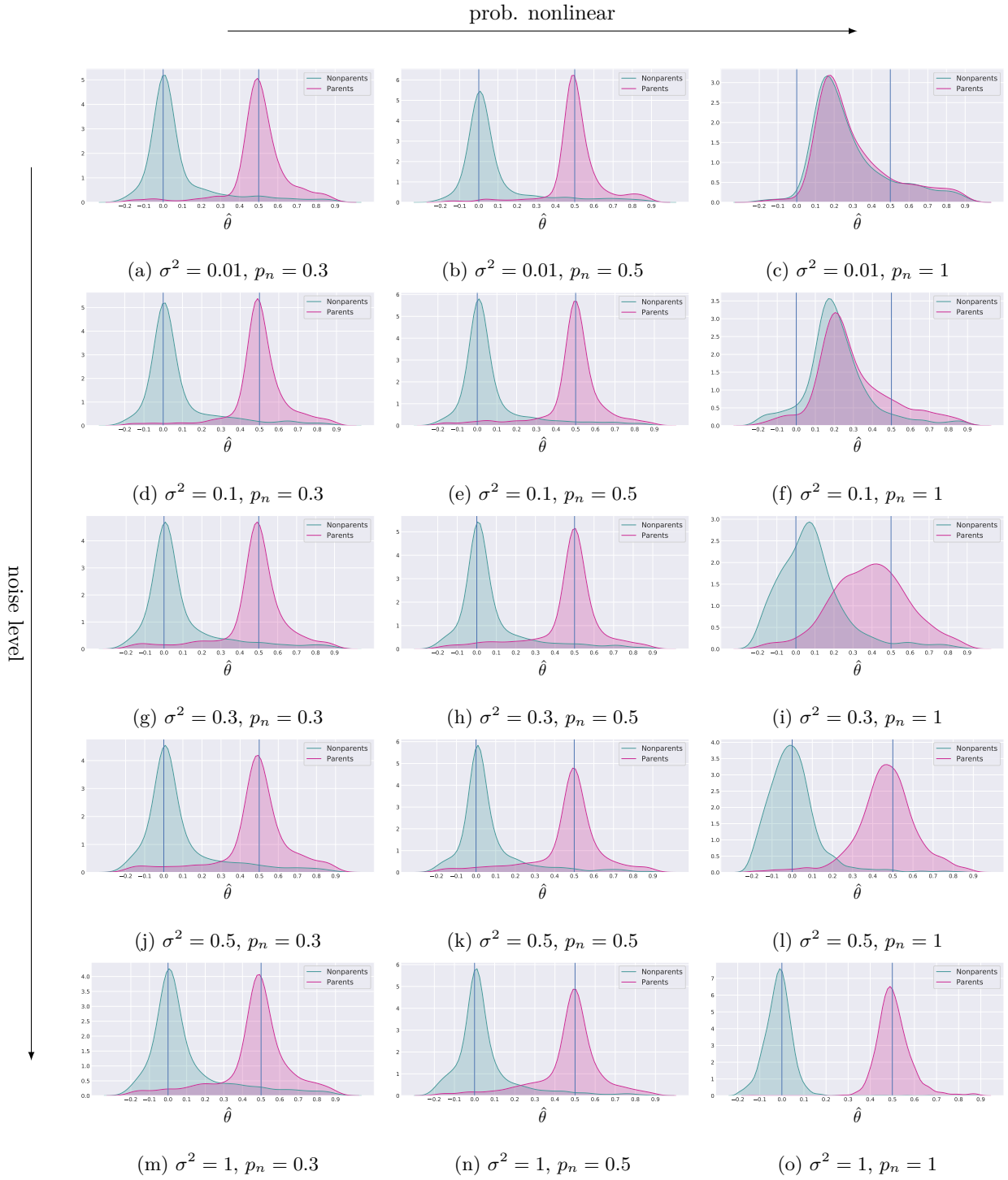

(a) $\sigma^2 = 0.01$, $p_n = 0.3$ (b) $\sigma^2 = 0.01$, $p_n = 0.5$ (c) $\sigma^2 = 0.01$, $p_n = 1$

(d) $\sigma^2 = 0.1$, $p_n = 0.3$ (e) $\sigma^2 = 0.1$, $p_n = 0.5$ (f) $\sigma^2 = 0.1$, $p_n = 1$

(g) $\sigma^2 = 0.3$, $p_n = 0.3$ (h) $\sigma^2 = 0.3$, $p_n = 0.5$ (i) $\sigma^2 = 0.3$, $p_n = 1$

(j) $\sigma^2 = 0.5$, $p_n = 0.3$ (k) $\sigma^2 = 0.5$, $p_n = 0.5$ (l) $\sigma^2 = 0.5$, $p_n = 1$

(m) $\sigma^2 = 1$, $p_n = 0.3$ (n) $\sigma^2 = 1$, $p_n = 0.5$ (o) $\sigma^2 = 1$, $p_n = 1$

Figure E.36: 0.5 connectivity, 50 nodes, 1000 observations, 100 simulations. Distribution of the estimated θ values for the true and false causal parents in 100 simulations. The vertical lines indicate the ground truth values for the causal parents linear coefficients. In general we observe that in all settings with enough observations the parameter estimation works reliably.

F Supplemntary Figures for Performace in Inferring Direct Causes, Accuracy as Metric

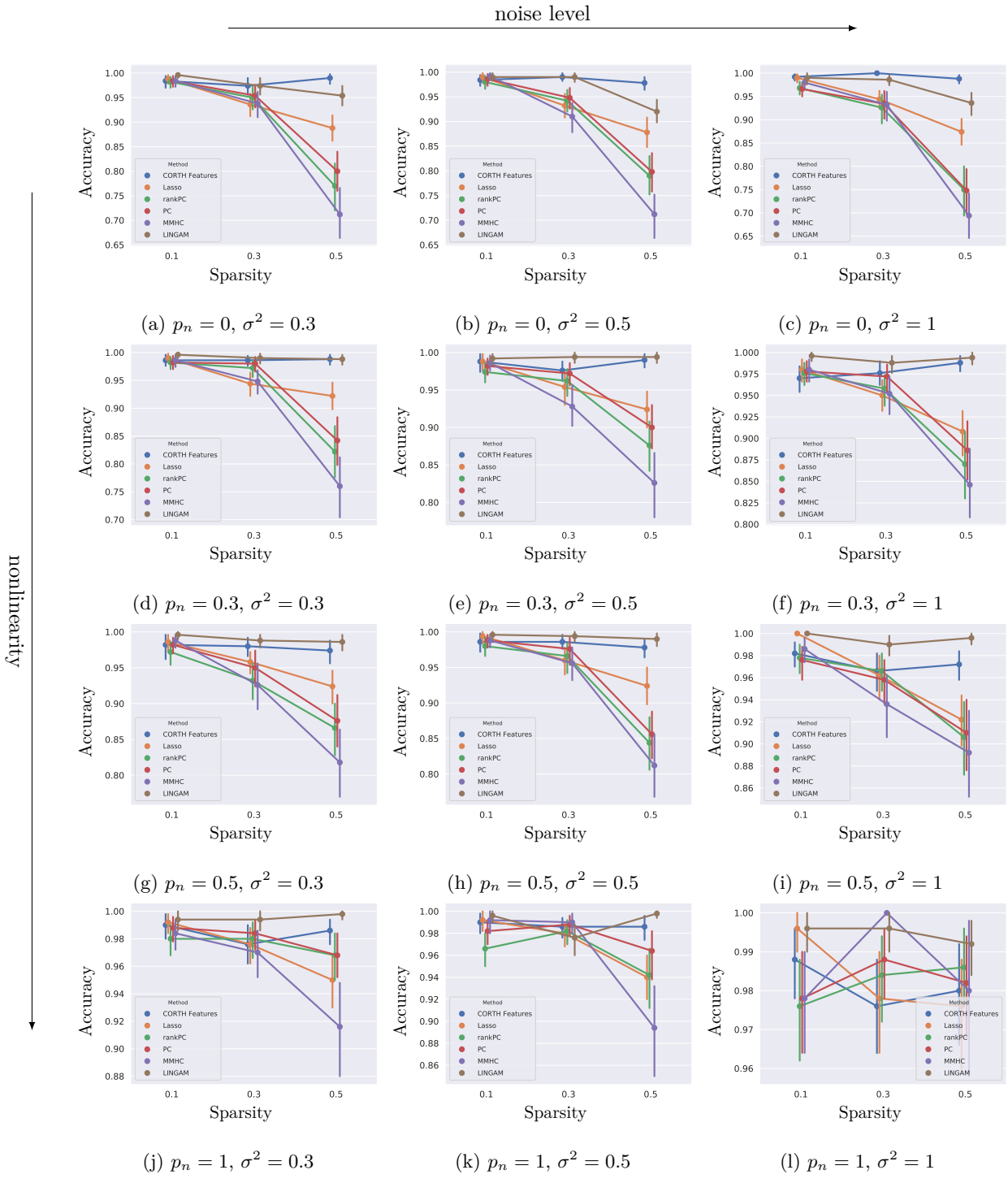

(a) $p_n = 0$, $\sigma^2 = 0.3$ (b) $p_n = 0$, $\sigma^2 = 0.5$ (c) $p_n = 0$, $\sigma^2 = 1$

(d) $p_n = 0.3$, $\sigma^2 = 0.3$ (e) $p_n = 0.3$, $\sigma^2 = 0.5$ (f) $p_n = 0.3$, $\sigma^2 = 1$

(g) $p_n = 0.5$, $\sigma^2 = 0.3$ (h) $p_n = 0.5$, $\sigma^2 = 0.5$ (i) $p_n = 0.5$, $\sigma^2 = 1$

(j) $p_n = 1$, $\sigma^2 = 0.3$ (k) $p_n = 1$, $\sigma^2 = 0.5$ (l) $p_n = 1$, $\sigma^2 = 1$

Figure F.1: 5 nodes, 100 observations, 100 simulations. Compared to other methods, our approach is stable wrt. noise level, connectivity and even partially non-linear relationships, significantly outperforming the majority of baselines.

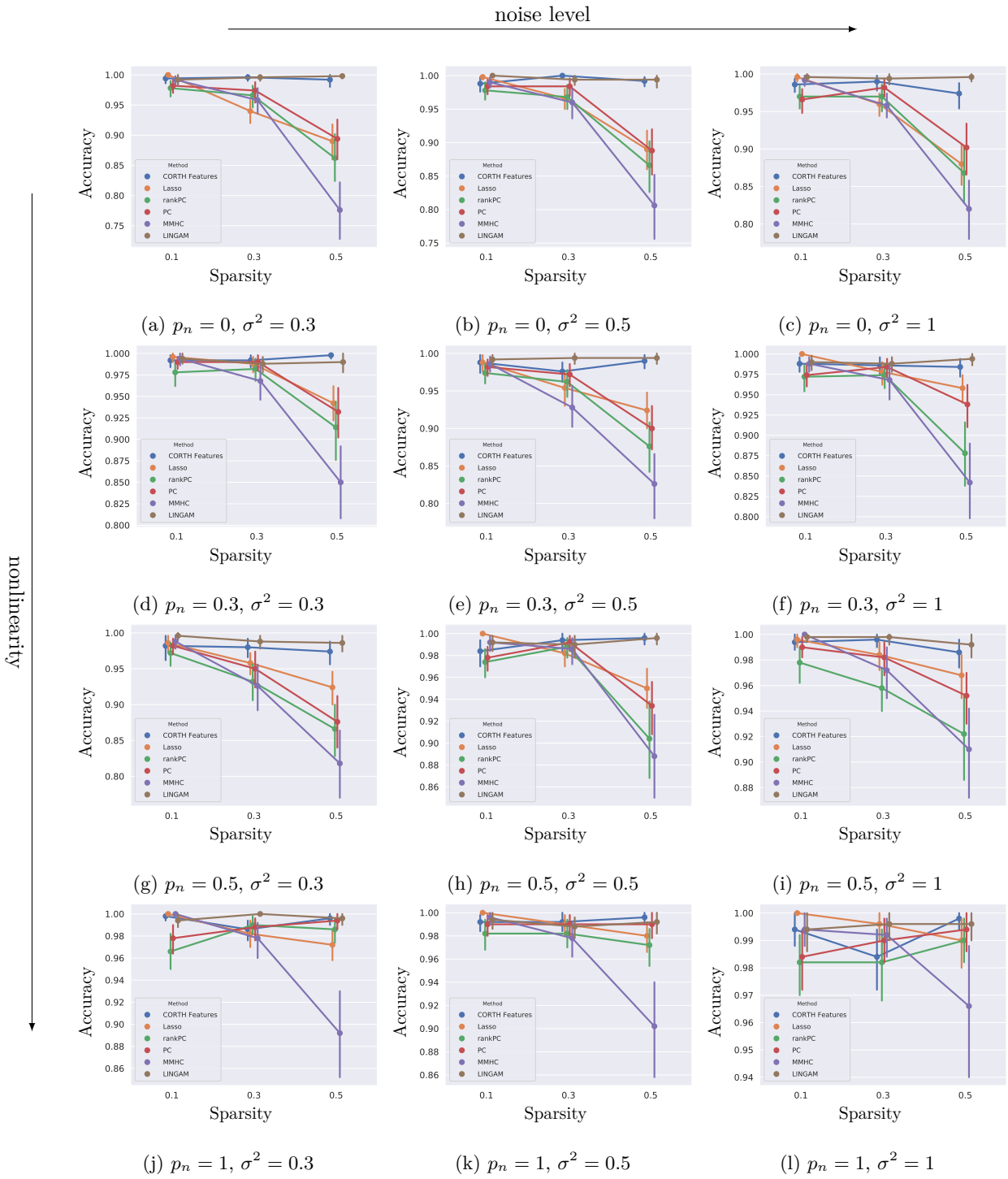

(a) $p_n = 0$, $\sigma^2 = 0.3$ (b) $p_n = 0$, $\sigma^2 = 0.5$ (c) $p_n = 0$, $\sigma^2 = 1$

(d) $p_n = 0.3$, $\sigma^2 = 0.3$ (e) $p_n = 0.3$, $\sigma^2 = 0.5$ (f) $p_n = 0.3$, $\sigma^2 = 1$

(g) $p_n = 0.5$, $\sigma^2 = 0.3$ (h) $p_n = 0.5$, $\sigma^2 = 0.5$ (i) $p_n = 0.5$, $\sigma^2 = 1$

(j) $p_n = 1$, $\sigma^2 = 0.3$ (k) $p_n = 1$, $\sigma^2 = 0.5$ (l) $p_n = 1$, $\sigma^2 = 1$

Figure F.2: 5 nodes, 500 observations, 100 simulations. Compared to other methods, our approach is stable wrt. noise level, connectivity and even partially non-linear relationships, significantly outperforming the majority of baselines.

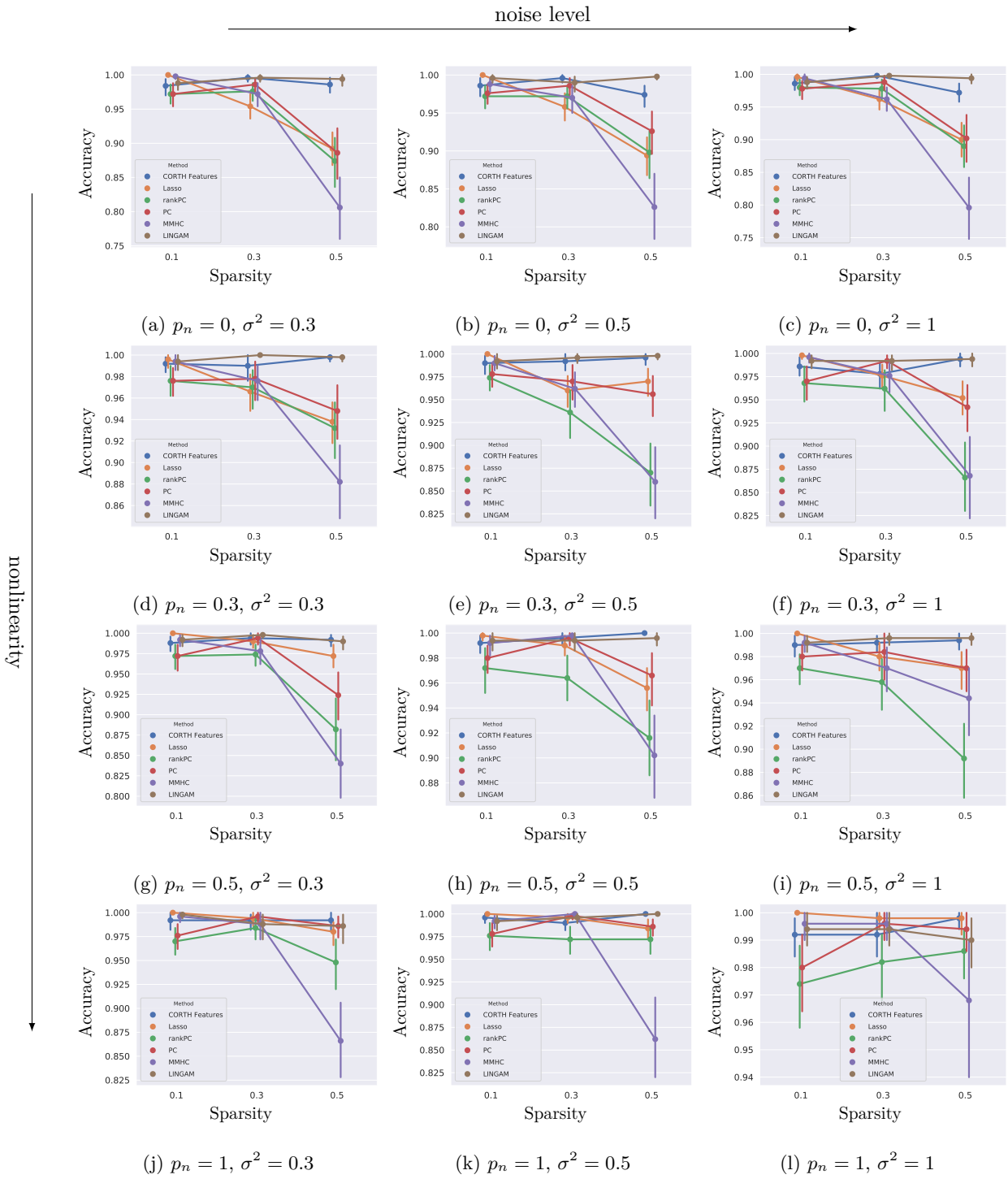

(a) $p_n = 0$, $\sigma^2 = 0.3$ (b) $p_n = 0$, $\sigma^2 = 0.5$ (c) $p_n = 0$, $\sigma^2 = 1$

(d) $p_n = 0.3$, $\sigma^2 = 0.3$ (e) $p_n = 0.3$, $\sigma^2 = 0.5$ (f) $p_n = 0.3$, $\sigma^2 = 1$

(g) $p_n = 0.5$, $\sigma^2 = 0.3$ (h) $p_n = 0.5$, $\sigma^2 = 0.5$ (i) $p_n = 0.5$, $\sigma^2 = 1$

(j) $p_n = 1$, $\sigma^2 = 0.3$ (k) $p_n = 1$, $\sigma^2 = 0.5$ (l) $p_n = 1$, $\sigma^2 = 1$

Figure F.3: 5 nodes, 1000 observations, 100 simulations. Compared to other methods, our approach is stable wrt. noise level, connectivity and even partially non-linear relationships, significantly outperforming the majority of baselines.

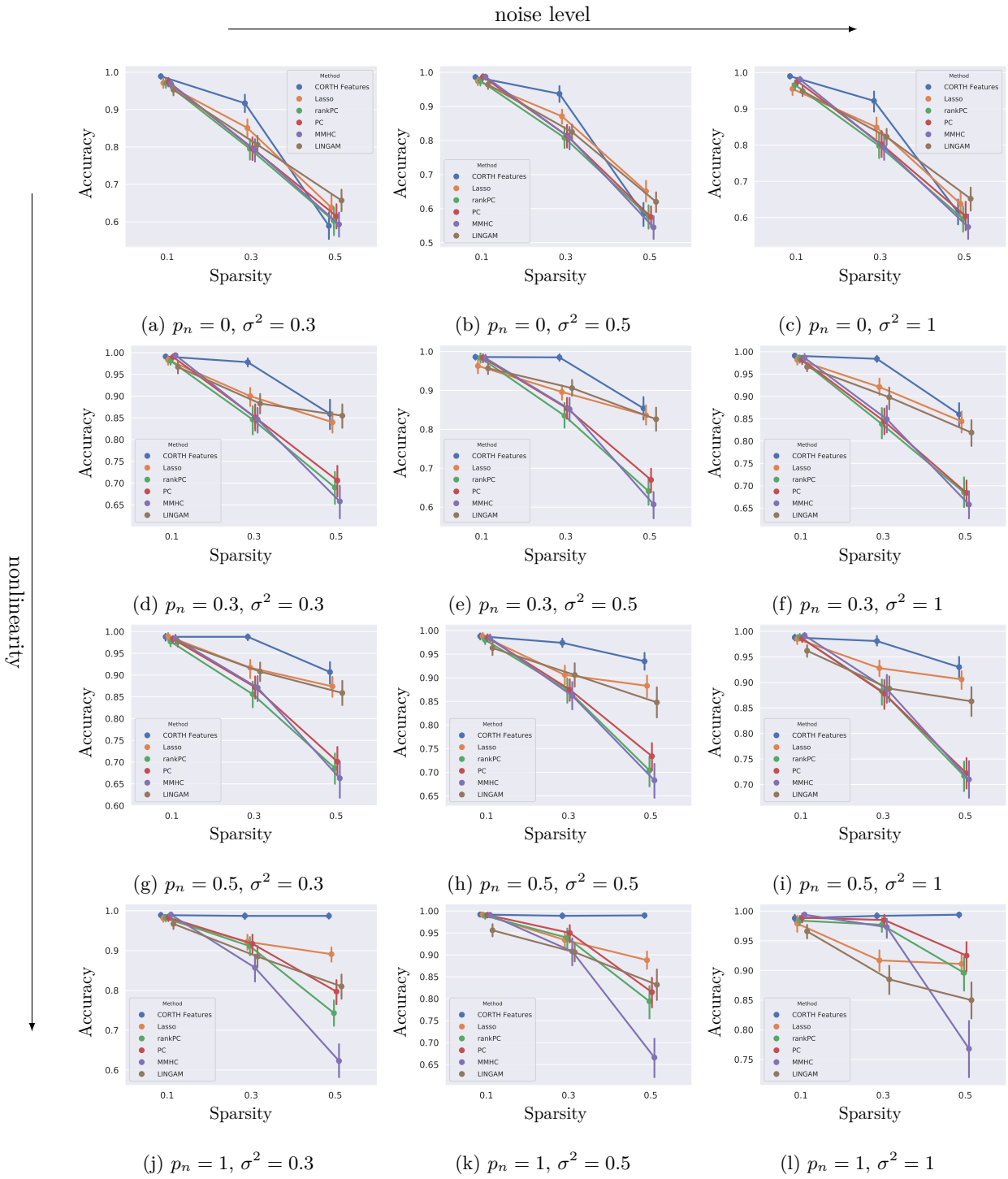

(a) $p_n = 0$, $\sigma^2 = 0.3$ (b) $p_n = 0$, $\sigma^2 = 0.5$ (c) $p_n = 0$, $\sigma^2 = 1$

(d) $p_n = 0.3$, $\sigma^2 = 0.3$ (e) $p_n = 0.3$, $\sigma^2 = 0.5$ (f) $p_n = 0.3$, $\sigma^2 = 1$

(g) $p_n = 0.5$, $\sigma^2 = 0.3$ (h) $p_n = 0.5$, $\sigma^2 = 0.5$ (i) $p_n = 0.5$, $\sigma^2 = 1$

(j) $p_n = 1$, $\sigma^2 = 0.3$ (k) $p_n = 1$, $\sigma^2 = 0.5$ (l) $p_n = 1$, $\sigma^2 = 1$

Figure F.4: 10 nodes, 100 observations, 100 simulations. Compared to other methods, our approach is stable wrt. noise level, connectivity and even partially non-linear relationships, significantly outperforming the majority of baselines.

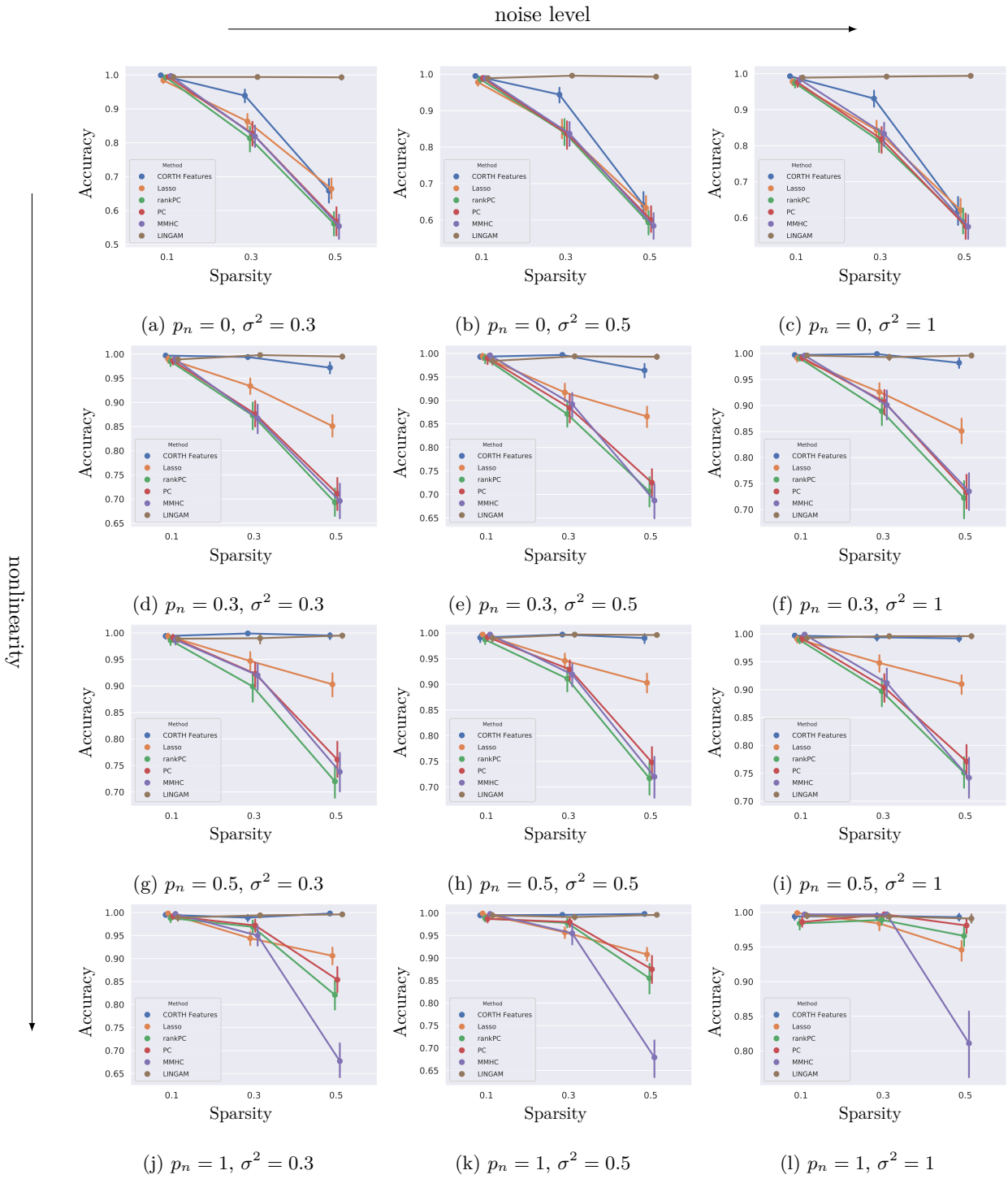

(a) $p_n = 0$, $\sigma^2 = 0.3$ (b) $p_n = 0$, $\sigma^2 = 0.5$ (c) $p_n = 0$, $\sigma^2 = 1$

(d) $p_n = 0.3$, $\sigma^2 = 0.3$ (e) $p_n = 0.3$, $\sigma^2 = 0.5$ (f) $p_n = 0.3$, $\sigma^2 = 1$

(g) $p_n = 0.5$, $\sigma^2 = 0.3$ (h) $p_n = 0.5$, $\sigma^2 = 0.5$ (i) $p_n = 0.5$, $\sigma^2 = 1$

(j) $p_n = 1$, $\sigma^2 = 0.3$ (k) $p_n = 1$, $\sigma^2 = 0.5$ (l) $p_n = 1$, $\sigma^2 = 1$

Figure F.5: 10 nodes, 500 observations, 100 simulations. Compared to other methods, our approach is stable wrt. noise level, connectivity and even partially non-linear relationships, significantly outperforming the majority of baselines.

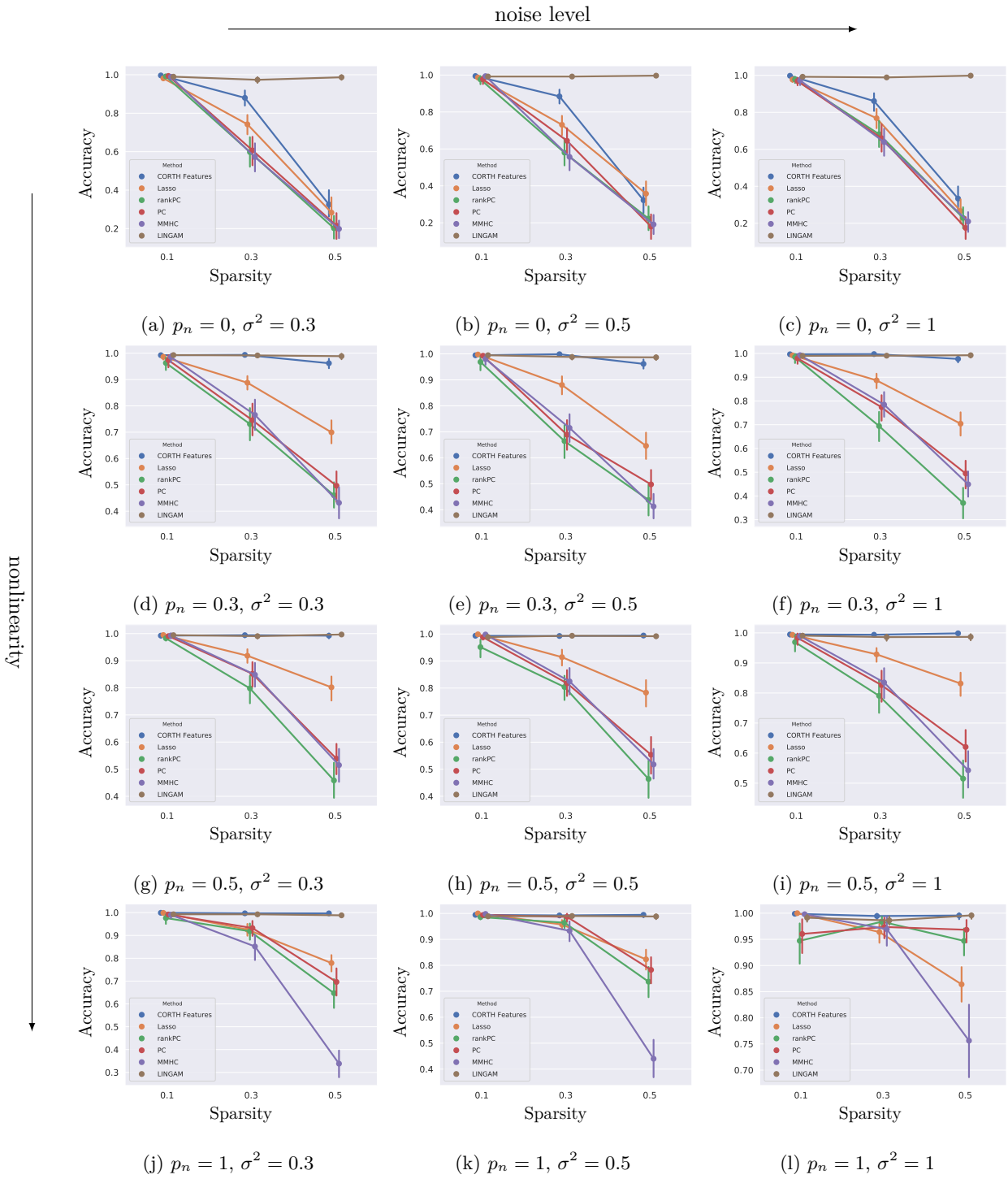

(a) $p_n = 0$, $\sigma^2 = 0.3$ (b) $p_n = 0$, $\sigma^2 = 0.5$ (c) $p_n = 0$, $\sigma^2 = 1$

(d) $p_n = 0.3$, $\sigma^2 = 0.3$ (e) $p_n = 0.3$, $\sigma^2 = 0.5$ (f) $p_n = 0.3$, $\sigma^2 = 1$

(g) $p_n = 0.5$, $\sigma^2 = 0.3$ (h) $p_n = 0.5$, $\sigma^2 = 0.5$ (i) $p_n = 0.5$, $\sigma^2 = 1$

(j) $p_n = 1$, $\sigma^2 = 0.3$ (k) $p_n = 1$, $\sigma^2 = 0.5$ (l) $p_n = 1$, $\sigma^2 = 1$

Figure F.6: 10 nodes, 1000 observations, 100 simulations. Compared to other methods, our approach is stable wrt. noise level, connectivity and even partially non-linear relationships, significantly outperforming the majority of baselines.

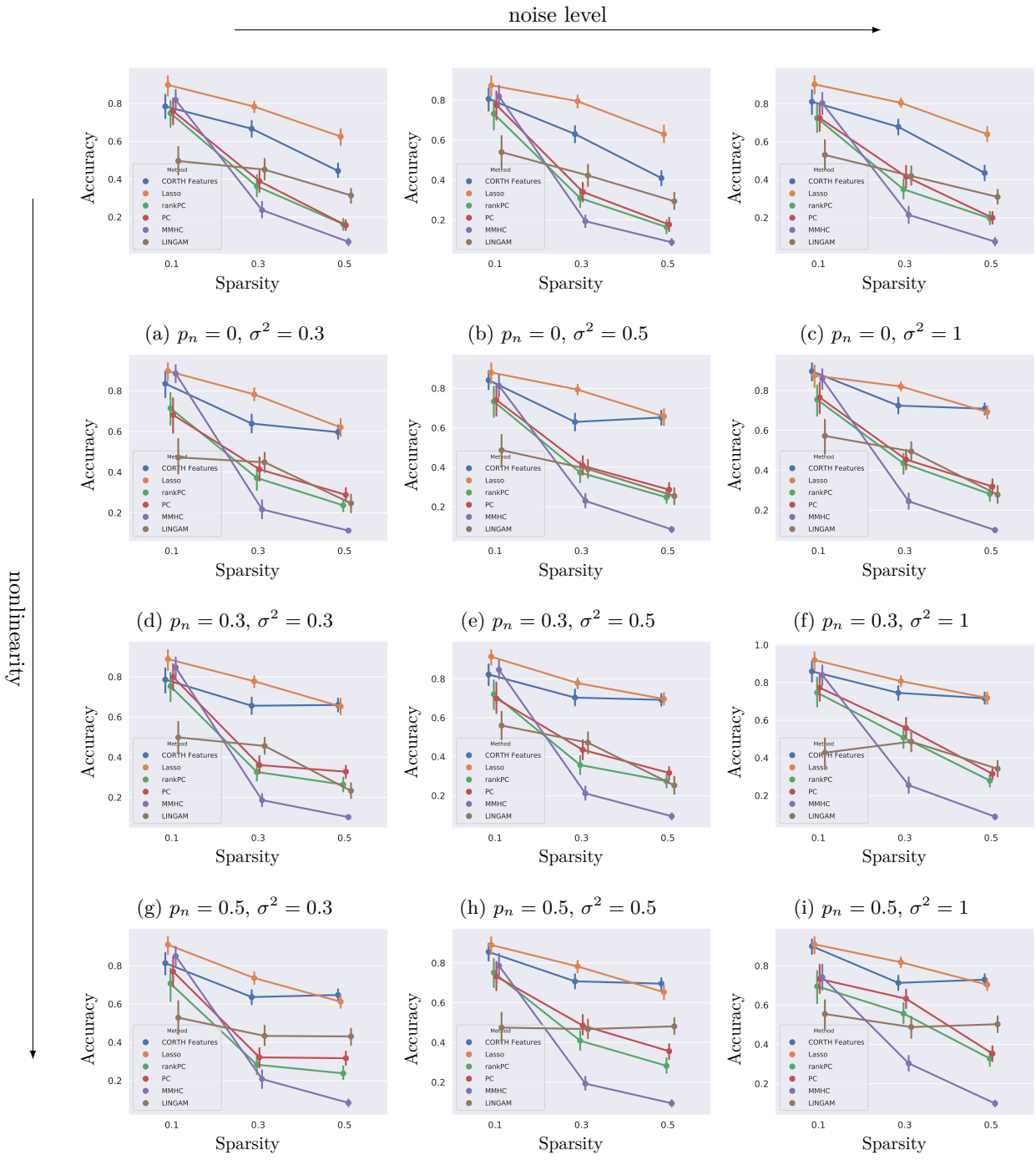

(a) $p_n = 0$, $\sigma^2 = 0.3$ (b) $p_n = 0$, $\sigma^2 = 0.5$ (c) $p_n = 0$, $\sigma^2 = 1$

(d) $p_n = 0.3$, $\sigma^2 = 0.3$ (e) $p_n = 0.3$, $\sigma^2 = 0.5$ (f) $p_n = 0.3$, $\sigma^2 = 1$

(g) $p_n = 0.5$, $\sigma^2 = 0.3$ (h) $p_n = 0.5$, $\sigma^2 = 0.5$ (i) $p_n = 0.5$, $\sigma^2 = 1$

(j) $p_n = 1$, $\sigma^2 = 0.3$ (k) $p_n = 1$, $\sigma^2 = 0.5$ (l) $p_n = 1$, $\sigma^2 = 1$

Figure F.7: 20 nodes, 100 observations, 100 simulations. Compared to other methods, our approach is stable wrt. noise level, connectivity and even partially non-linear relationships, significantly outperforming the majority of baselines.

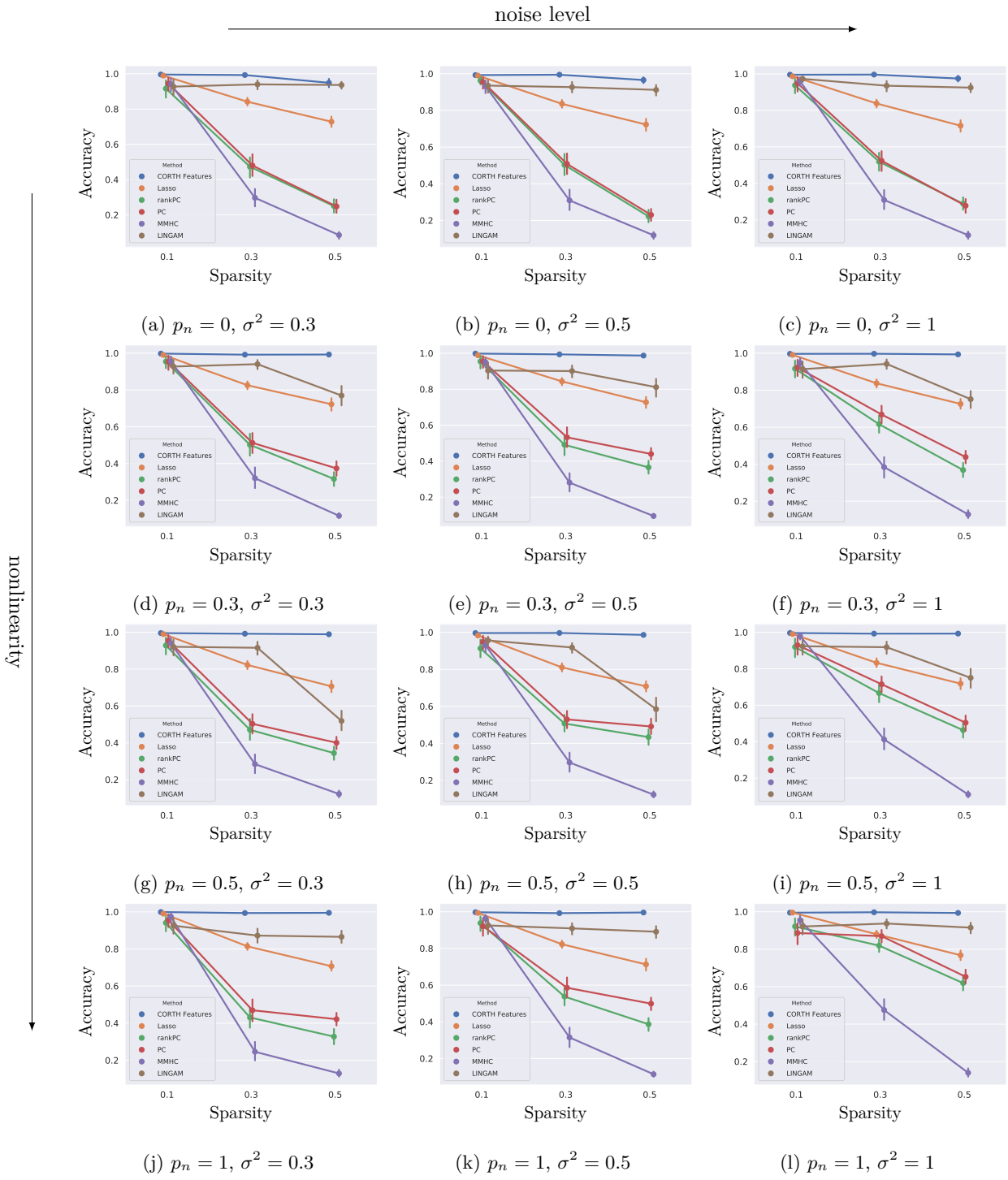

(a) $p_n = 0$, $\sigma^2 = 0.3$ (b) $p_n = 0$, $\sigma^2 = 0.5$ (c) $p_n = 0$, $\sigma^2 = 1$

(d) $p_n = 0.3$, $\sigma^2 = 0.3$ (e) $p_n = 0.3$, $\sigma^2 = 0.5$ (f) $p_n = 0.3$, $\sigma^2 = 1$

(g) $p_n = 0.5$, $\sigma^2 = 0.3$ (h) $p_n = 0.5$, $\sigma^2 = 0.5$ (i) $p_n = 0.5$, $\sigma^2 = 1$

(j) $p_n = 1$, $\sigma^2 = 0.3$ (k) $p_n = 1$, $\sigma^2 = 0.5$ (l) $p_n = 1$, $\sigma^2 = 1$

Figure F.8: 20 nodes, 500 observations, 100 simulations. Compared to other methods, our approach is stable wrt. noise level, connectivity and even partially non-linear relationships, significantly outperforming the majority of baselines.

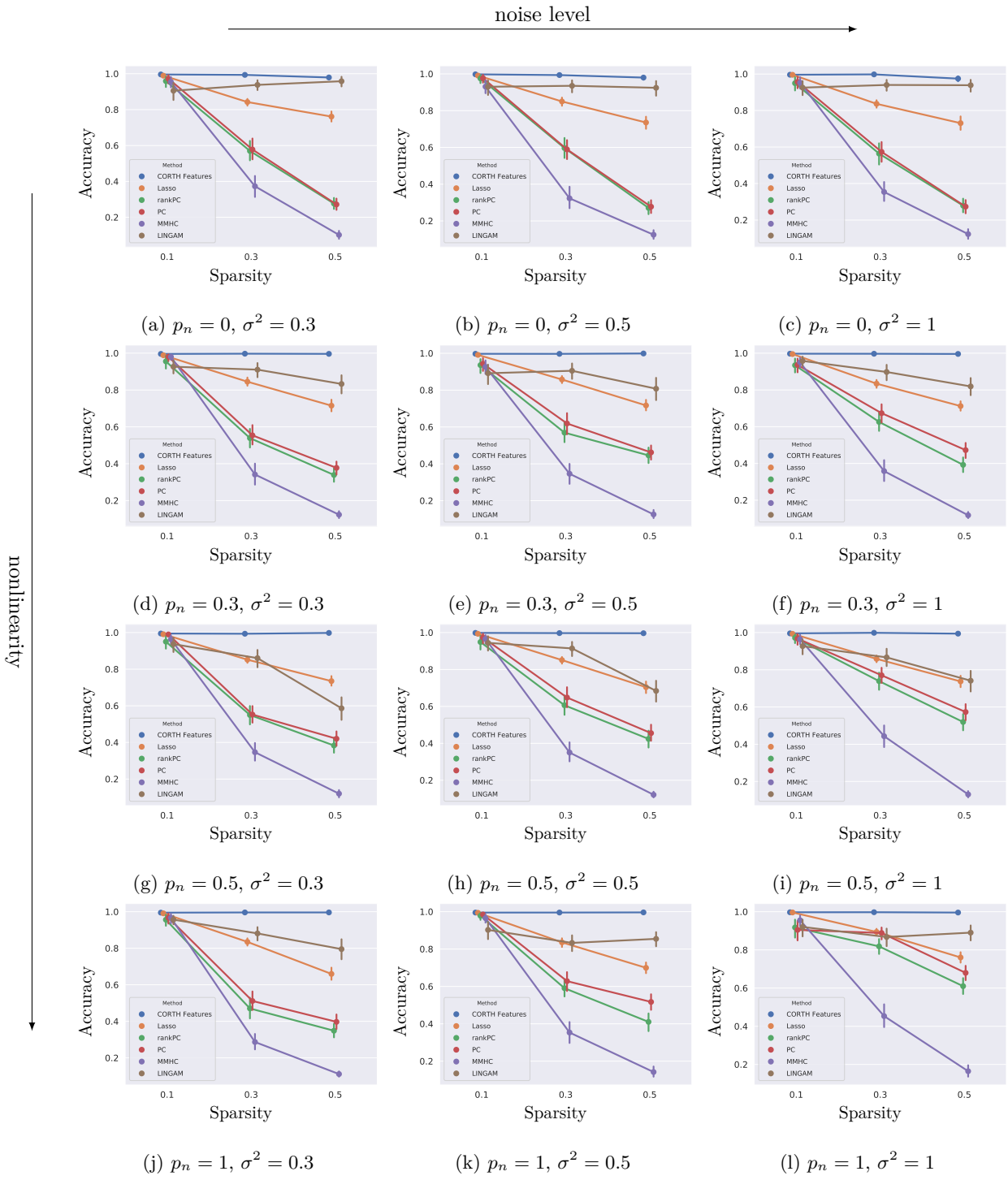

(a) $p_n = 0$, $\sigma^2 = 0.3$ (b) $p_n = 0$, $\sigma^2 = 0.5$ (c) $p_n = 0$, $\sigma^2 = 1$

(d) $p_n = 0.3$, $\sigma^2 = 0.3$ (e) $p_n = 0.3$, $\sigma^2 = 0.5$ (f) $p_n = 0.3$, $\sigma^2 = 1$

(g) $p_n = 0.5$, $\sigma^2 = 0.3$ (h) $p_n = 0.5$, $\sigma^2 = 0.5$ (i) $p_n = 0.5$, $\sigma^2 = 1$

(j) $p_n = 1$, $\sigma^2 = 0.3$ (k) $p_n = 1$, $\sigma^2 = 0.5$ (l) $p_n = 1$, $\sigma^2 = 1$

Figure F.9: 20 nodes, 1000 observations, 100 simulations. Compared to other methods, our approach is stable wrt. noise level, connectivity and even partially non-linear relationships, significantly outperforming the majority of baselines.

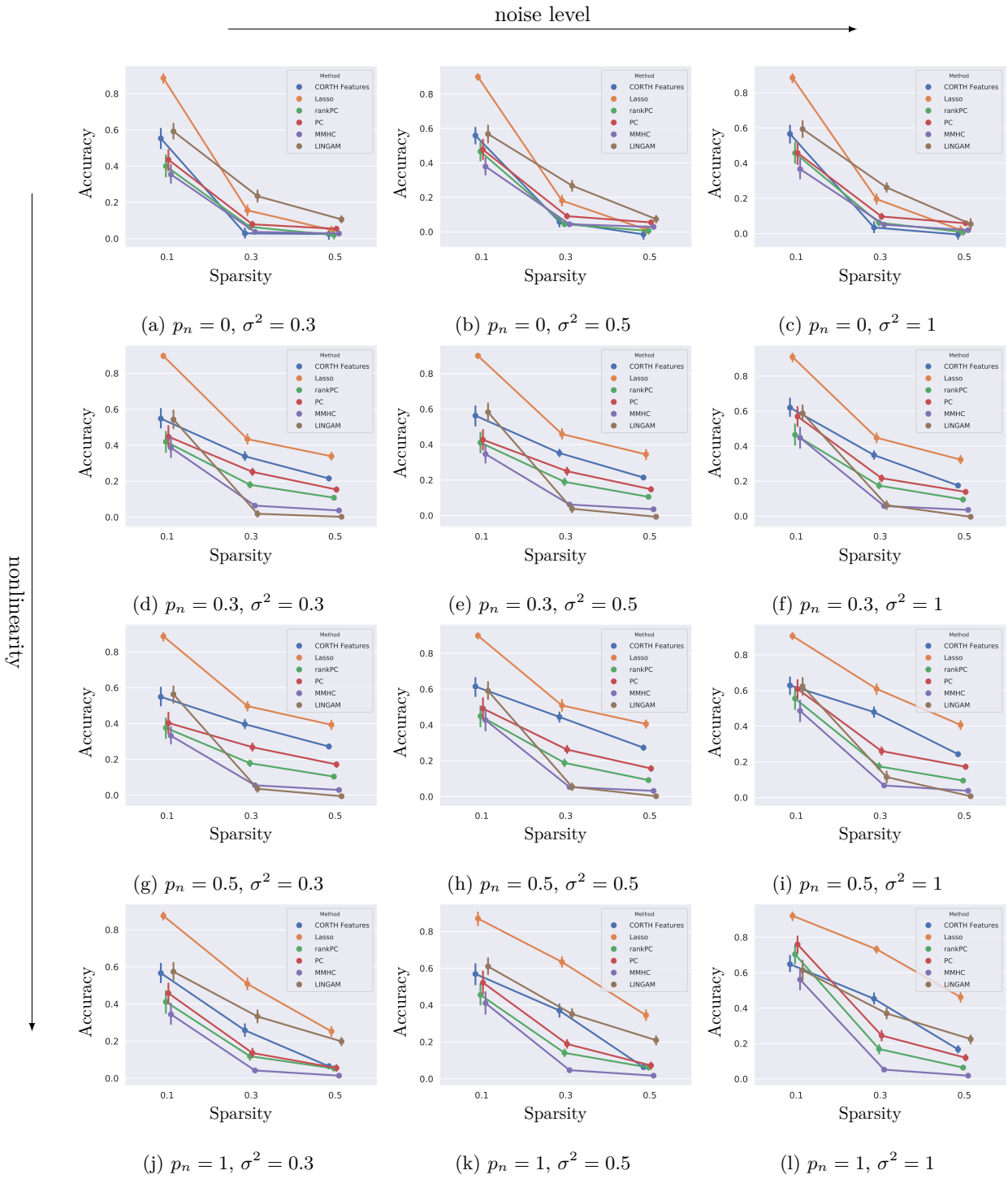

(a) $p_n = 0$, $\sigma^2 = 0.3$ (b) $p_n = 0$, $\sigma^2 = 0.5$ (c) $p_n = 0$, $\sigma^2 = 1$

(d) $p_n = 0.3$, $\sigma^2 = 0.3$ (e) $p_n = 0.3$, $\sigma^2 = 0.5$ (f) $p_n = 0.3$, $\sigma^2 = 1$

(g) $p_n = 0.5$, $\sigma^2 = 0.3$ (h) $p_n = 0.5$, $\sigma^2 = 0.5$ (i) $p_n = 0.5$, $\sigma^2 = 1$

(j) $p_n = 1$, $\sigma^2 = 0.3$ (k) $p_n = 1$, $\sigma^2 = 0.5$ (l) $p_n = 1$, $\sigma^2 = 1$

Figure F.10: 50 nodes, 100 observations, 100 simulations. Compared to other methods, our approach is stable wrt. noise level, connectivity and even partially non-linear relationships, significantly outperforming the majority of baselines.

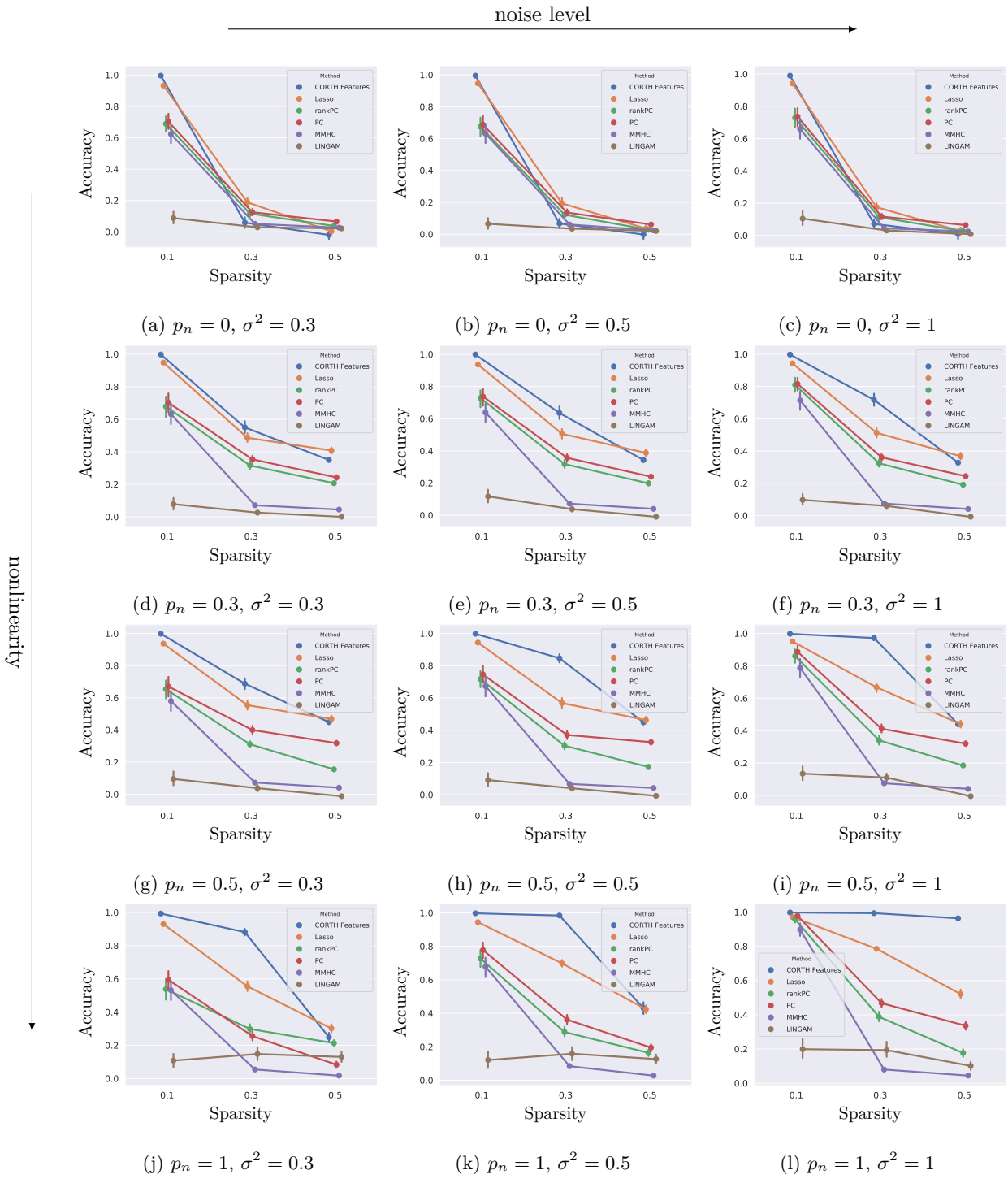

(a) $p_n = 0$, $\sigma^2 = 0.3$ (b) $p_n = 0$, $\sigma^2 = 0.5$ (c) $p_n = 0$, $\sigma^2 = 1$

(d) $p_n = 0.3$, $\sigma^2 = 0.3$ (e) $p_n = 0.3$, $\sigma^2 = 0.5$ (f) $p_n = 0.3$, $\sigma^2 = 1$

(g) $p_n = 0.5$, $\sigma^2 = 0.3$ (h) $p_n = 0.5$, $\sigma^2 = 0.5$ (i) $p_n = 0.5$, $\sigma^2 = 1$

(j) $p_n = 1$, $\sigma^2 = 0.3$ (k) $p_n = 1$, $\sigma^2 = 0.5$ (l) $p_n = 1$, $\sigma^2 = 1$

Figure F.11: 50 nodes, 500 observations, 100 simulations. Compared to other methods, our approach is stable wrt. noise level, connectivity and even partially non-linear relationships, significantly outperforming the majority of baselines.

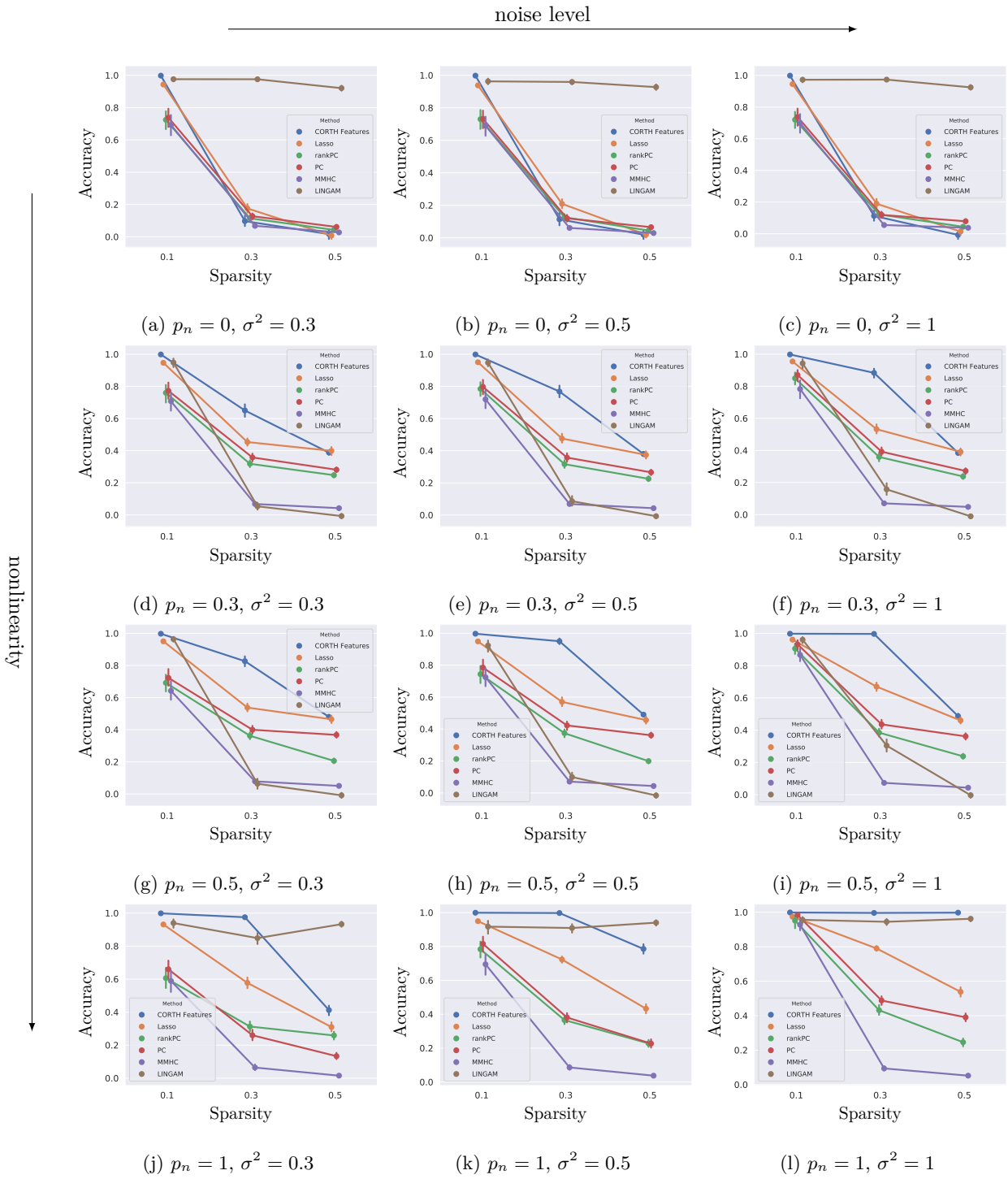

(a) $p_n = 0$, $\sigma^2 = 0.3$ (b) $p_n = 0$, $\sigma^2 = 0.5$ (c) $p_n = 0$, $\sigma^2 = 1$

(d) $p_n = 0.3$, $\sigma^2 = 0.3$ (e) $p_n = 0.3$, $\sigma^2 = 0.5$ (f) $p_n = 0.3$, $\sigma^2 = 1$

(g) $p_n = 0.5$, $\sigma^2 = 0.3$ (h) $p_n = 0.5$, $\sigma^2 = 0.5$ (i) $p_n = 0.5$, $\sigma^2 = 1$

(j) $p_n = 1$, $\sigma^2 = 0.3$ (k) $p_n = 1$, $\sigma^2 = 0.5$ (l) $p_n = 1$, $\sigma^2 = 1$

Figure F.12: 50 nodes, 1000 observations, 100 simulations. Compared to other methods, our approach is stable wrt. noise level, connectivity and even partially non-linear relationships, significantly outperforming the majority of baselines.

G Supplemntary Figures for Performace in Inferring Direct Causes, F1 Score as Metric

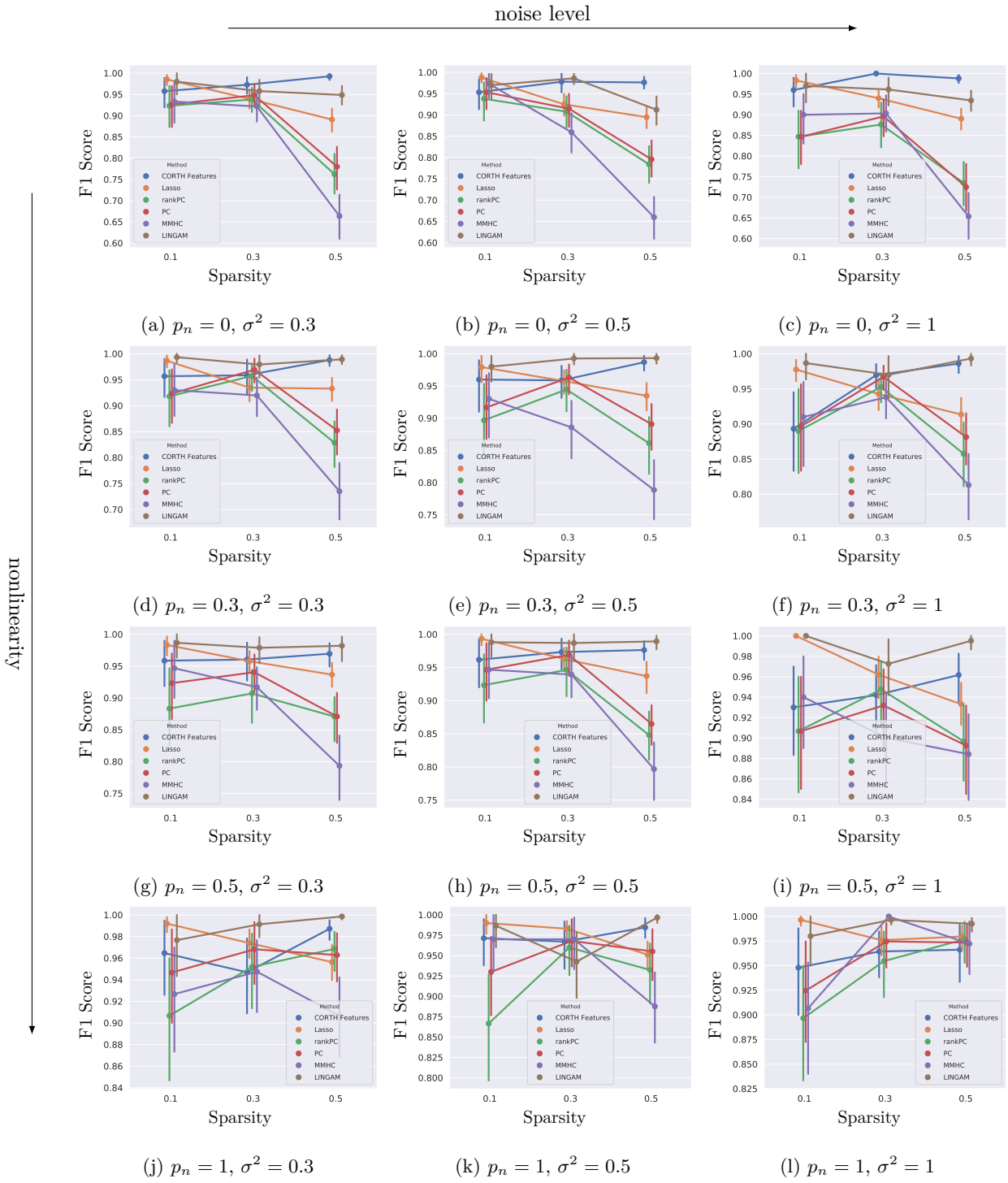

(a) $p_n = 0$, $\sigma^2 = 0.3$ (b) $p_n = 0$, $\sigma^2 = 0.5$ (c) $p_n = 0$, $\sigma^2 = 1$

(d) $p_n = 0.3$, $\sigma^2 = 0.3$ (e) $p_n = 0.3$, $\sigma^2 = 0.5$ (f) $p_n = 0.3$, $\sigma^2 = 1$

(g) $p_n = 0.5$, $\sigma^2 = 0.3$ (h) $p_n = 0.5$, $\sigma^2 = 0.5$ (i) $p_n = 0.5$, $\sigma^2 = 1$

(j) $p_n = 1$, $\sigma^2 = 0.3$ (k) $p_n = 1$, $\sigma^2 = 0.5$ (l) $p_n = 1$, $\sigma^2 = 1$

Figure G.1: 5 nodes, 100 observations, 100 simulations. Compared to other methods, our approach is stable wrt. noise level, connectivity and even partially non-linear relationships, significantly outperforming the majority of baselines.

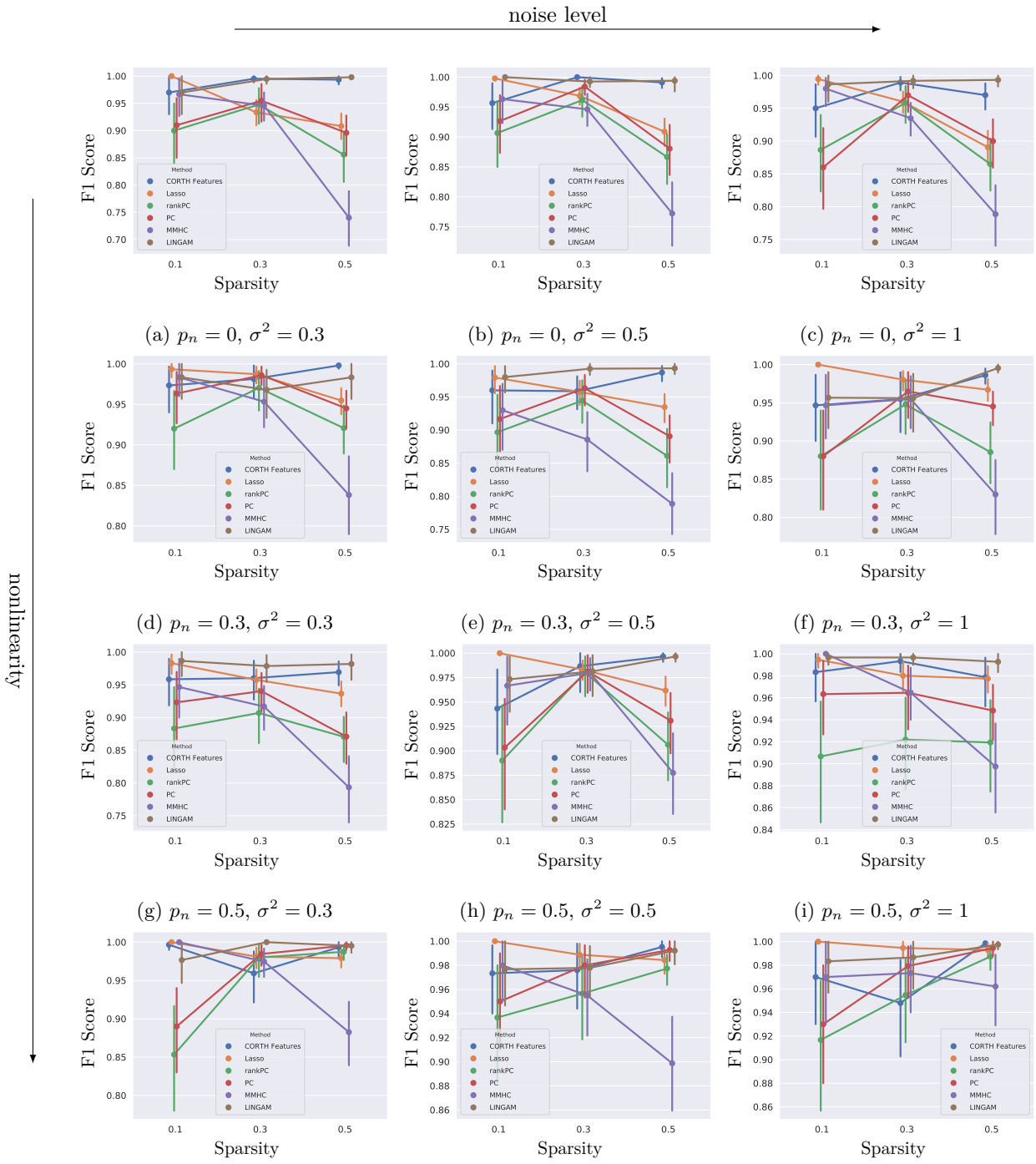

(a) $p_n = 0$, $\sigma^2 = 0.3$ (b) $p_n = 0$, $\sigma^2 = 0.5$ (c) $p_n = 0$, $\sigma^2 = 1$

(d) $p_n = 0.3$, $\sigma^2 = 0.3$ (e) $p_n = 0.3$, $\sigma^2 = 0.5$ (f) $p_n = 0.3$, $\sigma^2 = 1$

(g) $p_n = 0.5$, $\sigma^2 = 0.3$ (h) $p_n = 0.5$, $\sigma^2 = 0.5$ (i) $p_n = 0.5$, $\sigma^2 = 1$

(j) $p_n = 1$, $\sigma^2 = 0.3$ (k) $p_n = 1$, $\sigma^2 = 0.5$ (l) $p_n = 1$, $\sigma^2 = 1$

Figure G.2: 5 nodes, 500 observations, 100 simulations. Compared to other methods, our approach is stable wrt. noise level, connectivity and even partially non-linear relationships, significantly outperforming the majority of baselines.

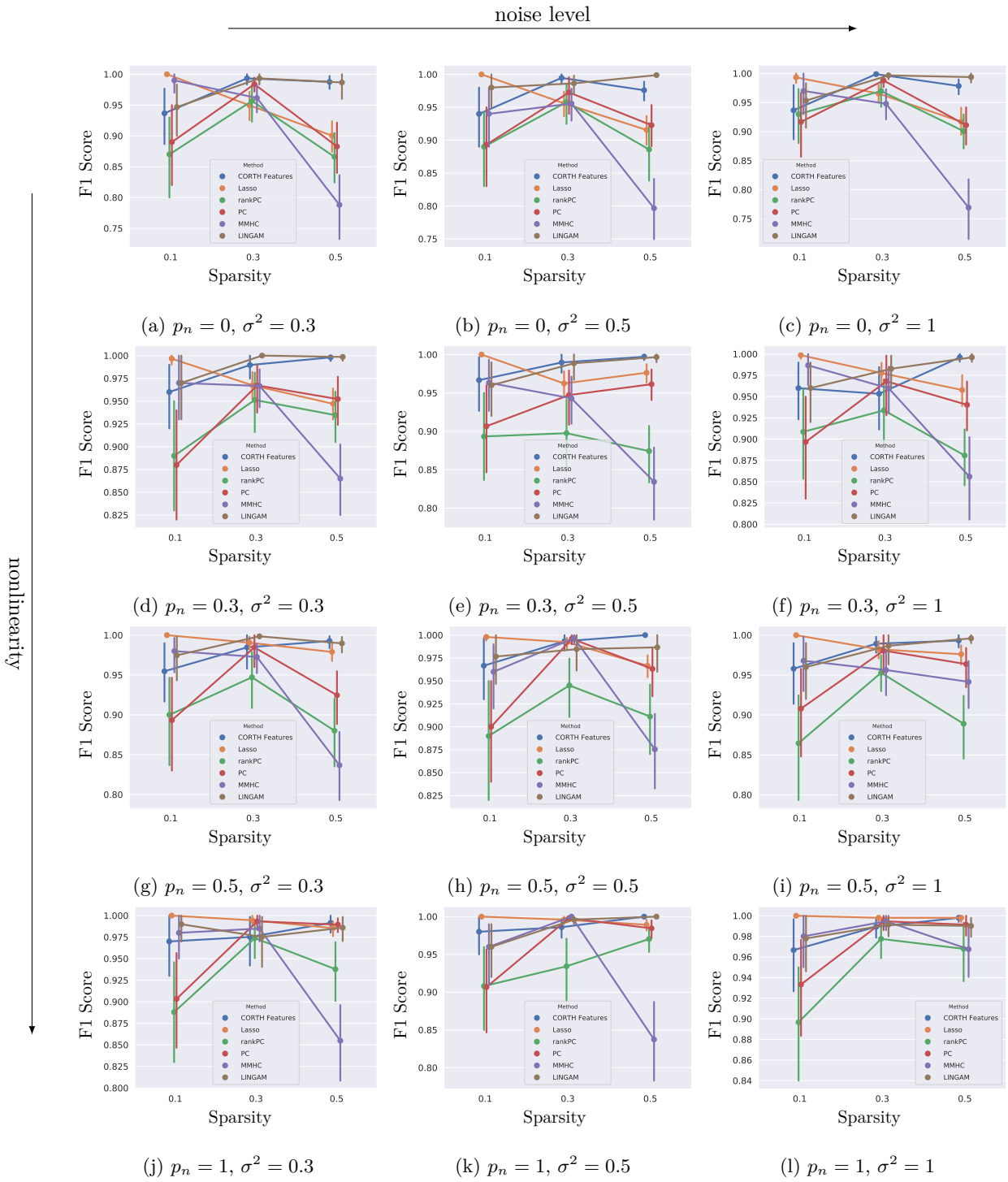

(a) $p_n = 0$, $\sigma^2 = 0.3$ (b) $p_n = 0$, $\sigma^2 = 0.5$ (c) $p_n = 0$, $\sigma^2 = 1$

(d) $p_n = 0.3$, $\sigma^2 = 0.3$ (e) $p_n = 0.3$, $\sigma^2 = 0.5$ (f) $p_n = 0.3$, $\sigma^2 = 1$

(g) $p_n = 0.5$, $\sigma^2 = 0.3$ (h) $p_n = 0.5$, $\sigma^2 = 0.5$ (i) $p_n = 0.5$, $\sigma^2 = 1$

(j) $p_n = 1$, $\sigma^2 = 0.3$ (k) $p_n = 1$, $\sigma^2 = 0.5$ (l) $p_n = 1$, $\sigma^2 = 1$

Figure G.3: 5 nodes, 1000 observations, 100 simulations. Compared to other methods, our approach is stable wrt. noise level, connectivity and even partially non-linear relationships, significantly outperforming the majority of baselines.

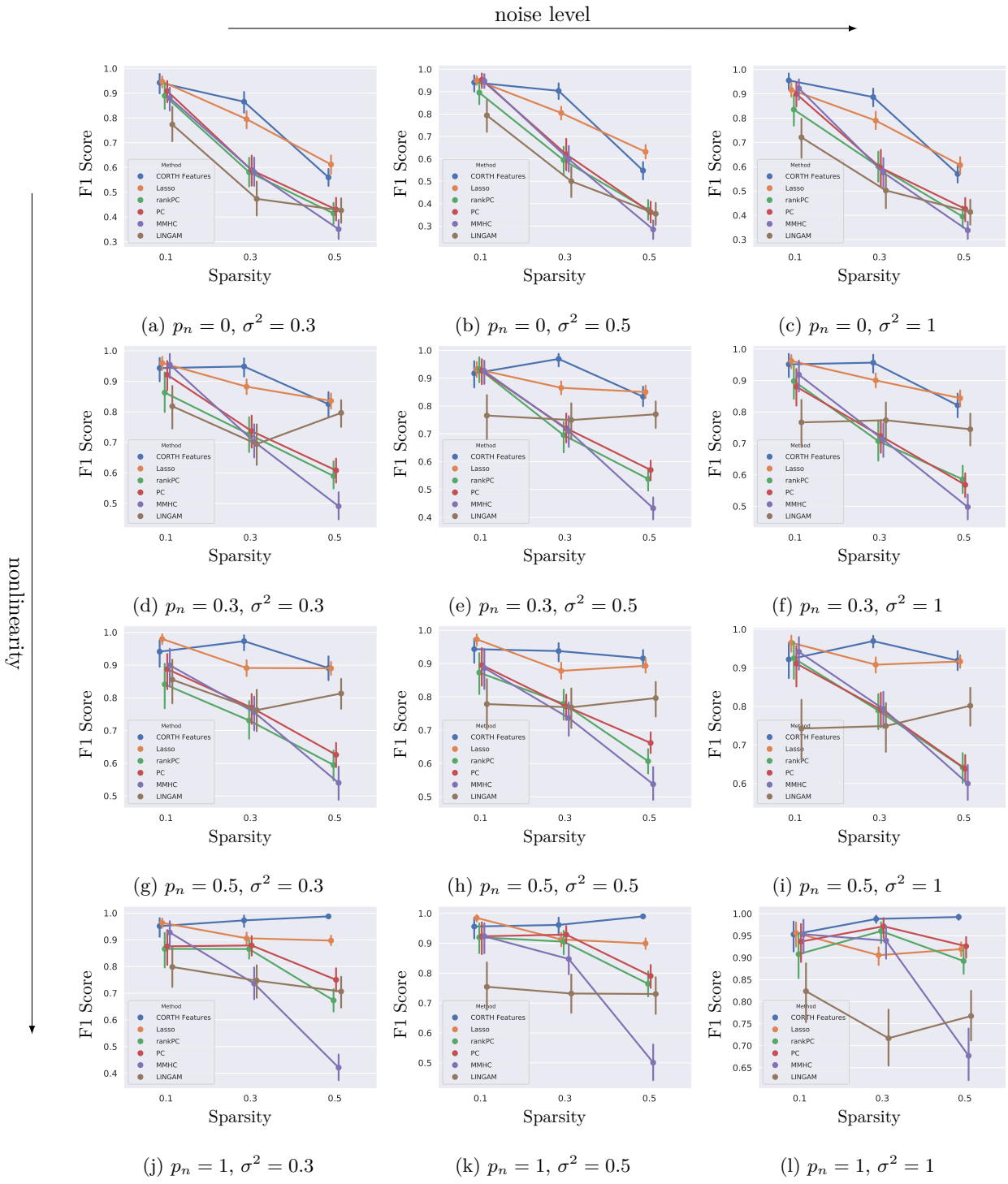

(a) $p_n = 0$, $\sigma^2 = 0.3$ (b) $p_n = 0$, $\sigma^2 = 0.5$ (c) $p_n = 0$, $\sigma^2 = 1$

(d) $p_n = 0.3$, $\sigma^2 = 0.3$ (e) $p_n = 0.3$, $\sigma^2 = 0.5$ (f) $p_n = 0.3$, $\sigma^2 = 1$

(g) $p_n = 0.5$, $\sigma^2 = 0.3$ (h) $p_n = 0.5$, $\sigma^2 = 0.5$ (i) $p_n = 0.5$, $\sigma^2 = 1$

(j) $p_n = 1$, $\sigma^2 = 0.3$ (k) $p_n = 1$, $\sigma^2 = 0.5$ (l) $p_n = 1$, $\sigma^2 = 1$

Figure G.4: 10 nodes, 100 observations, 100 simulations. Compared to other methods, our approach is stable wrt. noise level, connectivity and even partially non-linear relationships, significantly outperforming the majority of baselines.

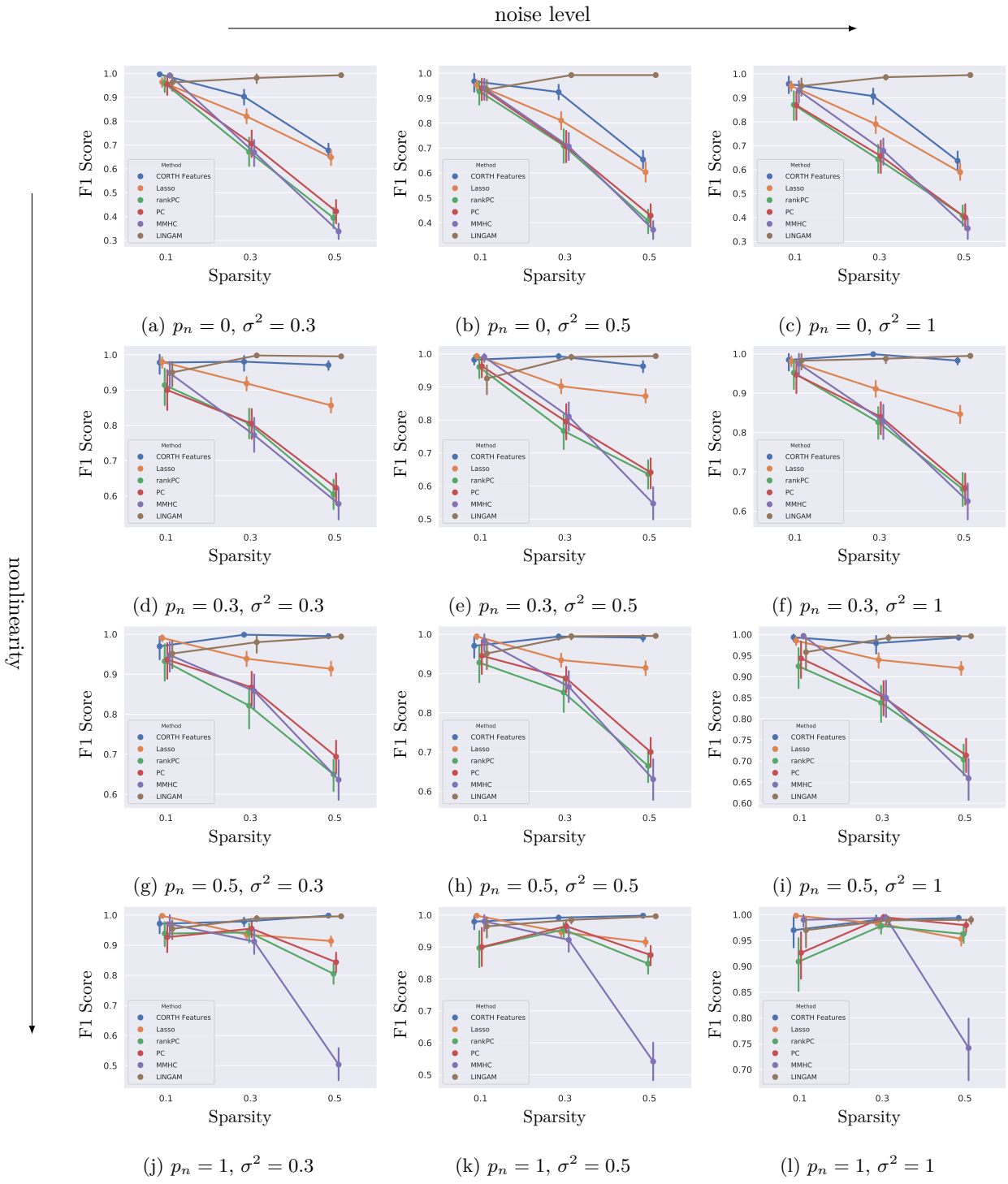

(a) $p_n = 0$, $\sigma^2 = 0.3$ (b) $p_n = 0$, $\sigma^2 = 0.5$ (c) $p_n = 0$, $\sigma^2 = 1$

(d) $p_n = 0.3$, $\sigma^2 = 0.3$ (e) $p_n = 0.3$, $\sigma^2 = 0.5$ (f) $p_n = 0.3$, $\sigma^2 = 1$

(g) $p_n = 0.5$, $\sigma^2 = 0.3$ (h) $p_n = 0.5$, $\sigma^2 = 0.5$ (i) $p_n = 0.5$, $\sigma^2 = 1$

(j) $p_n = 1$, $\sigma^2 = 0.3$ (k) $p_n = 1$, $\sigma^2 = 0.5$ (l) $p_n = 1$, $\sigma^2 = 1$

Figure G.5: 10 nodes, 500 observations, 100 simulations. Compared to other methods, our approach is stable wrt. noise level, connectivity and even partially non-linear relationships, significantly outperforming the majority of baselines.

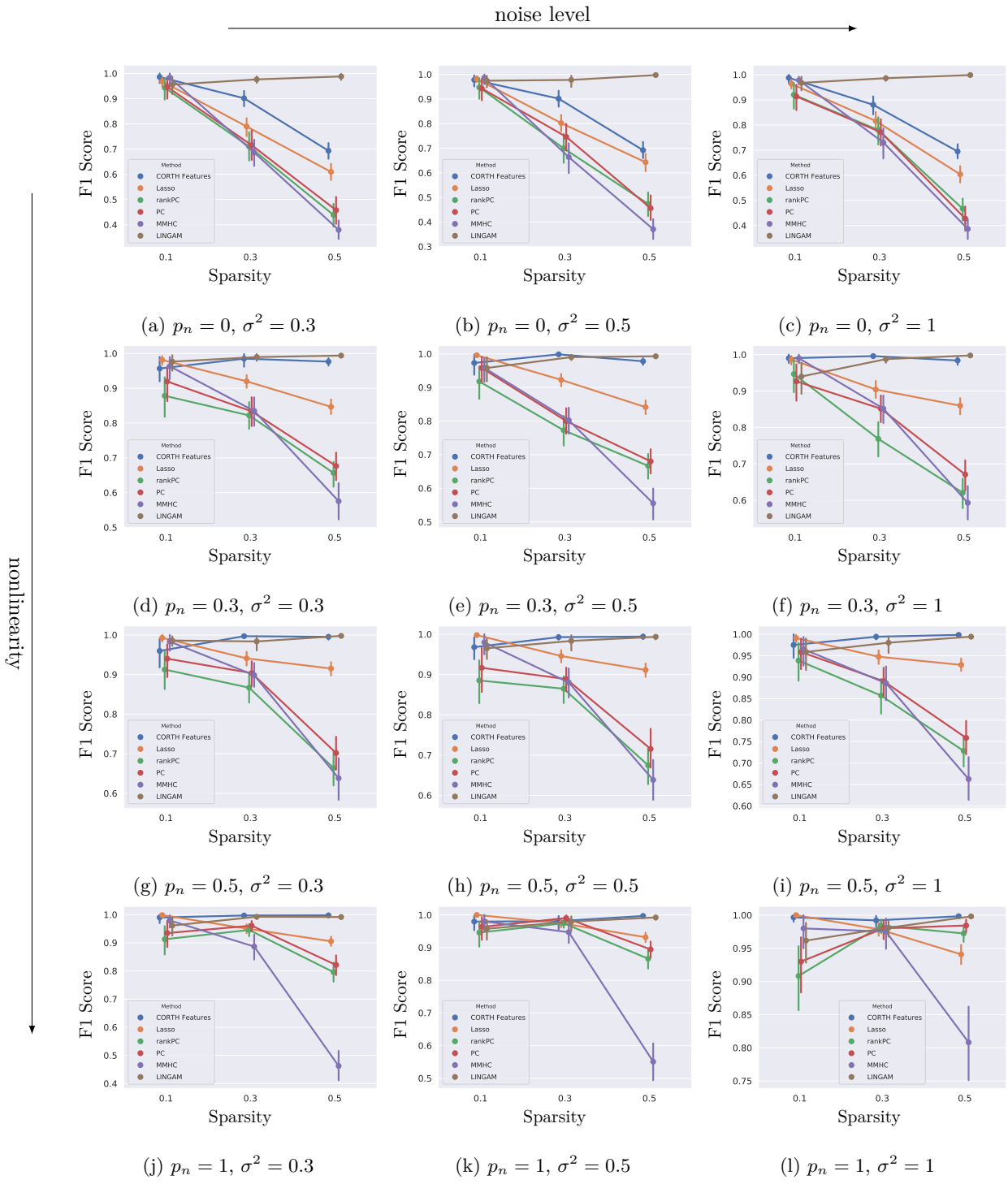

(a) $p_n = 0$, $\sigma^2 = 0.3$ (b) $p_n = 0$, $\sigma^2 = 0.5$ (c) $p_n = 0$, $\sigma^2 = 1$

(d) $p_n = 0.3$, $\sigma^2 = 0.3$ (e) $p_n = 0.3$, $\sigma^2 = 0.5$ (f) $p_n = 0.3$, $\sigma^2 = 1$

(g) $p_n = 0.5$, $\sigma^2 = 0.3$ (h) $p_n = 0.5$, $\sigma^2 = 0.5$ (i) $p_n = 0.5$, $\sigma^2 = 1$

(j) $p_n = 1$, $\sigma^2 = 0.3$ (k) $p_n = 1$, $\sigma^2 = 0.5$ (l) $p_n = 1$, $\sigma^2 = 1$

Figure G.6: 10 nodes, 1000 observations, 100 simulations. Compared to other methods, our approach is stable wrt. noise level, connectivity and even partially non-linear relationships, significantly outperforming the majority of baselines.

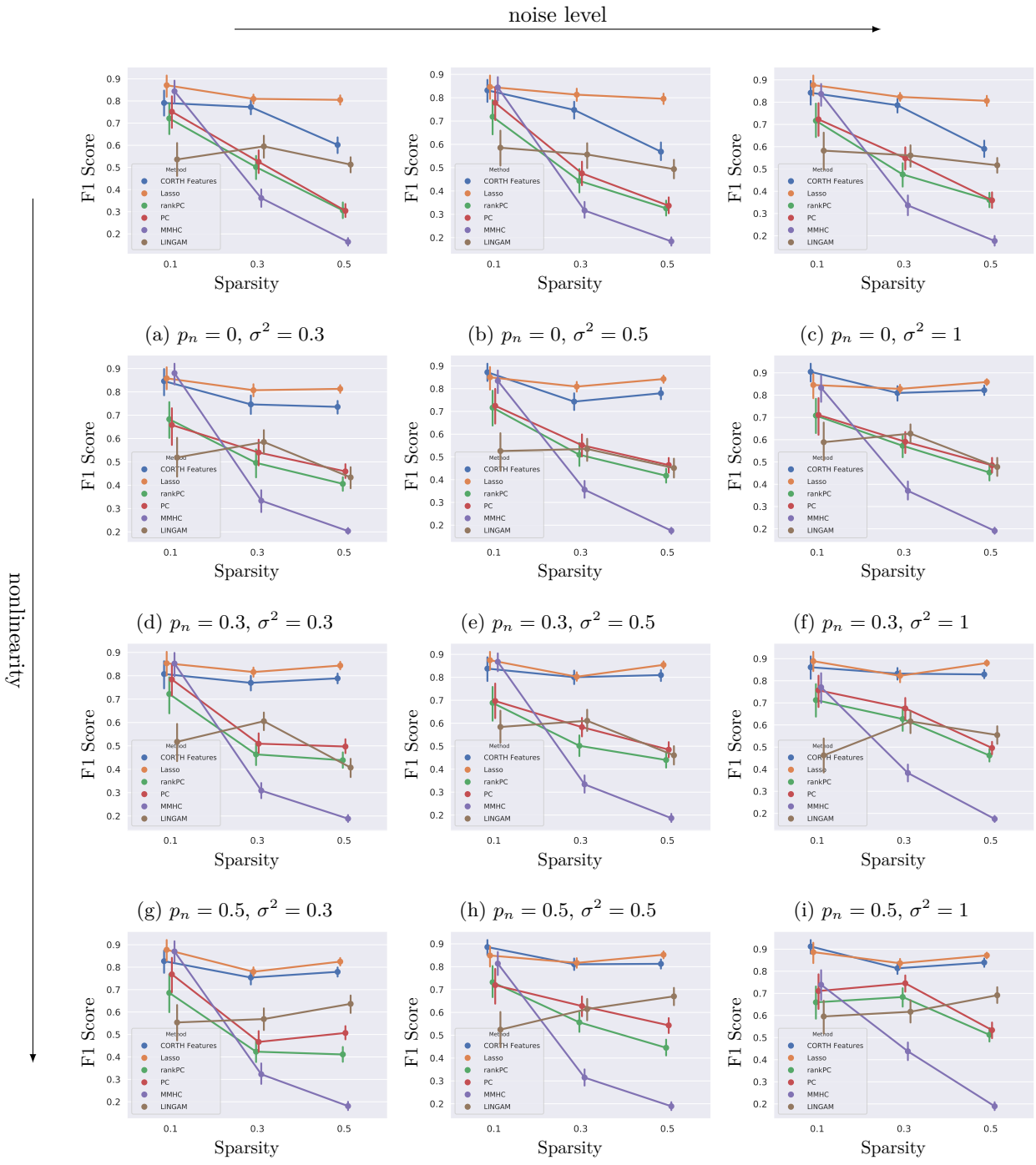

(a) $p_n = 0$, $\sigma^2 = 0.3$ (b) $p_n = 0$, $\sigma^2 = 0.5$ (c) $p_n = 0$, $\sigma^2 = 1$

(d) $p_n = 0.3$, $\sigma^2 = 0.3$ (e) $p_n = 0.3$, $\sigma^2 = 0.5$ (f) $p_n = 0.3$, $\sigma^2 = 1$

(g) $p_n = 0.5$, $\sigma^2 = 0.3$ (h) $p_n = 0.5$, $\sigma^2 = 0.5$ (i) $p_n = 0.5$, $\sigma^2 = 1$

(j) $p_n = 1$, $\sigma^2 = 0.3$ (k) $p_n = 1$, $\sigma^2 = 0.5$ (l) $p_n = 1$, $\sigma^2 = 1$

Figure G.7: 20 nodes, 100 observations, 100 simulations. Compared to other methods, our approach is stable wrt. noise level, connectivity and even partially non-linear relationships, significantly outperforming the majority of baselines.

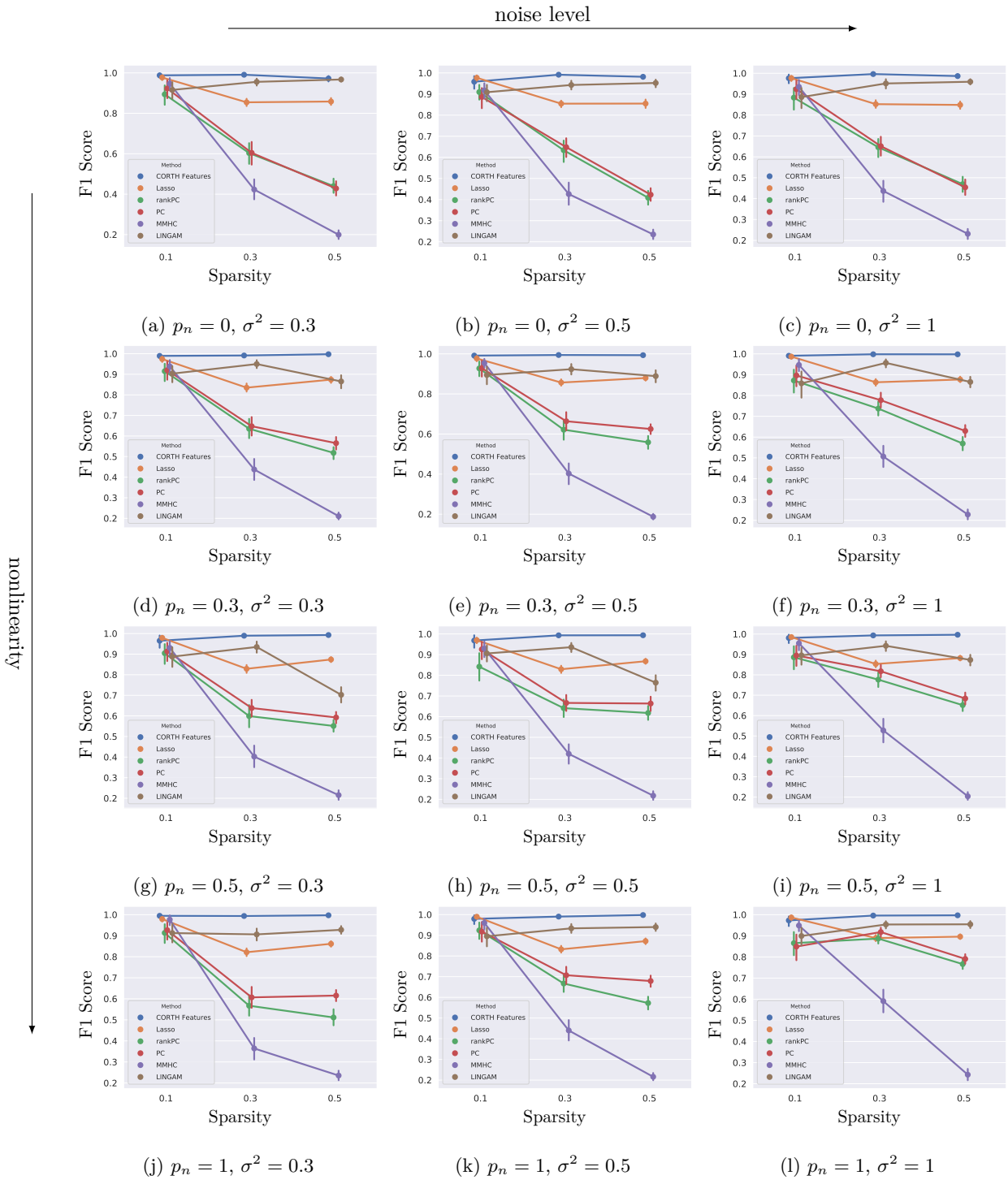

(a) $p_n = 0$, $\sigma^2 = 0.3$ (b) $p_n = 0$, $\sigma^2 = 0.5$ (c) $p_n = 0$, $\sigma^2 = 1$

(d) $p_n = 0.3$, $\sigma^2 = 0.3$ (e) $p_n = 0.3$, $\sigma^2 = 0.5$ (f) $p_n = 0.3$, $\sigma^2 = 1$

(g) $p_n = 0.5$, $\sigma^2 = 0.3$ (h) $p_n = 0.5$, $\sigma^2 = 0.5$ (i) $p_n = 0.5$, $\sigma^2 = 1$

(j) $p_n = 1$, $\sigma^2 = 0.3$ (k) $p_n = 1$, $\sigma^2 = 0.5$ (l) $p_n = 1$, $\sigma^2 = 1$

Figure G.8: 20 nodes, 500 observations, 100 simulations. Compared to other methods, our approach is stable wrt. noise level, connectivity and even partially non-linear relationships, significantly outperforming the majority of baselines.

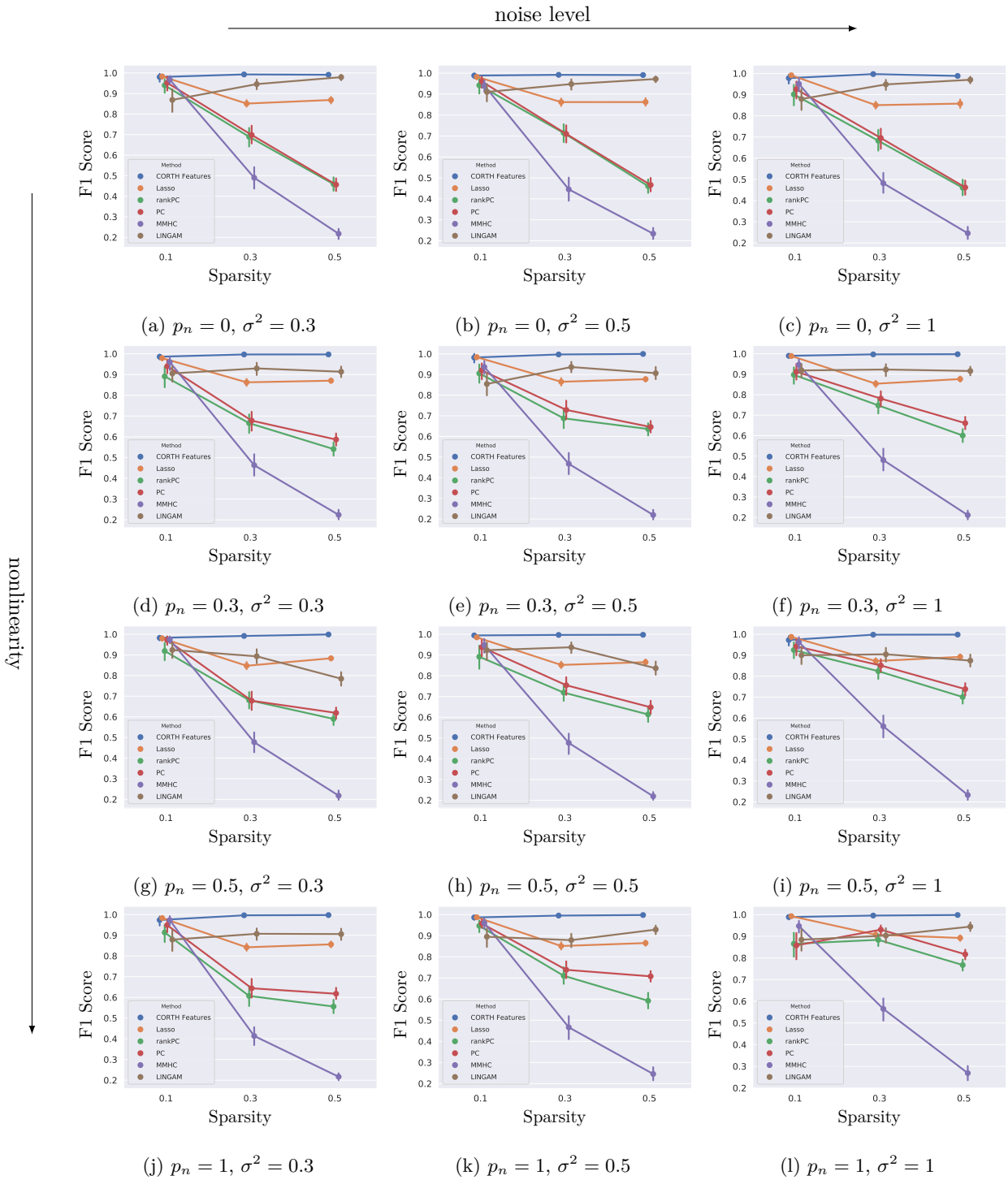

(a) $p_n = 0$, $\sigma^2 = 0.3$ (b) $p_n = 0$, $\sigma^2 = 0.5$ (c) $p_n = 0$, $\sigma^2 = 1$

(d) $p_n = 0.3$, $\sigma^2 = 0.3$ (e) $p_n = 0.3$, $\sigma^2 = 0.5$ (f) $p_n = 0.3$, $\sigma^2 = 1$

(g) $p_n = 0.5$, $\sigma^2 = 0.3$ (h) $p_n = 0.5$, $\sigma^2 = 0.5$ (i) $p_n = 0.5$, $\sigma^2 = 1$

(j) $p_n = 1$, $\sigma^2 = 0.3$ (k) $p_n = 1$, $\sigma^2 = 0.5$ (l) $p_n = 1$, $\sigma^2 = 1$

Figure G.9: 20 nodes, 1000 observations, 100 simulations. Compared to other methods, our approach is stable wrt. noise level, connectivity and even partially non-linear relationships, significantly outperforming the majority of baselines.

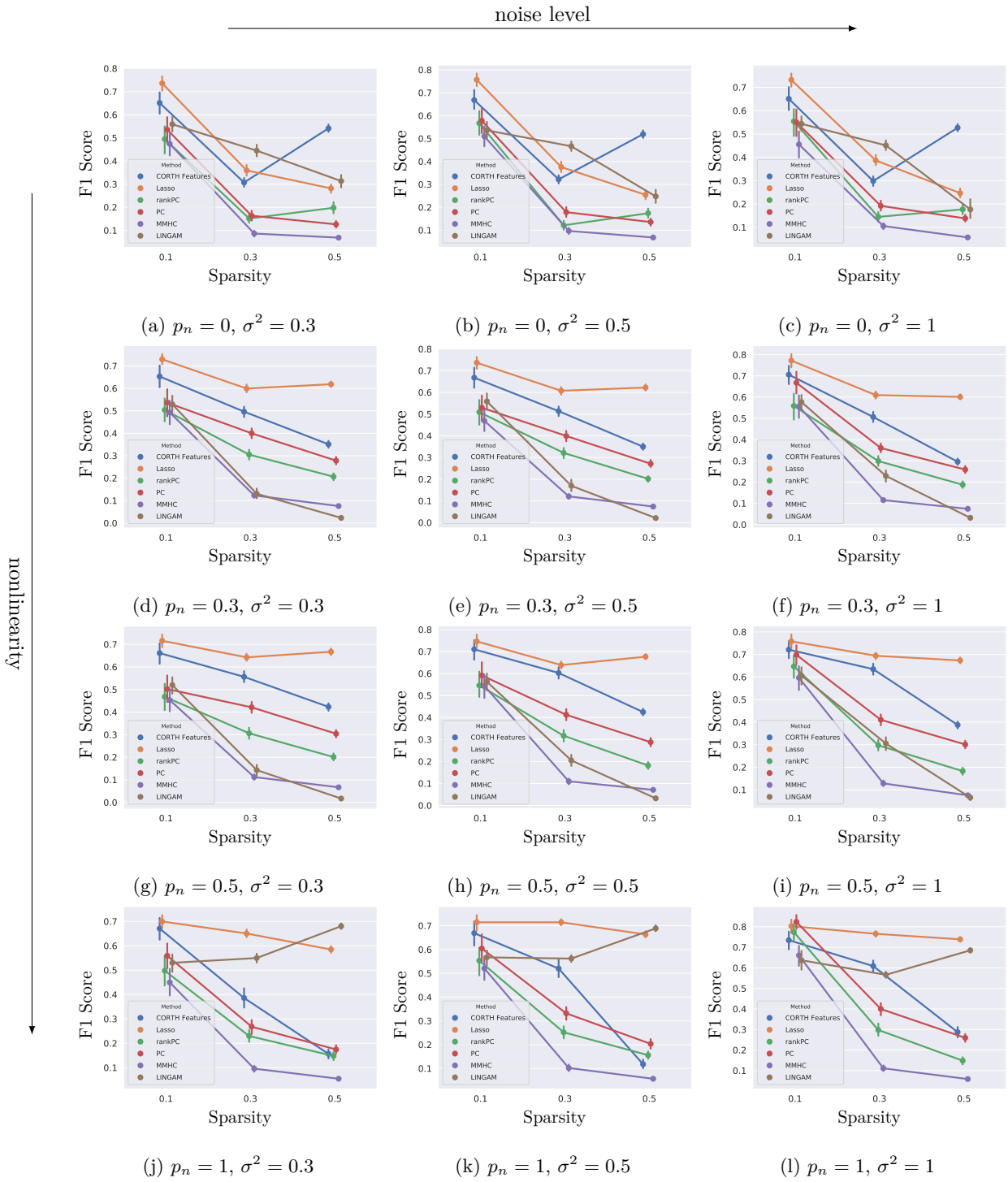

(a) $p_n = 0$, $\sigma^2 = 0.3$ (b) $p_n = 0$, $\sigma^2 = 0.5$ (c) $p_n = 0$, $\sigma^2 = 1$

(d) $p_n = 0.3$, $\sigma^2 = 0.3$ (e) $p_n = 0.3$, $\sigma^2 = 0.5$ (f) $p_n = 0.3$, $\sigma^2 = 1$

(g) $p_n = 0.5$, $\sigma^2 = 0.3$ (h) $p_n = 0.5$, $\sigma^2 = 0.5$ (i) $p_n = 0.5$, $\sigma^2 = 1$

(j) $p_n = 1$, $\sigma^2 = 0.3$ (k) $p_n = 1$, $\sigma^2 = 0.5$ (l) $p_n = 1$, $\sigma^2 = 1$

Figure G.10: 50 nodes, 100 observations, 100 simulations. Compared to other methods, our approach is stable wrt. noise level, connectivity and even partially non-linear relationships, significantly outperforming the majority of baselines.

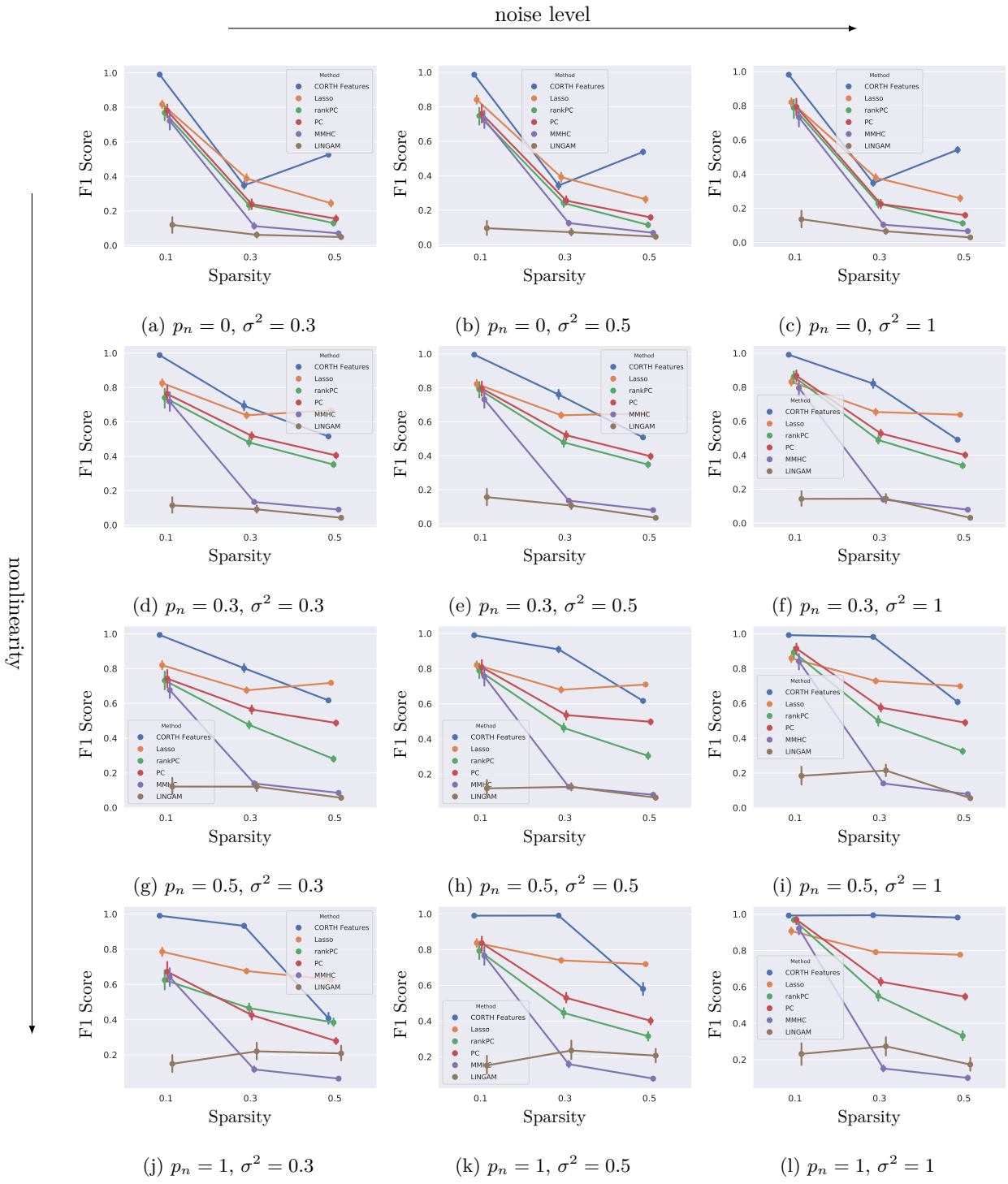

(a) $p_n = 0$, $\sigma^2 = 0.3$ (b) $p_n = 0$, $\sigma^2 = 0.5$ (c) $p_n = 0$, $\sigma^2 = 1$

(d) $p_n = 0.3$, $\sigma^2 = 0.3$ (e) $p_n = 0.3$, $\sigma^2 = 0.5$ (f) $p_n = 0.3$, $\sigma^2 = 1$

(g) $p_n = 0.5$, $\sigma^2 = 0.3$ (h) $p_n = 0.5$, $\sigma^2 = 0.5$ (i) $p_n = 0.5$, $\sigma^2 = 1$

(j) $p_n = 1$, $\sigma^2 = 0.3$ (k) $p_n = 1$, $\sigma^2 = 0.5$ (l) $p_n = 1$, $\sigma^2 = 1$

Figure G.11: 50 nodes, 500 observations, 100 simulations. Compared to other methods, our approach is stable wrt. noise level, connectivity and even partially non-linear relationships, significantly outperforming the majority of baselines.

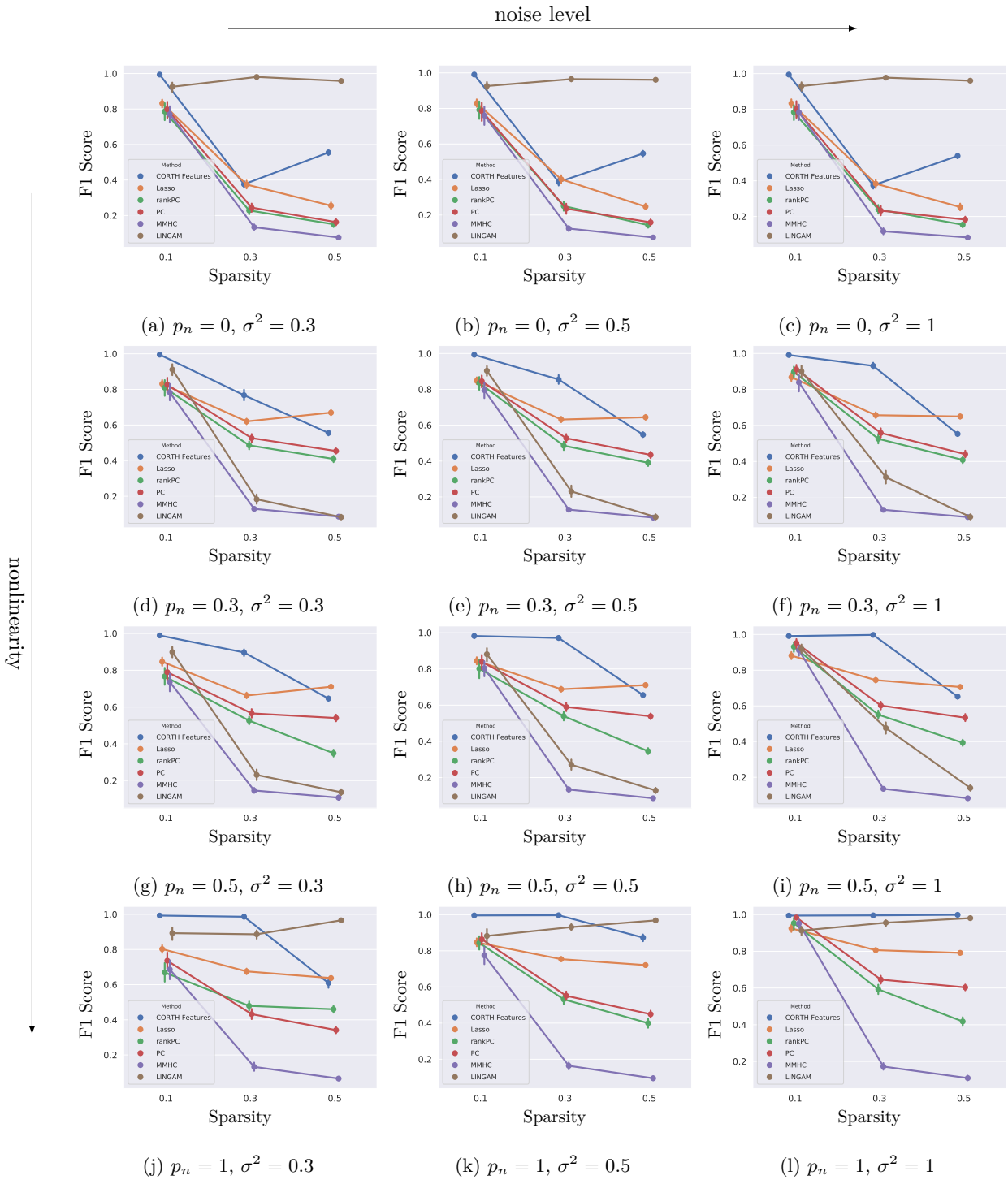

(a) $p_n = 0$, $\sigma^2 = 0.3$ (b) $p_n = 0$, $\sigma^2 = 0.5$ (c) $p_n = 0$, $\sigma^2 = 1$

(d) $p_n = 0.3$, $\sigma^2 = 0.3$ (e) $p_n = 0.3$, $\sigma^2 = 0.5$ (f) $p_n = 0.3$, $\sigma^2 = 1$

(g) $p_n = 0.5$, $\sigma^2 = 0.3$ (h) $p_n = 0.5$, $\sigma^2 = 0.5$ (i) $p_n = 0.5$, $\sigma^2 = 1$

(j) $p_n = 1$, $\sigma^2 = 0.3$ (k) $p_n = 1$, $\sigma^2 = 0.5$ (l) $p_n = 1$, $\sigma^2 = 1$

Figure G.12: 50 nodes, 1000 observations, 100 simulations. Compared to other methods, our approach is stable wrt. noise level, connectivity and even partially non-linear relationships, significantly outperforming the majority of baselines.